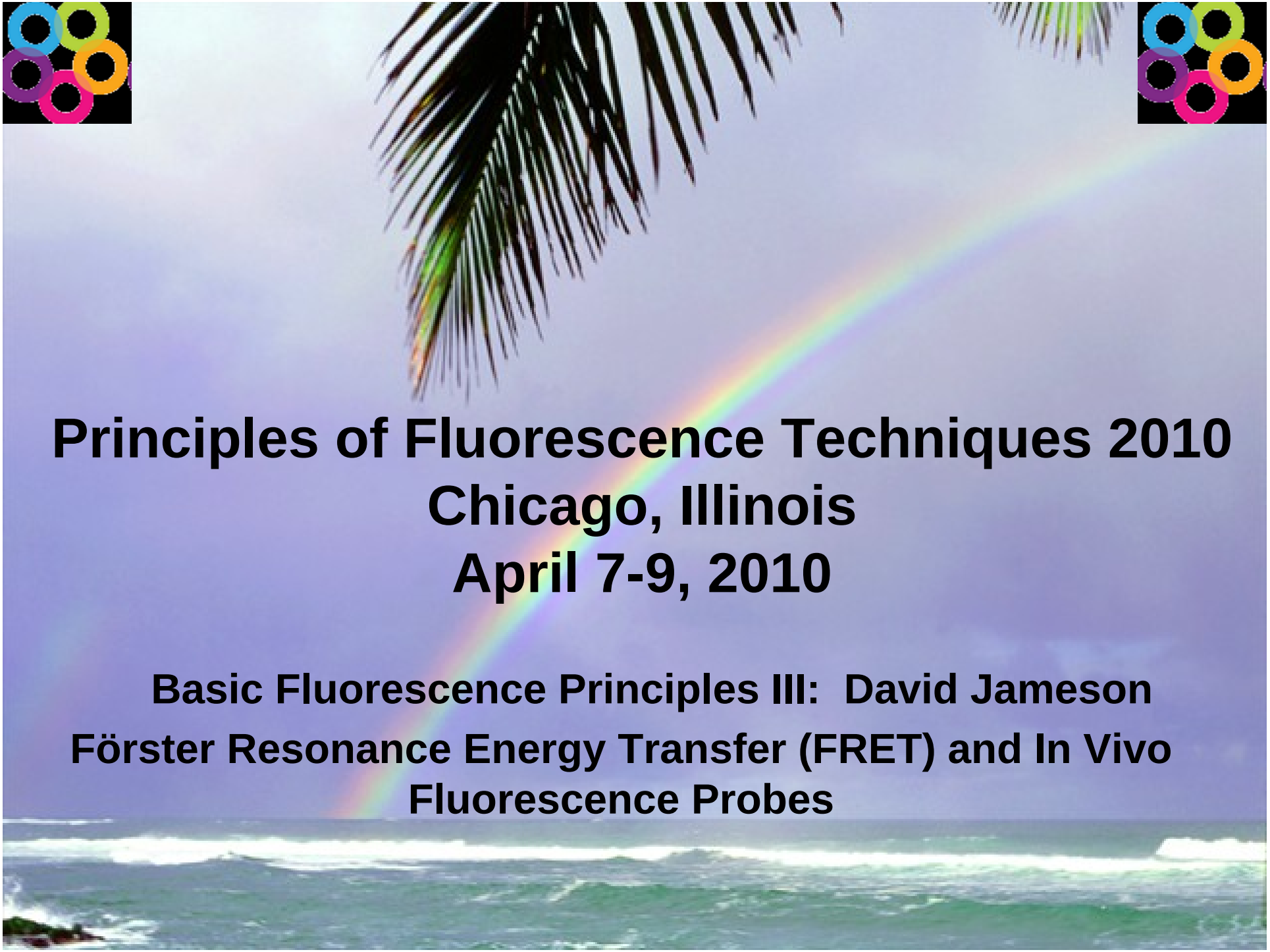

Principles of Fluorescence Techniques 2010
Chicago, Illinois
April 7-9, 2010

Basic Fluorescence Principles III: David Jameson

Förster Resonance Energy Transfer (FRET) and In Vivo Fluorescence Probes

Förster Resonance Energy Transfer
FRET

I should note before we start that the Merriam-Webster online dictionary defines “FRET” as:

“to cause to suffer emotional strain”

Some of these slides were prepared by Pierre Moens

This sentence appears in a 2006 book!

Let's correct this mistake!

More than 50 years ago, the German scientist Förster discovered that close proximity of two chromophores changes their spectral properties in predictable ways (Förster, 1948a).

Milestones in the Theory of Resonance Energy Transfer

1922 G. Cario and J. Franck demonstrate that excitation of a mixture of mercury and thallium atomic vapors with 254nm (the mercury resonance line) also displayed thallium (sensitized) emission at 535nm.

1924 E. Gaviola and P. Pringsham observed that an increase in the concentration of fluorescein in viscous solvent was accompanied by a progressive depolarization of the emission.

1925 J. Perrin proposed the mechanism of resonance energy transfer

1928 H. Kallmann and F. London developed the quantum theory of resonance energy transfer between various atoms in the gas phase. The dipole-dipole interaction and the parameter R_0 are used for the first time

1932 F. Perrin published a quantum mechanical theory of energy transfer between molecules of the same specie in solution. Qualitative discussion of the effect of the spectral overlap between the emission spectrum of the donor and the absorption spectrum of the acceptor

1946-1949 T. Förster develop the first complete quantitative theory of molecular resonance energy transfer


André Marie Ampère

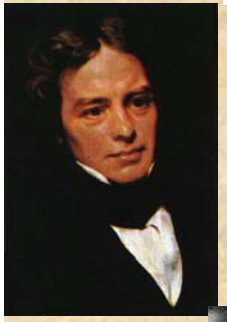


Heinrich Rudolf Hertz

From Förster's famous book
"Fluoreszenz Organischer Verbindungen";
which everyone references, but few read,

setzt, wobei n_{AB} die Häufigkeit des zwischenmolekularen Energieüberganges ist. Sie ist gleich der Zahl der Übergänge in der Zeiteinheit unter der Annahme, daß nach jedem Übergang stets wieder der ursprüngliche Zustand hergestellt wird. Aus Gl. (13,5) erhält man so, indem man gleichzeitig von der bisher benutzten Kreisfrequenz ω zur Frequenz ν selbst übergeht:

$$(13,6) \qquad n_{A,B} = \frac{\varkappa^2 e^4}{16\pi^2 n^4 m^2 R^6} \int_0^\infty f_e^{(A)}(\nu) \cdot f_a^{(B)}(\nu) \frac{d\nu}{\nu^2}.$$

Statt der Oszillatorenstärkefunktionen $f_e^{(A)}(\nu)$ und $f_a^{(B)}(\nu)$ führt man hier zweckmäßig die leichter zugänglichen Größen $f_Q^{(A)}(\nu)$ (Quantenspektrum des energieabgebenden Moleküls A) und $\varepsilon^{(B)}(\nu)$ (molarer dekadischer Extinktionskoeffizient des energieaufnehmenden Moleküls B) nach Gln. (12,46′) und (12,43′) ein. Man erhält so für die Übergangshäufigkeit

$$(13,7) \quad n_{A,B} = \frac{9 \cdot \ln 10}{128\pi^6} \frac{\varkappa^2 c^4}{n^4 N' \tau_e R^6} \int_0^\infty f_Q^{(A)}(\nu) \cdot \varepsilon^{(B)}(\nu) \frac{d\nu}{\nu^4}.$$

Diese Beziehung ist auch auf exakter quantenmechanischer Grundlage zu gewinnen [FÖRSTER (1947a)].

Die dimensionslose Konstante $\varkappa$ ist nach Gl. (13,1) durch die Feldstärkekomponente des Oszillators A am Ort und in der Richtung des Oszillators B bestimmt. Sie hängt daher von der Orientierung beider Oszillatoren zueinander und zu deren Verbindungslinie ab. Seien φ_A und φ_B die Winkel zwischen den einzelnen Oszillationsrichtungen und dieser Verbindungslinie und φ_{AB} der Winkel zwischen den Oszillationsrichtungen, so ist nach einer elementaren Formel für die Wechselwirkungsenergie zweier Dipole:

$$(13,8) \qquad \varkappa = \cos\varphi_{AB} - 3\cos\varphi_A \cdot \cos\varphi_B.$$

Wegen der Rotationsbewegung der Moleküle wechseln sämtliche Richtungen in den meisten Fällen so rasch, daß statt der Momentanwerte von $\varkappa^2$ dessen *statistischer Mittelwert* über sämtliche Orientierungen einzusetzen ist. Dieser ergibt sich am einfachsten durch

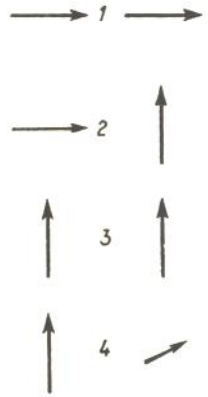

Fig. 16. Hauptlagen für die gegenseitige Orientierung zweier Oszillatoren. Der rechte Vektor zeigt in der Lage 4 nach hinten. Die nach Gl. (13,8) berechneten Werte von $\varkappa^2$ und die statistischen Gewichte der Hauptlagen sind:
$\varkappa_1^2 = 4\,(\frac{1}{9})$, $\varkappa_2^2 = 0\,(\frac{4}{9})$,
$\varkappa_3^2 = 1\,(\frac{2}{9})$, $\varkappa_4^2 = 0\,(\frac{2}{9})$.

gleichen Wert.

Thanks to Bob Clegg for this slide

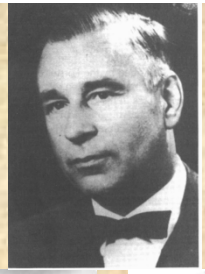

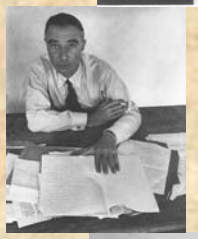

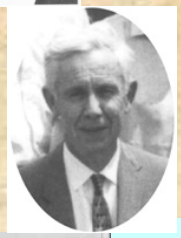

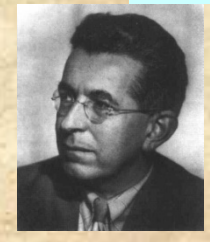

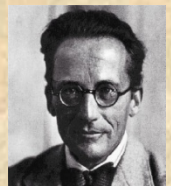


Werner Heisenberg

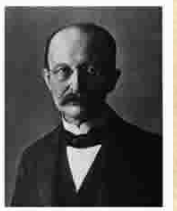
Max Planck

FRET applications in life sciences (from Valeur, 2002)

- Ligand-receptor interactions
- Conformational changes of biomolecules
- Proteins: in vivo protein-protein interactions, protein folding kinetics, protein subunit exchange, enzyme activity assay, etc…
- Membranes and models: membrane organization (e.g. membrane domains, lipid distribution, peptide association, lipid order in vesicles, membrane fusion assays, etc…)
- Nucleic acid structure and sequences: primary and secondary structure of DNA fragments, translocation of genes between two chromosomes, detection of nucleic acid hybridization, formation of hairpin structure, interaction with drugs, DNA triple helix, DNA-protein interaction, automated DNA sequencing, etc…
- Nucleic acid-protein interaction
- Immunoassays
- Biosensors

What is FRET ?

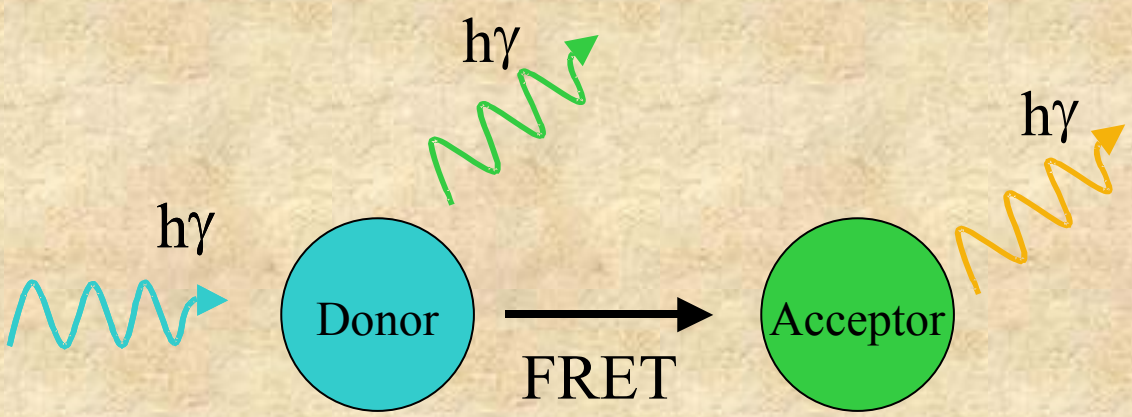

When the donor molecule absorbs a photon, and there is an acceptor molecule close to the donor molecule, radiationless energy transfer can occur from the donor to the acceptor.

FRET results in a decrease of the fluorescence intensity and lifetime of the donor probe, It enhance the fluorescence of the acceptor probe when the acceptor is fluorescent.

PM

Tuning fork analogy for resonance energy transfer

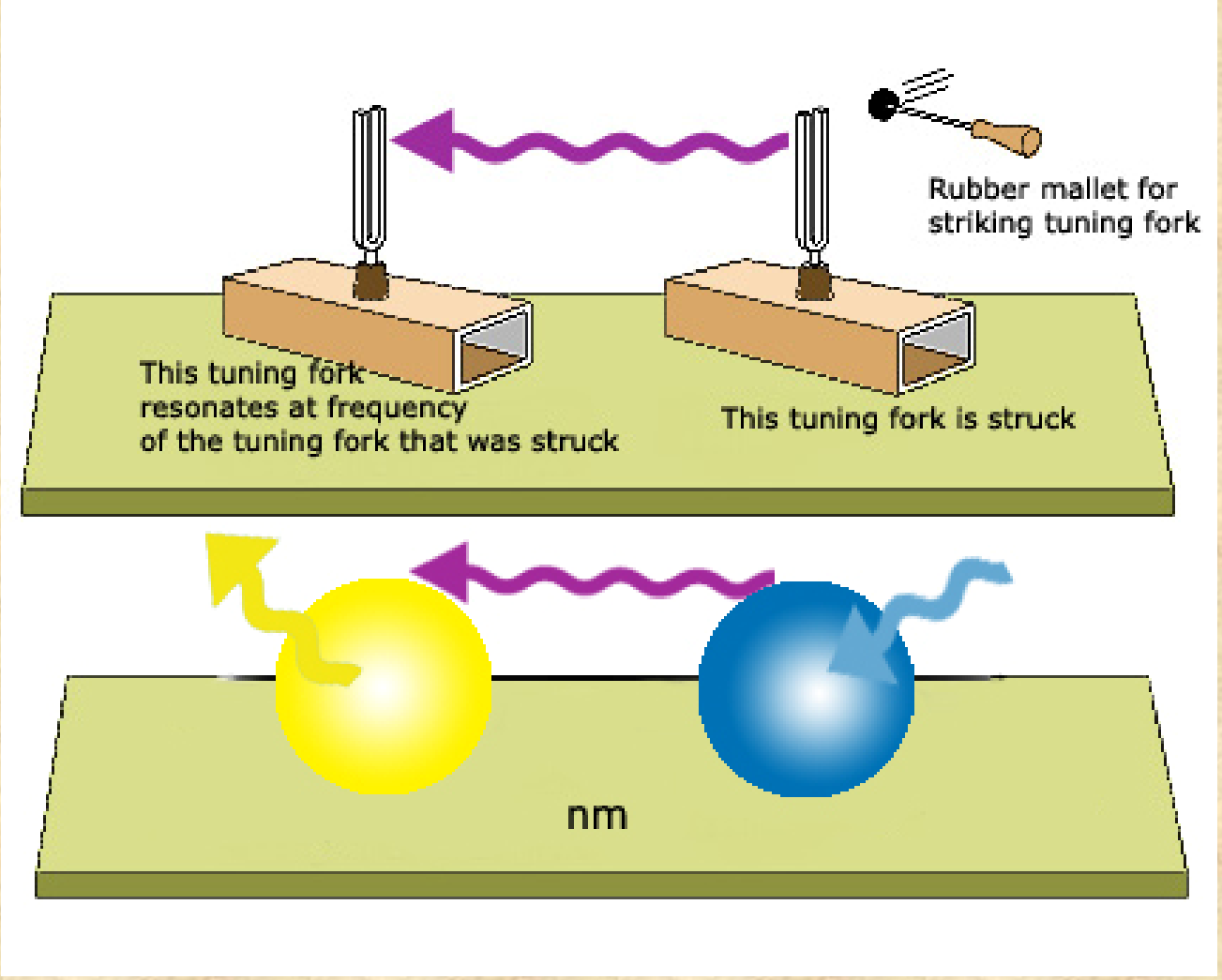

Simplified FRET Energy Diagram

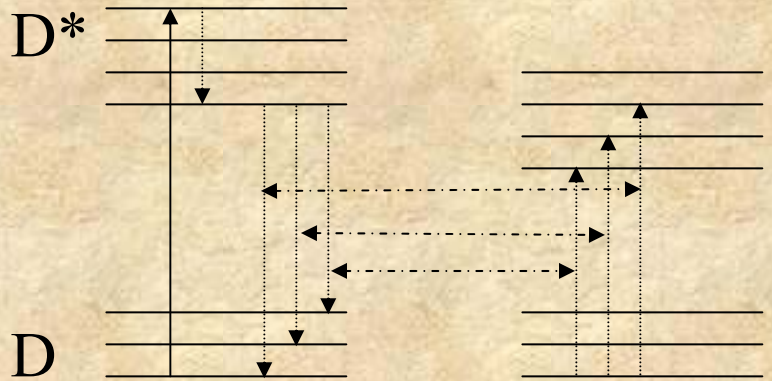

Coupled transitions

Suppose that the energy difference for one of these possible deactivation processes in the donor molecule matches that for a possible absorption transition in a nearby acceptor molecule. Then, with sufficient energetic coupling between these molecules (overlap of the emission spectrum of the donor and absorption spectrum of the acceptor), both processes may occur simultaneously, resulting in a transfer of excitation from the donor to the acceptor molecule

The interaction energy is of a dipole-dipole nature and depends on the distance between the molecules as well as the relative orientation of the dipoles

PM

Dipole-dipole interaction

The rate of transfer (k_T) of excitation energy is given by:

$$k_T = (1/\tau_d)(R_0/r)^6$$

Where τ_d is the fluorescence lifetime of the donor in the absence of acceptor, r the distance between the centers of the donor and acceptor molecules and R_0 the Förster critical distance at which 50% of the excitation energy is transferred to the acceptor and can be approximated from experiments independent of energy transfer.

Förster critical distance

$$R_0 = 0.2108\,(n^{-4} Q_d \kappa^2 J)^{1/6} \text{ Å}$$

n is the refractive index of the medium in the wavelength range where spectral overlap is significant (usually between 1.2-1.4 for biological samples)

Q_d is the fluorescence quantum yield of the donor in absence of acceptor (i.e. number of quanta emitted / number of quanta absorbed)

κ^2 (pronounced “kappa squared”) is the orientation factor for the dipole-dipole interaction

J is the normalized spectral overlap integral [$\varepsilon(\lambda)$ is in $M^{-1}\,cm^{-1}$, λ is in nm and J units are $M^{-1}\,cm^{-1}\,(nm)^4$]

The overlap integral *J* is defined by:

$$J = \int_0^\infty I_D(\lambda)\varepsilon_A(\lambda)\lambda^4 d\lambda$$

Where λ is the wavelength of the light, $\varepsilon_A(\lambda)$ is the molar absorption coefficient at that wavelength and $I_D(\lambda)$ is the fluorescence spectrum of the donor normalized on the wavelength scale:

$$I_D(\lambda) = \frac{F_{D\lambda}(\lambda)}{\int_0^\infty F_{D\lambda}(\lambda)d\lambda}$$

Where $F_{D\,\lambda}(\lambda)$ is the donor fluorescence per unit wavelength interval

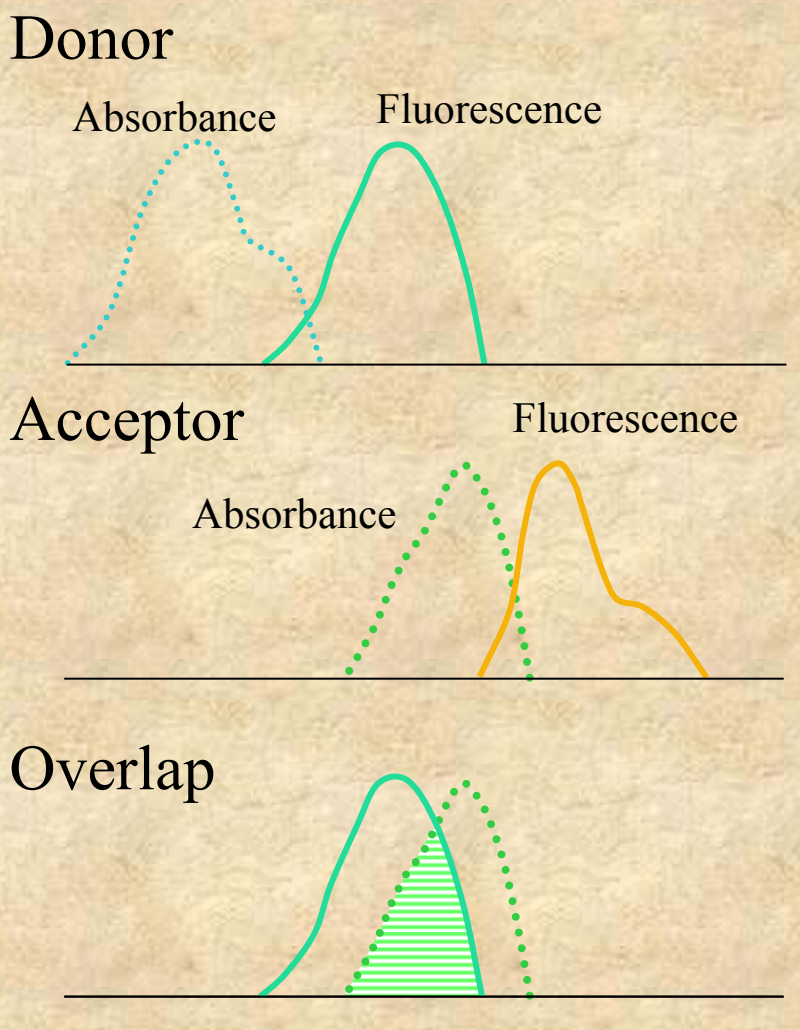

Determination of the efficiency of energy transfer (*E*)

Steady state method: *Decrease in donor fluorescence.* the fluorescence intensity of the donor is determined in absence and presence of the acceptor.

$$E = 1 - \frac{F_{da}}{F_d}$$

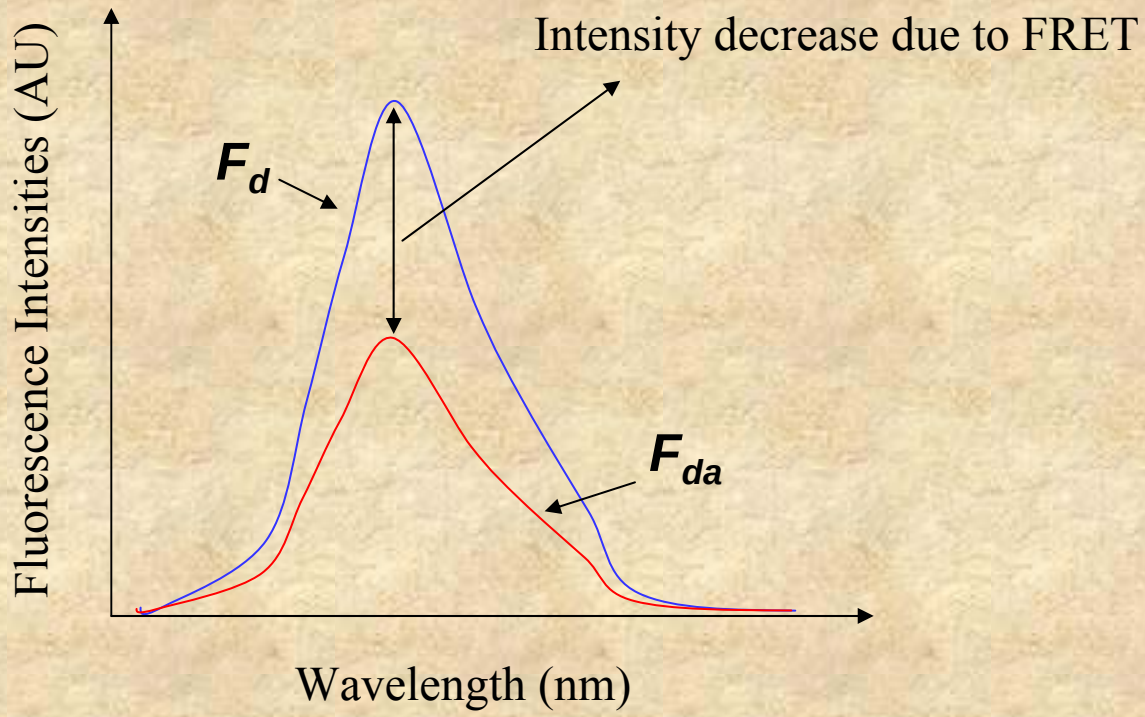

Determination of the efficiency of energy transfer (*E*)

Time-resolved method: Decrease in the lifetime of the donor

If the fluorescence decay of the donor is a single exponential then:

$$E = 1 - \frac{\tau_D}{\tau_D^0}$$

Where τ_D and τ_D^0 are the lifetime of the donor in the presence and absence of acceptor, respectively

Determination of the efficiency of energy transfer (*E*)

If the donor fluorescence decay in absence of acceptor is not a single exponential (probably resulting from heterogeneity of the probe's microenvironment) , then it may be modeled as a sum of exponential and the transfer efficiency can be calculated using the average decay times of the donor in absence and presence of acceptor:

$$E = 1 - {}^{\tau}\frac{\left\langle \tau_D \right\rangle}{\left\langle \tau_D^0 \right\rangle}$$

Where $<\tau>$ is the amplitude-average decay time and is defined as:

$$\left\langle \tau \right\rangle = \frac{\sum_i \alpha_i \tau_i}{\sum_i \alpha_i}$$

The distance dependence of the energy transfer efficiency (*E*)

$$r = \left(\frac{1}{E} - 1 \right)^{1/6} R_0$$

Where *r* is the distance separating the donor and acceptor fluorophores, R_0 is the Förster distance.

Many equivalent forms of this equation is found in the literature, such as:

$$E = R_0^6 / (R_0^6 + r^6) \text{ or } E = 1 / \left[1 + \left(r/R_0 \right)^6 \right]$$

The distance dependence of the energy transfer efficiency (*E*)

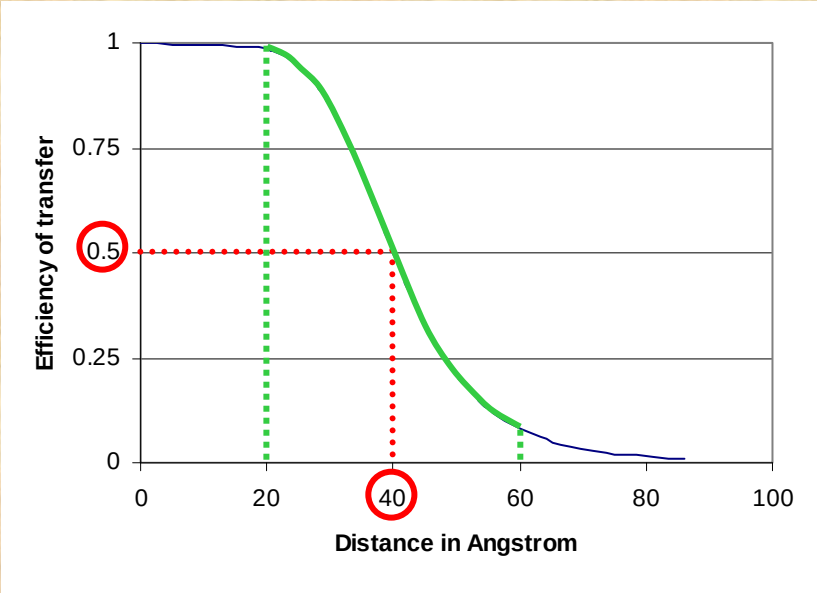

The efficiency of transfer varies with the inverse sixth power of the distance.

R_0 in this example was set to 40 Å. When the *E* is 50%, $R=R_0$

Distances can usually be measured between 0.5 R_0 and ~1.5R_0. Beyond these limits, we can often only say that the distance is smaller than 0.5 R_0 or greater than 1.5R_0. If accurate distance measurement is required then a probe pair with a different R_0 is necessary.

How was FRET theory tested experimentally?

Energy Transfer. A System with Relatively Fixed Donor–Acceptor Separation

JACS 87:995(1965)

S. A. Latt, H. T. Cheung, and E. R. Blout

Contribution from the Department of Biological Chemistry, Harvard Medical School, Boston, Massachusetts. *Received August 24, 1964*

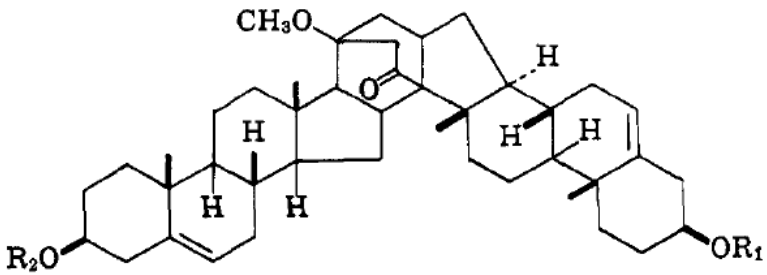

XIb, R_1 = *p*-methoxyphenylacetyl; R_2 = 1-naphthoyl
XIIb, R_1 = 1-naphthoyl; R_2 = anthracene-9-carbonyl

Table III

Compound	$\overline{K^2}$	R_{calcd}, Å.	R_{measd} (from Dreiding models), Å.
XI	$^2/_3$	21.3 ± 1.6	21.8 ± 2.0 (linear av.)
			19.2 ± 2.0 ($[\overline{1/R^6}]^{-6}$)
XII	$^2/_3$	16.7 ± 1.4	21.5 ± 2.0 (linear av.)
			19.4 ± 2.0 ($[\overline{1/R^6}]^{-6}$)

The most likely explanation for this discrepancy between the predicted and observed transfer in compound XII is that the value of the average orientation factor is greater than the estimate of $^2/_3$ which was used to calculate the predicted separation.

*DEPENDENCE OF THE KINETICS OF SINGLET-SINGLET ENERGY TRANSFER ON SPECTRAL OVERLAP**

BY RICHARD P. HAUGLAND,† JUAN YGUERABIDE,‡ AND LUBERT STRYER‡

DEPARTMENT OF CHEMISTRY, STANFORD UNIVERSITY, AND
DEPARTMENT OF BIOCHEMISTRY, STANFORD UNIVERSITY SCHOOL OF MEDICINE

Communicated by Harden M. McConnell, February 19, 1969

PNAS

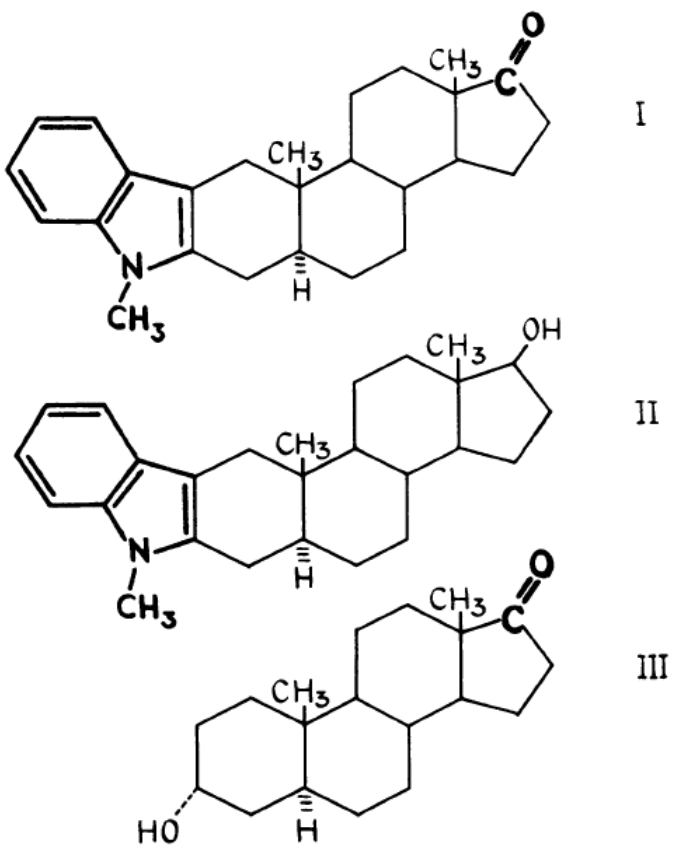

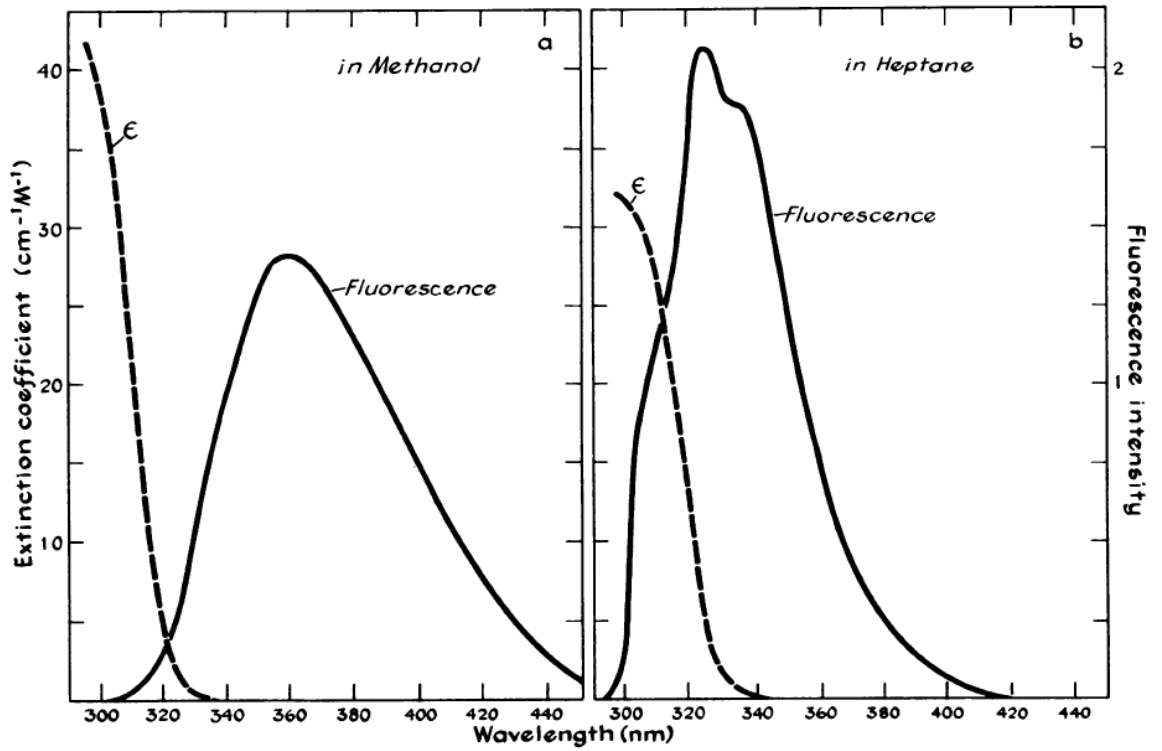

FIG. 2.—Overlap of the emission spectrum of the N-methylindole energy donor (II) and the absorption spectrum of the ketone energy acceptor (III) in (*a*) methanol and (*b*) heptane. III is nonfluorescent.

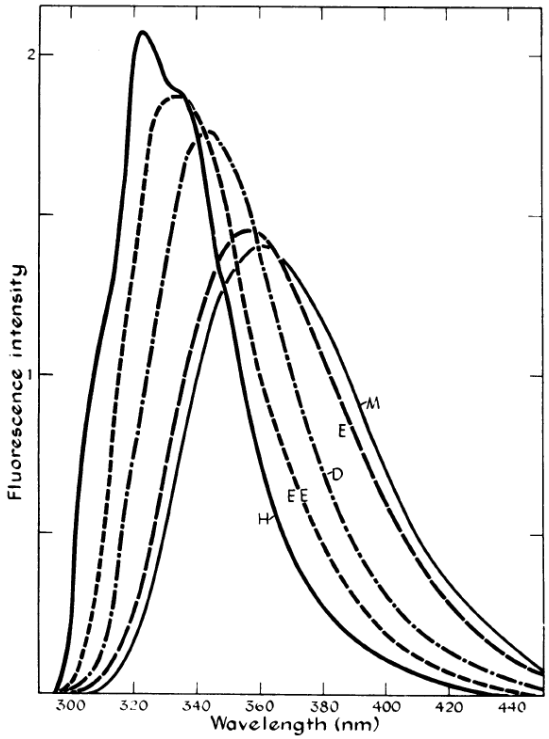

FIG. 3.—Fluorescence emission spectra of II in n-heptane (*H*), ethyl ether (*EE*), p-dioxane (*D*), ethanol (*E*), and methanol (*M*). The spectrum of II in ethyl acetate is virtually identical to that obtained in dioxane. The intensities have been normalized so that the areas under the curves are equal. The excitation wavelength was 290 nm.

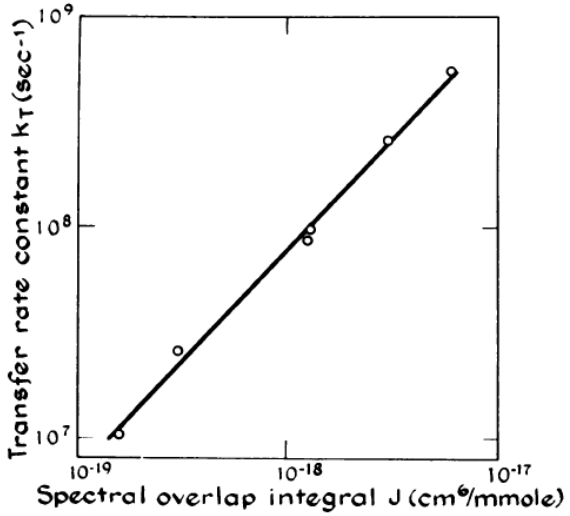

TABLE I. *Fluorescence properties of I and II in a series of solvents.*

Solvent	τ_I (nsec)	τ_{II} (nsec)	Fluorescence Quantum Yield Q_I	Q_{II}	Transfer Efficiency E_K	E_{SS}
Methanol	5.3	5.6	0.397	0.420	0.053	0.055
Ethanol	5.6	6.5	0.440	0.510	0.14	0.138
Dioxane	3.6	5.4	0.360	0.535	0.33	0.328
Ethyl acetate	3.3	4.7	0.286	0.418	0.30	0.315
Ethyl ether	2.1	4.5	0.247	0.515	0.53	0.52
Heptane	1.1	2.8	0.136	0.346	0.606	0.608

TABLE 2. *Transfer kinetics and spectral overlap integral of I in a series of solvents.*

Solvent	Transfer rate, k_T(sec^{-1}) $\times 10^{-7}$	Spectral overlap integral, J(cm^6 mmole^{-1}) $\times 10^{19}$	k_F (sec^{-1}) $\times 10^{-7}$	n_D	k_T/J $\times 10^{-26}$	$k_T/(Jk_F)$ $\times 10^{-18}$
Methanol	1.0	1.5	7.50	1.331	0.67	0.89
Ethanol	2.5	3.0	7.85	1.362	0.83	1.06
Dioxane	9.6	13.0	9.9	1.423	0.74	0.75
Ethyl acetate	11.3	12.8	8.9	1.372	0.88	0.99
Ethyl ether	25.5	30.0	11.5	1.349	0.83	0.72
Heptane	55.2	60.3	12.4	1.387	0.92	0.74

r^{-6} distance dependence?

$$k_T = (1/\tau_d)(R_0/r)^6$$

*ENERGY TRANSFER: A SPECTROSCOPIC RULER**

By Lubert Stryer and Richard P. Haugland†

DEPARTMENT OF BIOCHEMISTRY, STANFORD UNIVERSITY SCHOOL OF MEDICINE, PALO ALTO, AND THE DEPARTMENT OF CHEMISTRY, STANFORD UNIVERSITY

Communicated by Arthur Kornberg, May 29, 1967 PNAS

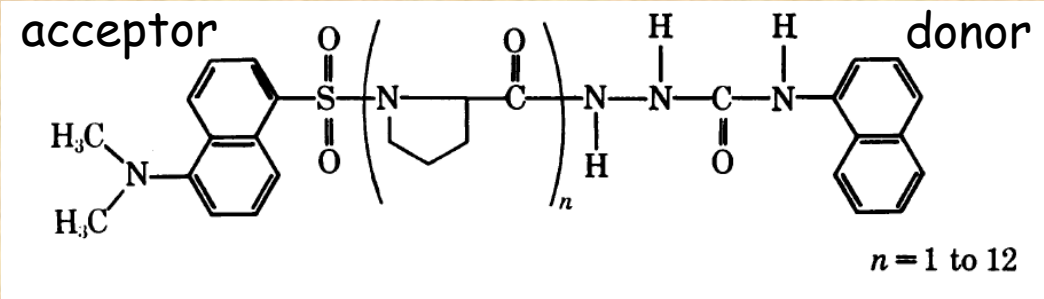

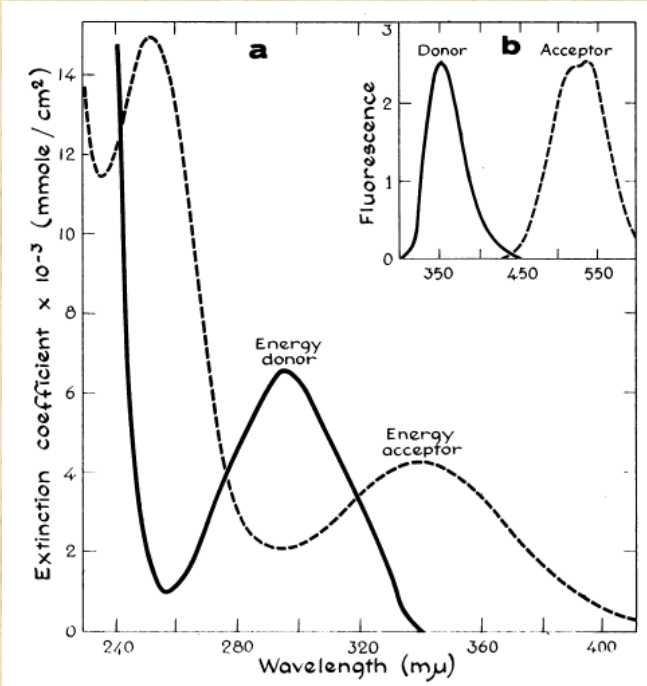

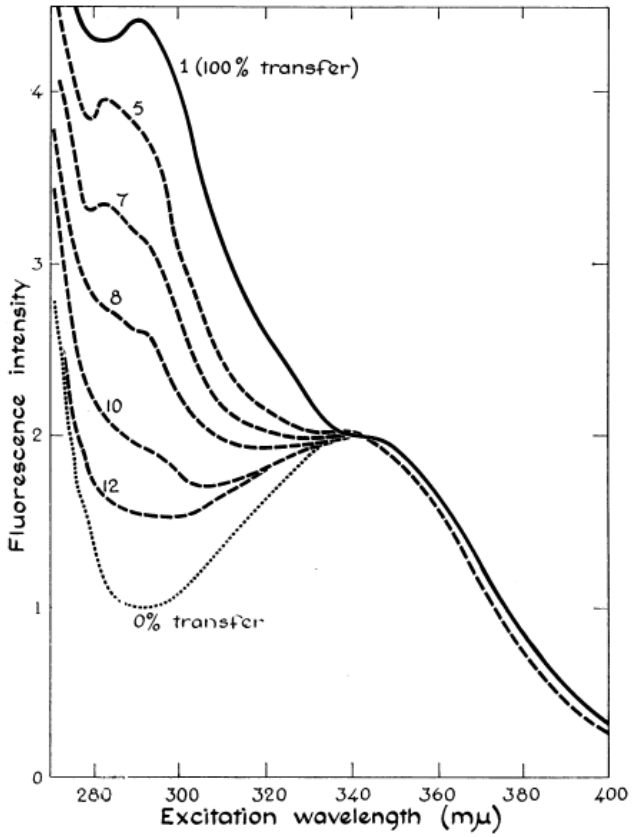

FIG. 3.—Excitation spectrum of dansyl-L-prolyl-hydrazide (·····, 0% transfer), dansyl-L-prolyl-α-naphthyl (———, 100% transfer), and dansyl-(L-prolyl)$_n$-α-naphthyl (- - - -, n = 5, 7, 8, 10, 12) in ethanol.

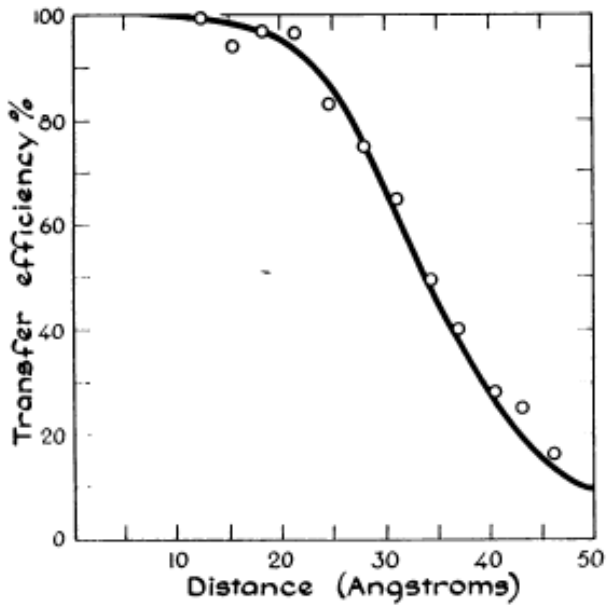

FIG. 4.—Efficiency of energy transfer as a function of distance in dansyl-(L-prolyl)$_n$-α-naphthyl, n = 1 to 12. The α-naphthyl and dansyl groups were separated by defined distances ranging from 12 to 46 Å. The energy transfer is 50% efficient at 34.6 Å. The solid line corresponds to an r^{-6} distance dependence.

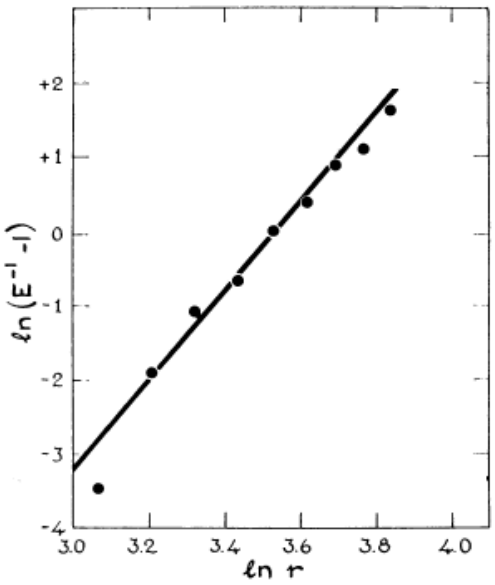

FIG. 5.—The dependence of the efficiency of energy transfer on distance is given by the slope in this plot of ln (E^{-1} − 1) versus ln r. The slope is 5.9, in excellent agreement with the r^{-6} dependence predicted by Förster.

For these parameters, R_0 is calculated to be 27.2 Å, *while the observed value is* 34.6 Å (Figs. 4 and 5). A rigorous comparison of the observed and calculated R_0 distances should be deferred until the value of K^2 is better defined. It would also be desirable to have independent confirmation of the estimated distances between the energy donor and acceptor groups.

More to the story???

Effect of flexibility and *cis* residues in single-molecule FRET studies of polyproline

Robert B. Best*†, Kusai A. Merchant*, Irina V. Gopich*, Benjamin Schuler*‡, Ad Bax*, and William A. Eaton*§

18964–18969 | PNAS | November 27, 2007 | vol. 104 | no. 48

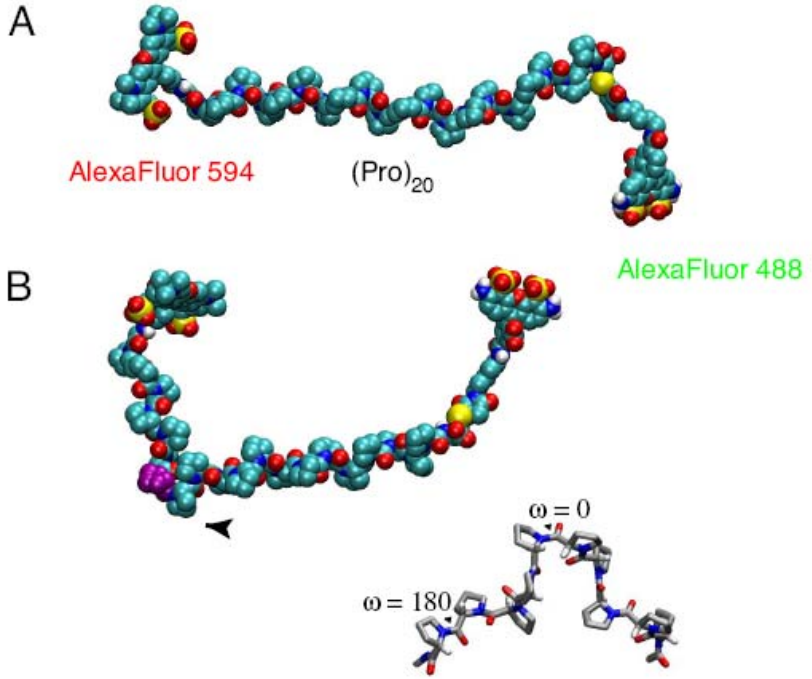

Fig. 1. Polyproline structures. Space-filling representation of polyproline-20 labeled with Alexa Fluor 488 (FRET donor) at the C-terminal cysteine and Alexa Fluor 594 (FRET acceptor) at the N-terminal glycine in the *all-trans* conformation (*A*) and with residue 8 (purple) in the *cis* conformation (*B*). (*B Inset*) A polyproline fragment with one *cis* peptide bond (shown as "$\omega = 0$"). One of the remaining *trans* peptide bonds is also indicated ("$\omega = 180$").

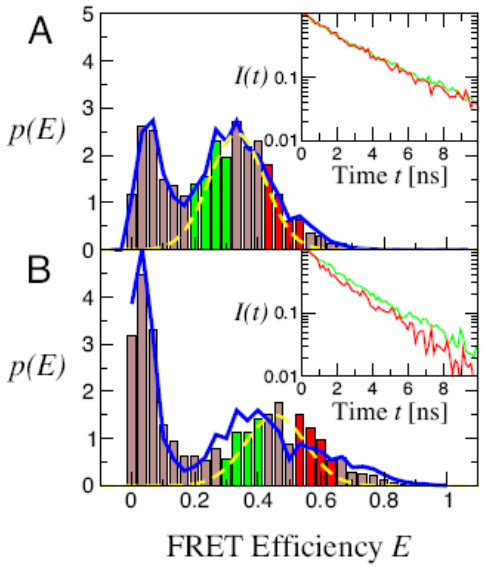

Fig. 3. Distributions of FRET efficiency for polyproline-20. The efficiency of each molecule $E = n_A/(n_A + n_D)$ was calculated from the (γ-corrected) n_A acceptor and n_D donor photons detected as it passes through the observation volume, in TFE (*A*) and water (*B*) (solid bars). Broken yellow lines indicate the shot-noise-limited width of the distribution (24, 19). Solid blue line in *A* gives a maximum likelihood fit of the data a multistate model. Solid blue line in *B* gives the expected efficiency distribution for a heterogeneous mixture of species containing *cis* proline, taking the relative populations from NMR and the efficiencies from simulation. (*Insets*) The donor fluorescence decays for donor photons from the subpopulations with corresponding colors in the efficiency histograms.

More to the story???

Polyproline has recently been used as a spacer between donor and acceptor chromophores to help establish the accuracy of distances determined from single-molecule Förster resonance energy transfer (FRET) measurements. This work showed that the FRET efficiency in water is higher than expected for a rigid spacer and was attributed to the flexibility of the polypeptide. Here, we investigate this issue further, using a combination of single-molecule fluorescence intensity and lifetime measurements, NMR, theory, and molecular dynamics simulations of polyproline-20 that include the dyes and their linkers to the polypeptide. NMR shows that in water ≈30% of the molecules contain internal *cis* prolines, whereas none are detectable in trifluoroethanol. Simulations suggest that the *all-trans* form of polyproline is relatively stiff, with persistence lengths of 9–13 nm using different established force fields, and that the kinks arising from internal *cis* prolines are primarily responsible for the higher mean FRET efficiency in water. We show that the observed efficiency histograms and distributions of donor fluorescence lifetimes are explained by the presence of multiple species with efficiencies consistent with the simulations and populations determined by NMR. In calculating FRET efficiencies from the simulation, we find that the fluctuations of the chromophores, attached to long flexible linkers, also play an important role. A similar simulation approach suggests that the flexibility of the chromophore linkers is largely responsible for the previously unexplained high value of R_0 required to fit the data in the classic study of Stryer and Haugland.

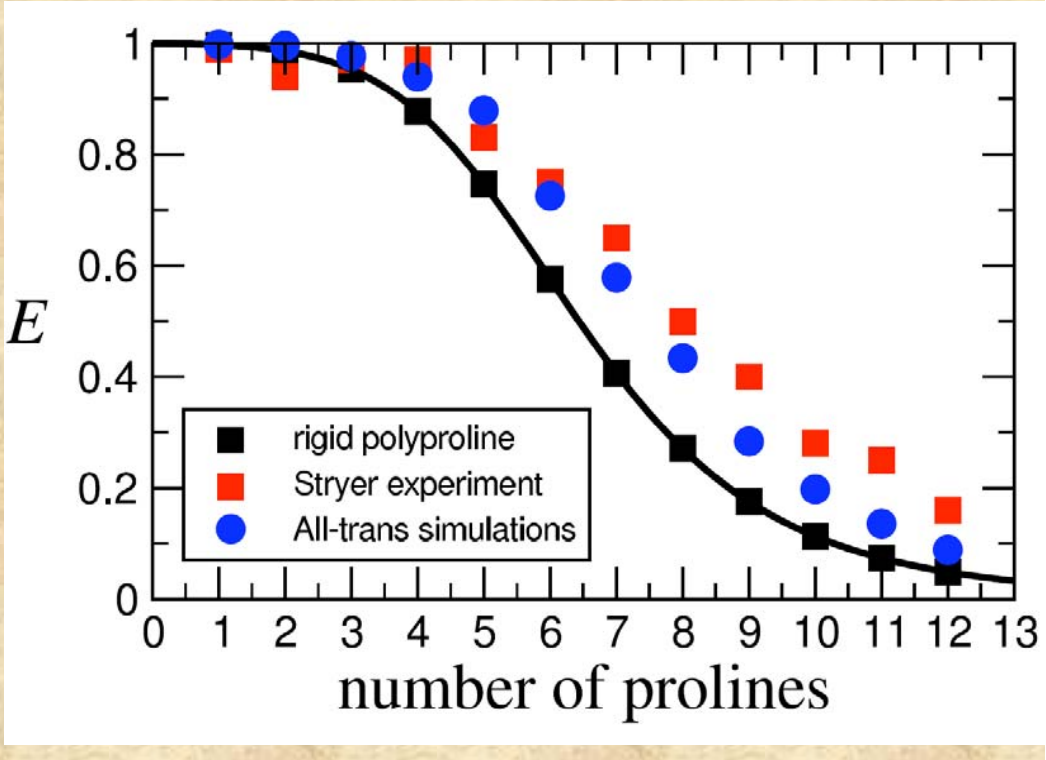

A related question that arose in the course of this work was whether donor/acceptor dynamics might explain the discrepancy mentioned earlier concerning the R_0 in the classic study of Stryer and Haugland (1). We found that simulations that included the dynamics of a naphthyl donor and dansyl acceptor resulted in increased FRET efficiency, explaining a large part of the difference between the calculated curves using the experimentally determined R_0 and the fitted R_0 (see SI Fig. 11).

Distributions

Proc. Nat. Acad. Sci. USA
Vol. 68, No. 9, pp. 2099–2101, September 1971

Determination of Distance Distribution Functions by Singlet-Singlet Energy Transfer

(flexibility/Förster theory/fluorescence/molecular structure)

CHARLES R. CANTOR AND PHILIP PECHUKAS

Proc. Nat. Acad. Sci. USA
Vol. 69, No. 8, pp. 2273–2277, August 1972

Evaluation of the Distribution of Distances Between Energy Donors and Acceptors by Fluorescence Decay

(energy transfer/fluorescence/decay/conformation/polymers)

A. GRINVALD, E. HAAS, AND I. Z. STEINBERG

$$E(R_0) = \int_0^\infty dR\, f(R)\, \frac{R_0^6}{R_0^6 + R^6}$$

Distributions

Proc. Nat. Acad. Sci. USA
Vol. 72, No. 5, pp. 1807–1811, May 1975

Distribution of End-to-End Distances of Oligopeptides in Solution as Estimated by Energy Transfer

(fluorescence decay/conformation)

ELISHA HAAS, MEIR WILCHEK, EPHRAIM KATCHALSKI-KATZIR, AND IZCHAK Z. STEINBERG

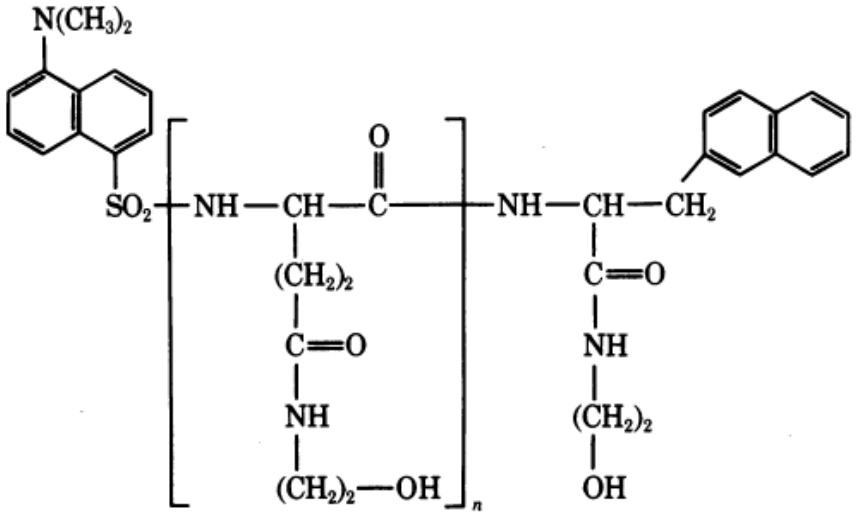

[I]

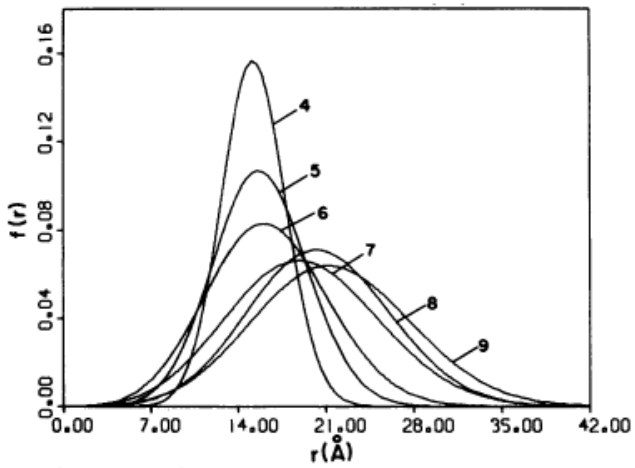

FIG. 4. The distribution function of the distances between donor and acceptor for the series of oligopeptides I, n = 4, 5, 6, 7, 8, and 9. The numbers in the figure refer to the values of n.

Distributions

Biochemistry **1988**, *27*, 9149–9160

Distance Distributions in Proteins Recovered by Using Frequency-Domain Fluorometry. Applications to Troponin I and Its Complex with Troponin C†

Joseph R. Lakowicz,*,‡ Ignacy Gryczynski,‡,§ Herbert C. Cheung,∥ Chien-Kao Wang,∥ Michael L. Johnson,⊥ and Nanda Joshi‡

Biochemistry **1991**, *30*, 5238–5247

Distance Distributions and Anisotropy Decays of Troponin C and Its Complex with Troponin I†

Herbert C. Cheung,*,‡ Chien-Kao Wang,‡,§ Ignacy Gryczynski,∥ Wieslaw Wiczk,∥ Gabor Laczko,∥ Michael L. Johnson,⊥ and Joseph R. Lakowicz∥

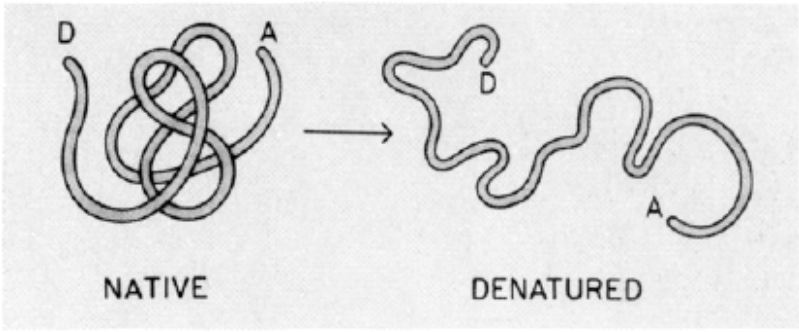

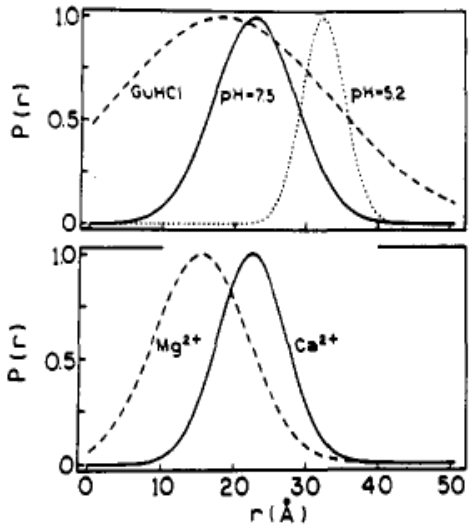

FIGURE 4: Distance distributions for TnC–DNZ–IAE in the absence of cations (top) and in the presence of Mg^{2+} and Ca^{2+} (pH 7.5, bottom). The pH for guanidine hydrochloride (GuHCl) was 7.5.

Proc. Natl. Acad. Sci. USA
Vol. 88, pp. 9355–9359, October 1991
Biochemistry

Differential flexibilities in three branches of an N-linked triantennary glycopeptide

(resonance energy transfer/oligosaccharides)

PENGGUANG WU, KEVIN G. RICE*, L. BRAND†, AND Y. C. LEE

Department of Biology, The Johns Hopkins University, Baltimore, MD 21218

ABSTRACT **The solution conformation behavior of complex oligosaccharides was studied by resonance energy transfer, as measured by the time-resolved fluorescence method, to determine the conformational heterogeneity of a triantennary glycopeptide at various temperatures. Groups that acted as a fluorescence donor (naphthyl-2-acetyl, Nap) or acceptor (dansylethylenediamine, Dan) were selectively attached to the N terminus of the peptide and a Gal residue [either 6′ (shown below), 6, or 8] of the oligosaccharide, respectively.**

(6′) Dan-Galβ4GlcNAcβ2Manα6↘
Manβ4GlcNAcβ4GlcNAcβ-Asn-Ala-NH-Nap
(6) Galβ4GlcNAcβ2Manα3↗
(8) Galβ4GlcNAcβ4↗

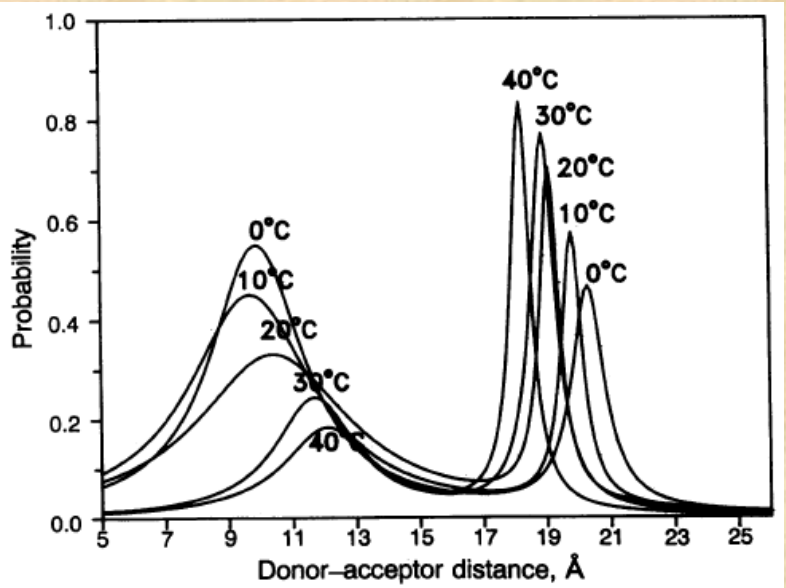

FIG. 6. Distance distribution of GP-6′-DanNap at various temperatures. Two distance populations were used to fit the data. The data were plotted to show the relative concentrations of each population by the peak at each temperature and for the same population (extended or folded) at different temperatures.

An impressive example of the use of FRET methodologies to study protein systems is given by the work of Lillo et al. ("Design and characterization of a multisite fluorescence energy-transfer system for protein folding studies: a steady-state and time-resolved study of yeast phosphoglycerate kinase" Biochemistry. 1997 Sep 16;36(37):11261-72 and "Real-time measurement of multiple intramolecular distances during protein folding reactions: a multisite stopped-flow fluorescence energy-transfer study of yeast phosphoglycerate kinase" Biochemistry. 1997 Sep 16;36(37):11273-81)

Site-directed mutagenesis was used to introduce pairs of cysteine residues in the protein at the positions shown

The pairs studied were:

135 – 290; 75 – 290

290 – 412; 412 – 202

135 – 412; 412 - 75

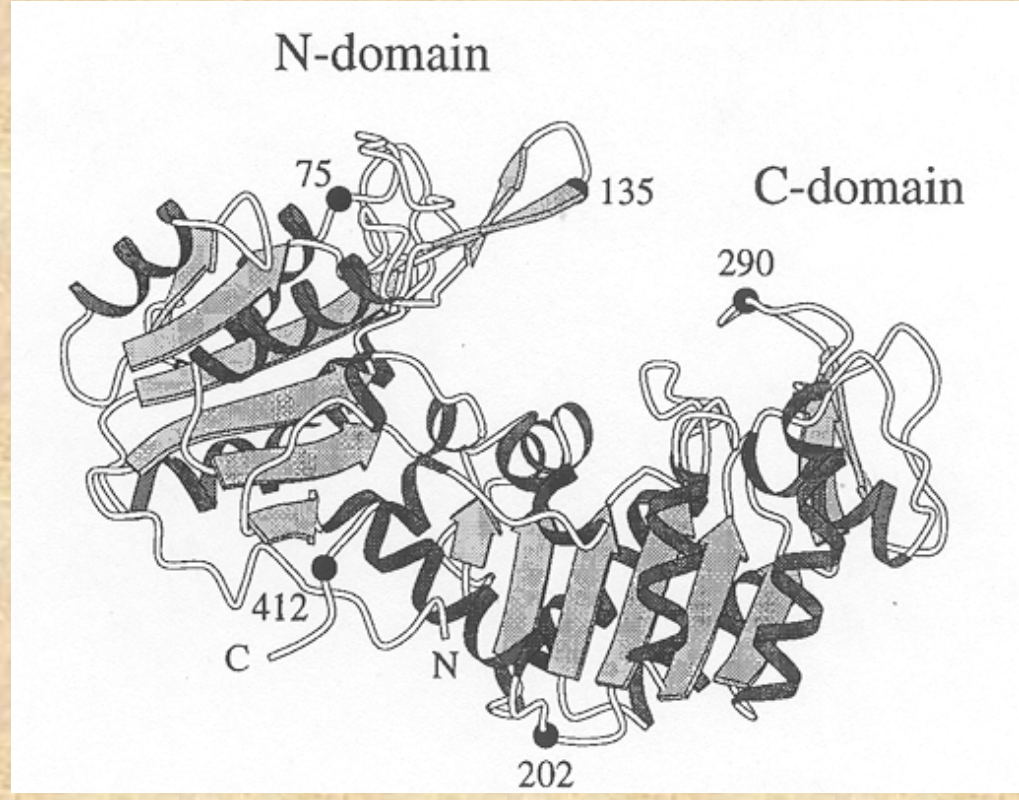

The donor was IAEDANS and the acceptor was IAF (iodoacetamindo-fluorescein). The various labeled protein products were separated by chromatography!

Table 1: Summary of the Labeled Proteins Examined for the Photophysical Characterization of Each Energy-Transfer Pair Cys*i* → Cys*j*

sample	name	Cys*i* → Cys*j*	no. of cysteines	fluorophore
donor only (D-PGK)	*i*-single cysteine	D- - -	1 (*i*)	AEDANS (*i*)
	j-single cysteine	- - -D	1 (*j*)	AEDANS (*j*)
	i-two cysteines	D- - -Cys	2 (*i*, *j*)	AEDANS (*i*)
	j-two cysteines	Cys- - -D	2 (*i*, *j*)	AEDANS (*j*)
	(*i*, *j*)-two cysteine average	D- - -Cys + Cys- - -D	2 (*i*, *j*)	AEDANS (*i*) + AEDANS (*j*)
	(*i*, *j*)-two cysteine "double donor"	D- - -D	2 (*i*, *j*)	AEDANS (*i*, *j*)
acceptor only	*i*-single cysteine	A- - -	1 (*i*)	AF (*i*)
	j-single cysteine	- - -A	1 (*j*)	AF (*j*)
donor-acceptor (D-PGK-A)	*i*, *j* specific label	D → A	2 (*i*, *j*)	AEDANS (*i*) and AF (*j*)
	j, *i* specific label	A ← D	2 (*i*, *j*)	AEDANS (*j*) and AF (*i*)
	i, *j* average label	D → A + A ← D	2 (*i*, *j*)	AEDANS (*i*) and AF (*j*) and + AEDANS (*j*) and AF (*i*)

Lifetime measurements were carried out on all samples

Table 5: Comparison of the Measured FRET Distances with That Predicted from the Crystal Structure[e]

energy-transfer pair	measured steady-state distance (Å)	measured time-resolved discrete distance		measured time-resolved distance distribution			crystal structure $C_\alpha \rightarrow C_\alpha$ (Å)[a]	estimated dye-to-dye distances (Å)[b]
		R (Å)	χ^2	R_c (Å) [±2]	σ (Å)	χ^2		
135 ↔ 290	43	43.3	2.7	39.4	7.3	1.3	39	39
		40.3[c]	1.6	38.8[c]	6.1	1.2		
135 ↔ 412	40	40.4	2.7	39.5	3.8	1.3	40	46
412 → 135	40	39.5	2.1	38.0	3.9	1.2		
		38.7	1.4	38.1[c]	3.4	1.3		
290 ↔ 412	69	63.6	1.4	64.8	13.5	1.3	48	56
		56.6[c]	1.8	58.6[c]	13.2	1.4		
75 ↔ 290	50	51.7	4.3	46.6	13.5	1.2	40	46
202 ↔ 412	39	41.7	1.5	37.8	6.6	1.1	26	34
412 → 75	47	48.2	3.1	44.8	13.5	1.4	32	46
all[d]	–	60–70	1.1	60–80	15–30	1.1	–	–

[a] Watson et al. (1982). [b] Donor-to-acceptor distance from MD simulations based on Watson et al. (1982) crystal structure. [c] Acceptor-side FRET measurements. [d] Unfolded samples (MOPS buffer at pH 7.5 and 25 °C and 2 M GuHCl). [e] MOPS buffer at pH 7.5 and 25 °C. D ↔ A: average labeled samples (donor distributed between the two Cys sites). D → A: specific labeled samples. Unless otherwise indicated, distance determinations are from donor-side experiments. The errors on the recovered distances are dominated by "nonfitting" sources and are estimated to be ±3 Å (see the text).

The intramolecular distances for the six energy transfer pairs are recovered for the each intermediate formed during the GuHCL induced unfolding of PGK

The authors proposed a specific structural transition associated with the unfolding of PGK from the native state (left) to the first unfolded state (right).

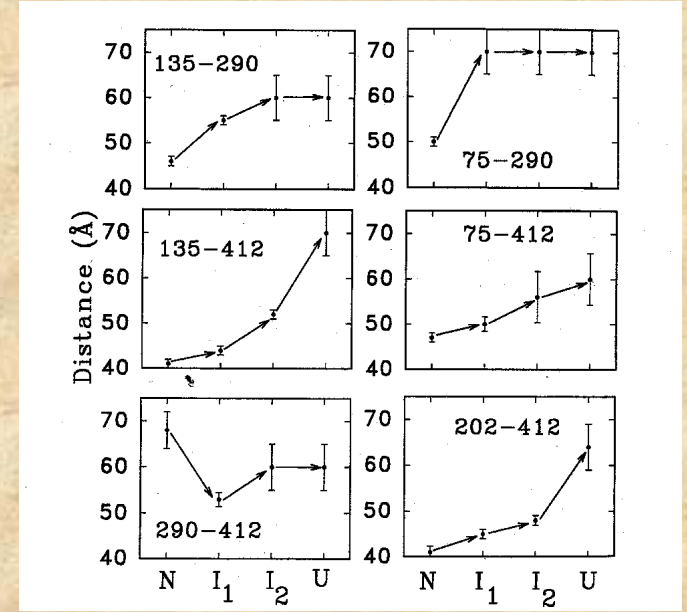

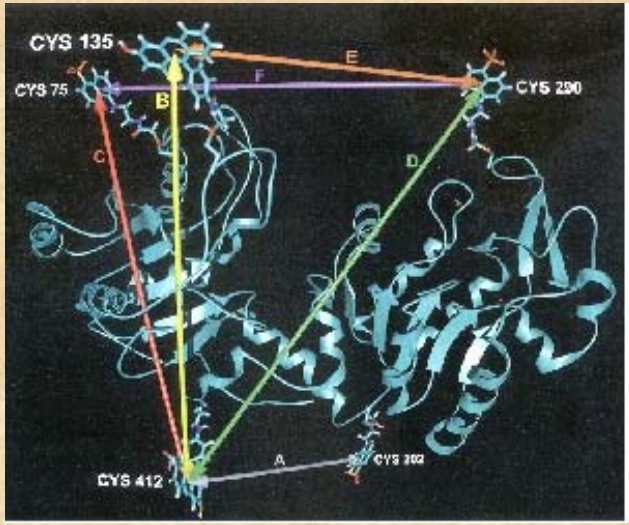

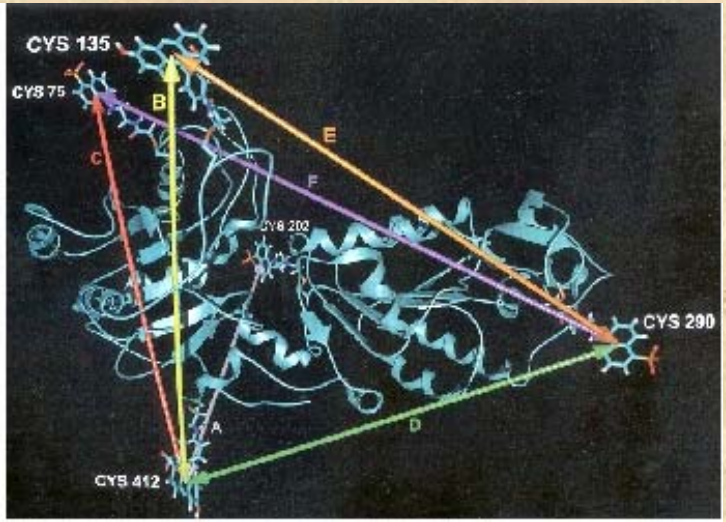

The C terminal domain (on the right of the monomer) is twisted by approximately 90º relative to the N-terminal domain resulting in an increase in the distances A,E and F and a shortening of the distance D.

The orientation factor κ^2

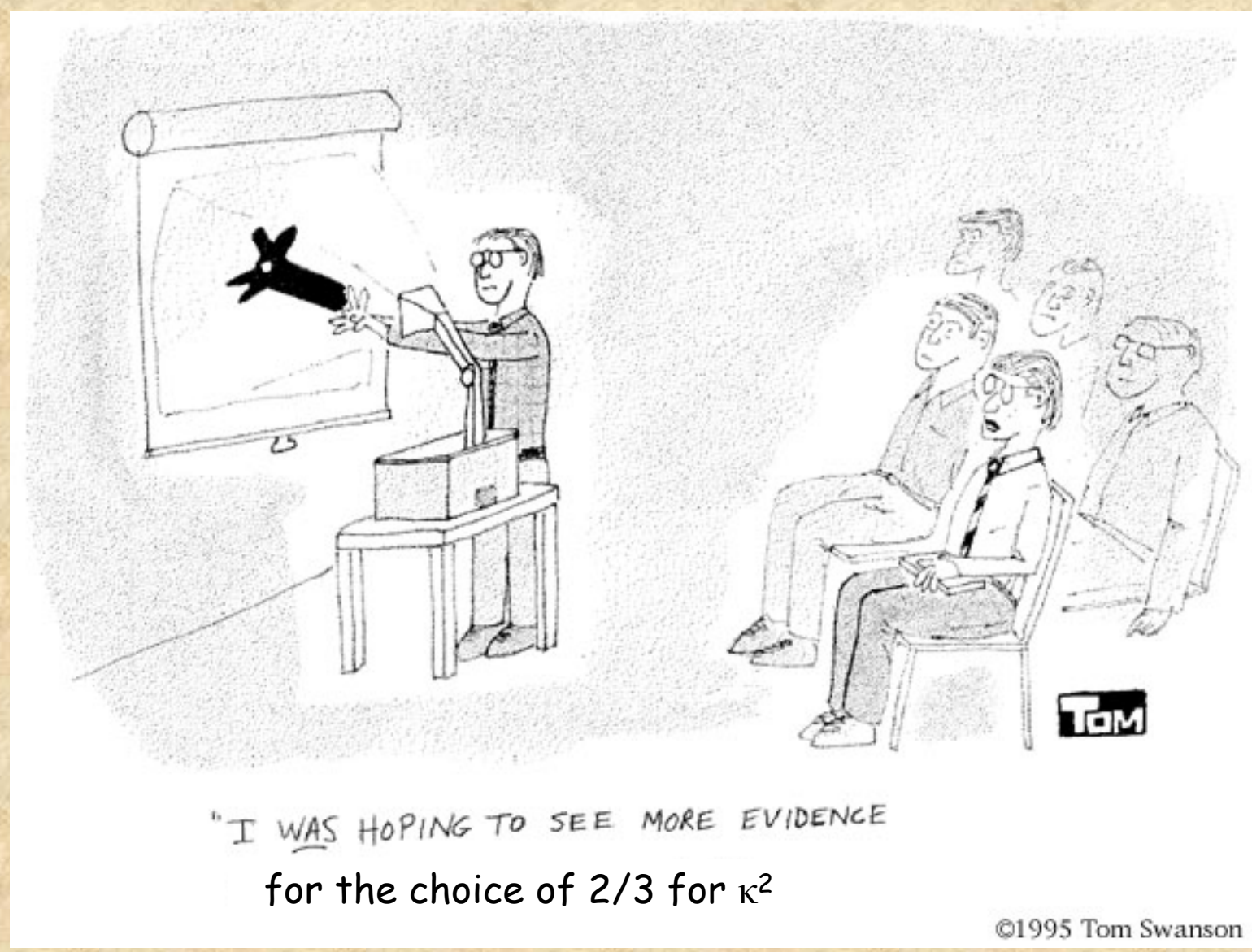

for the choice of 2/3 for κ^2

The orientation factor κ^2

$$\kappa^2 = (\cos\theta_T - 3\cos\theta_D \cos\theta_A)^2$$

Where θ_T is the angle between the D and A moments, given by

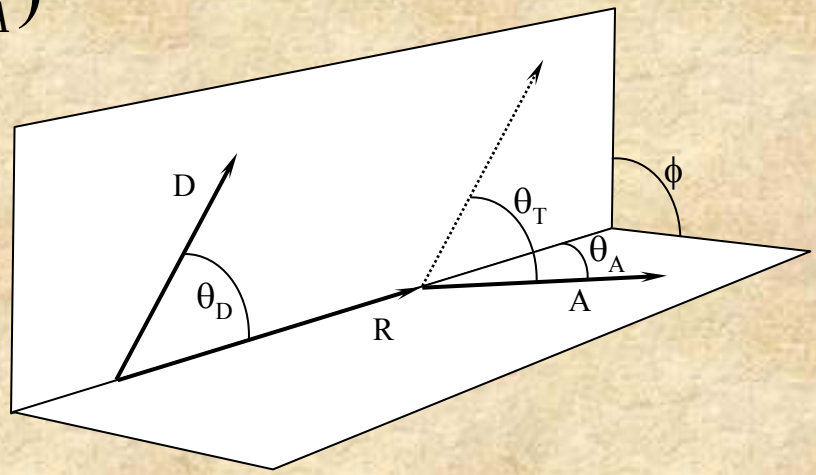

$$\cos\theta_T = \sin\theta_D \sin\theta_A \cos\phi + \cos\theta_D \cos\theta_A$$

In which θ_D, θ_A are the angles between the separation vector R, and the D and A moment, respectively, and ϕ is the azimuth between the planes (D,R) and (A,R)

The orientation factor κ^2

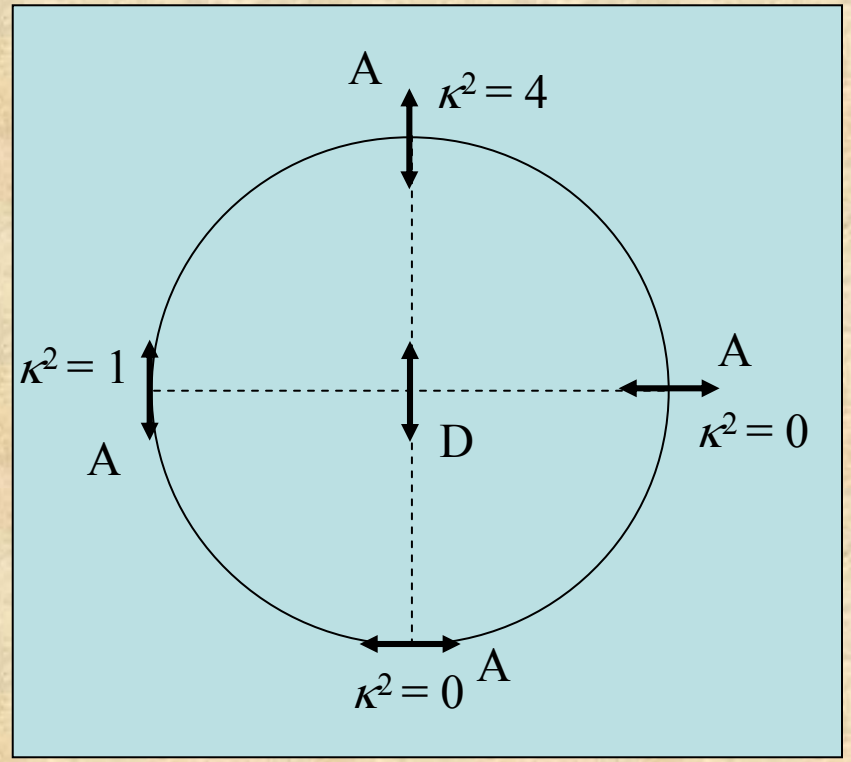

The limits for κ^2 are 0 to 4, The value of 4 is only obtained when both transitions moments are in line with the vector R. The value of 0 can be achieved in many different ways.

If the molecules undergo fast isotropic motions (dynamic averaging) then $\kappa^2 = 2/3$

From Eisinger and Dale in:"Excited States of Biological Molecules" Edited by John Birks (1976)

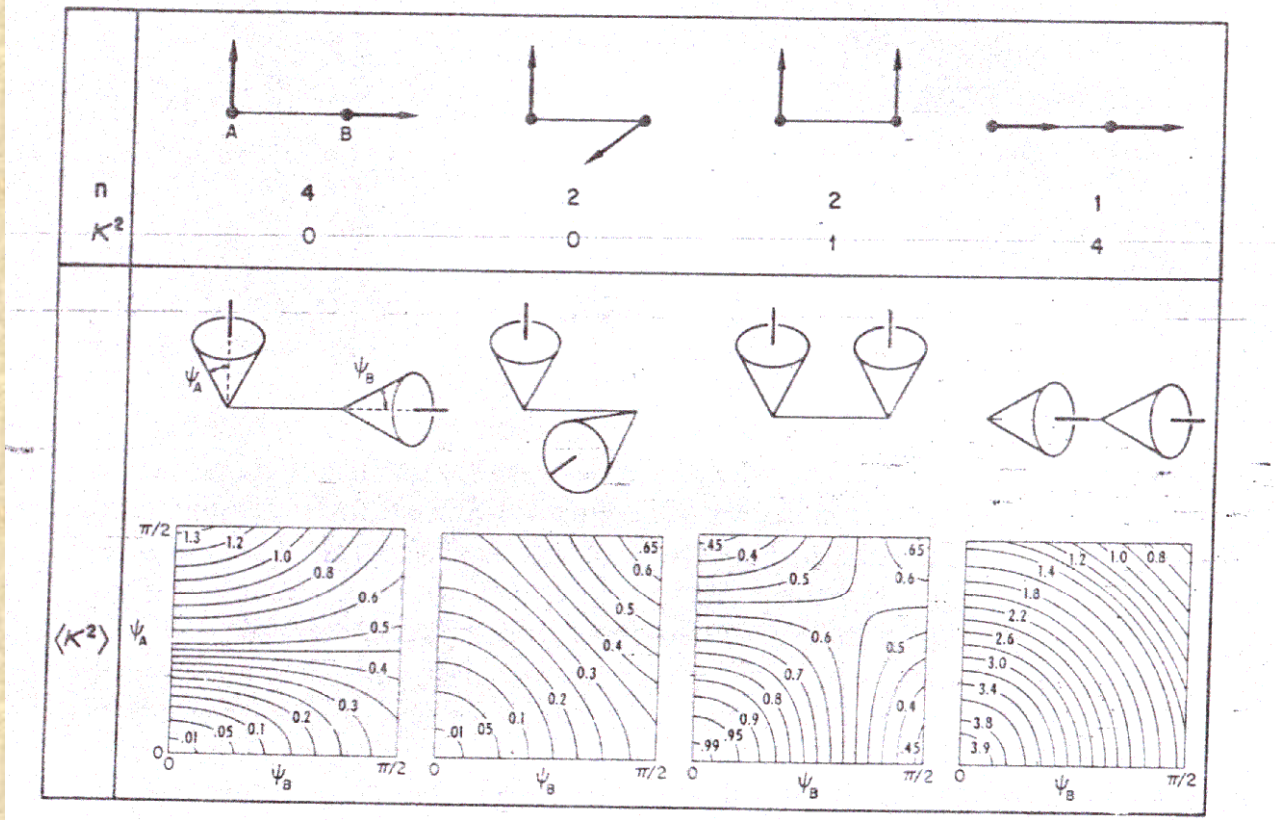

Figure 1 The upper part of the diagram illustrates the nine possible relative orientations of two transition dipoles each of which is fixed and can lie along either the x, y or z axis of a Cartesian triad. The corresponding κ^2 values are shown along with their statistical weights (n) and they are seen to lead to an average for κ^2 of 2/3, the same as for isotropically random orientations of the transition dipole moments. The lower part of the figure illustrates how these $\langle\kappa^2\rangle$ values change as the transition dipole directions are permitted orientational freedom within cones of half-angles ψ_A and ψ_B. Note that $\langle\kappa^2\rangle$ departs quite slowly from its fixed minimum and maximum values (0 and 4) as the two cones open up and that when each cone half-angle is $\pi/2$, corresponding to an isotropic distribution of the transition dipole directions, $\langle\kappa^2\rangle$ is equal to 2/3 for each of the cases considered

What if the system is static but randomly oriented?

For example for a system in a highly viscous solvent or in general if the fluorescence lifetimes are very short relative to any rotational motion.

Then $\kappa^2 = 0.476$

THE JOURNAL OF CHEMICAL PHYSICS VOLUME 48, NUMBER 6 15 MARCH 1968

Nonradiative Energy Transfer in Systems in which Rotatory Brownian Motion is Frozen

IZCHAK Z. STEINBERG

The Weizmann Institute of Science, Rehovoth, Israel

(Received 28 August 1967)

The effect of the complete restriction of rotatory Brownian motion of donor and acceptor molecules on the extent of nonradiative energy transfer in systems containing many donors and acceptors has been investigated. It is assumed that the molecules under discussion are randomly distributed and randomly oriented in space at the moment of excitation. The number of donor molecules which retain their excitation energy at time t after excitation is found to decrease exponentially with the sum of two terms: one proportional to t and the other proportional to $t^{1/2}$. This time dependence is similar in form to that found by Förster for systems in which donor and acceptor molecules undergo rapid rotatory diffusion. While the coefficient of $-t$ in the exponent is the same in both cases, the coefficient of $-t^{1/2}$ is smaller for systems in which molecular rotation is frozen than for systems in which rotatory Brownian motion is rapid.

But don't ask me to prove it!

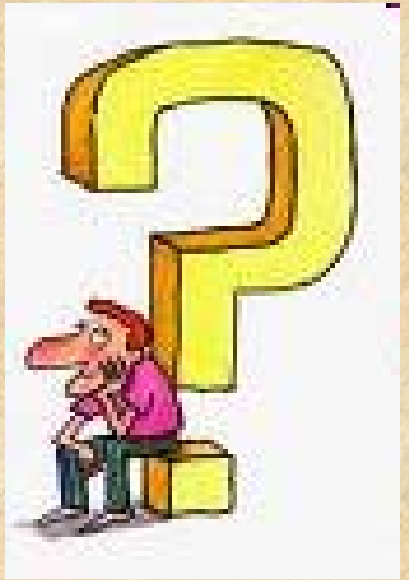

So how do we determine κ^2?

Except in very rare cases, κ^2 can not be uniquely determined in solution.

What value of κ^2 should be used ?

We can **assume** fast isotropic motions of the probes and value of $\kappa^2 = 2/3$, and verify experimentally that it is indeed the case.

We can **calculate** the lower and upper limit of κ^2 using polarization spectroscopy (Dale, Eisinger and Blumberg 1979).

Assuming $\kappa^2 = 2/3$

We can test this assumption experimentally:

***By swapping probes*:** The micro-environment of the probes will be different. Therefore, if the micro-environment affect the probes mobility and, κ^2 is not equal to 2/3, once swapped, the value of κ^2 will changed and hence the distance measured by FRET.

By using different probes: If the distance measured using different probe pairs are similar (taking into account the size of the probes) then the assumption that κ^2 is equal to 2/3 is probably valid.

Lower and upper limit of κ^2

We can **<u>calculate</u>** the lower and upper limit of κ^2 using polarization (Dale, Eisinger and Blumberg 1979).

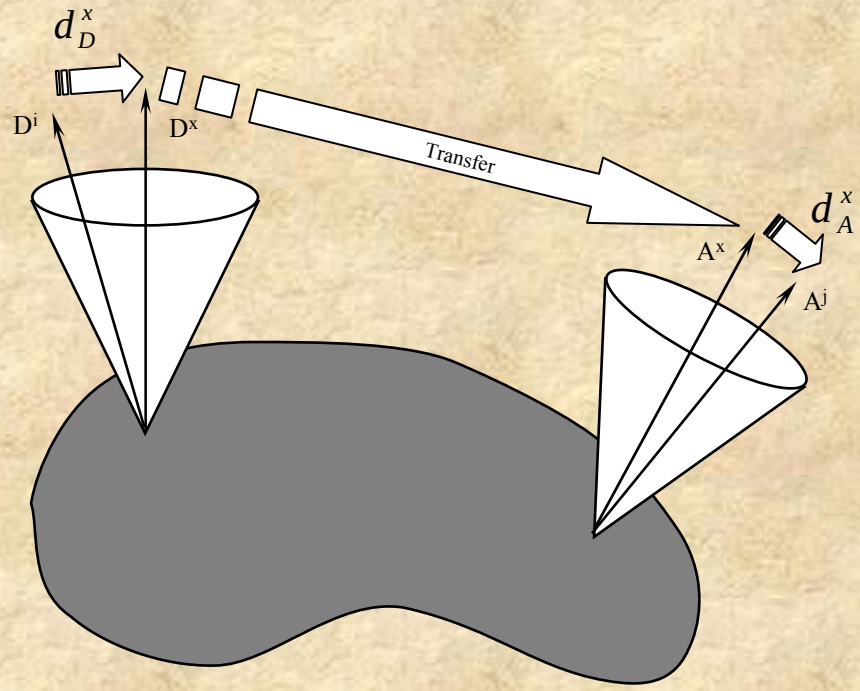

Lets consider that the each probe are rotating within a cone of axes D^x and A^x for the donor and acceptor, respectively, then 3 depolarization steps occurs after the absorption of the excitation energy by the donor: An axial depolarization of the donor, a depolarization due to transfer and an axial depolarization of the acceptor

In the Dale-Eisinger-Blumberg approach, one measures the ratio of the observed polarizations of donors and acceptors to their limiting polarizations and then uses the calculated contour plots to put limits on κ^2

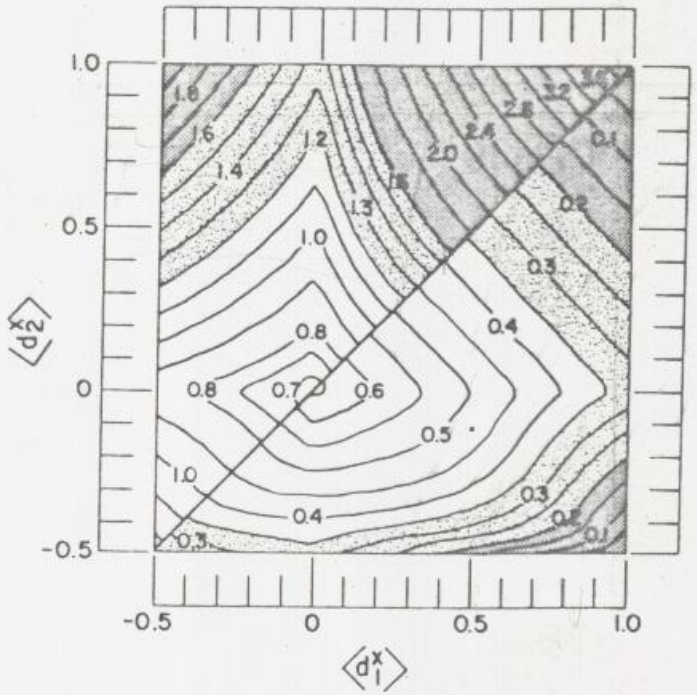

FIGURE 9 Contour plot similar to those shown in Figs. 4–8, but applicable in situations in which $\langle d_T \rangle$, and hence d_T^x, is unknown. It is obtained by maximizing and minimizing Eq. 21 and can be seen to lead to larger ranges between $\langle \kappa^2 \rangle_{min}$ and $\langle \kappa^2 \rangle_{max}$ than the plots of Figs. 4–8. In the heavily stippled regions the error in R resulting from the use of $\langle \kappa^2 \rangle = \frac{2}{3}$ instead of the indicated $\langle \kappa^2 \rangle_{min}$ and $\langle \kappa^2 \rangle_{max}$ is greater than 20%. It is between 10% and 20% in the lightly stippled regions and less than 10% in the unstippled ones.

This approach was used in:
Arbildua et al.,
Fluorescence resonance energy transfer and molecular modeling studies on 4',6-diamidino-2-phenylindole (DAPI) complexes with tubulin.
Protein Sci. (2006) 15(3):410-9.

FRET occurs between DAPI and TNP-GTP bound to tubulin – a heterodimer protein

DAPI

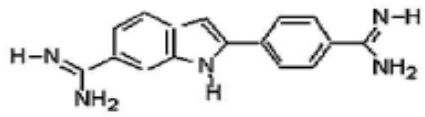

TNP-GTP

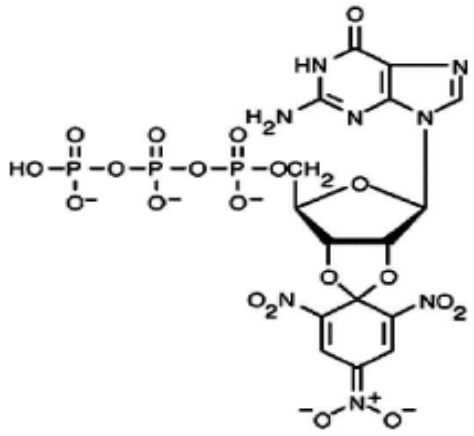

Figure 1. Structures of 4′-6-diamidino-2-phenylindole (DAPI) and 2′,3′-*O*-(2,4,6-trinitrocyclohexadienylidene)-GTP (TNP-GTP) at neutral or basic pH.

Assuming a κ^2 value of 2/3, one would calculate the DAPI-TNP-GTP distance to be ~43 Angstoms

But DAPI is bound non-covalently - hence has no local motion so its polarization is high (~0.42)

And, TNP-GTP is also non-covalently bound and has a short lifetime and hence a high polarization (~0.48)

These observed polarization values are close to the limiting polarization values for these probes: 93% and 100% respectively, for DAPI and TNP-GTP

Using the Dale-Eisenger-Blumberg plot one can then estimate that κ^2 can be anywhere between 0.02 and 3.7!

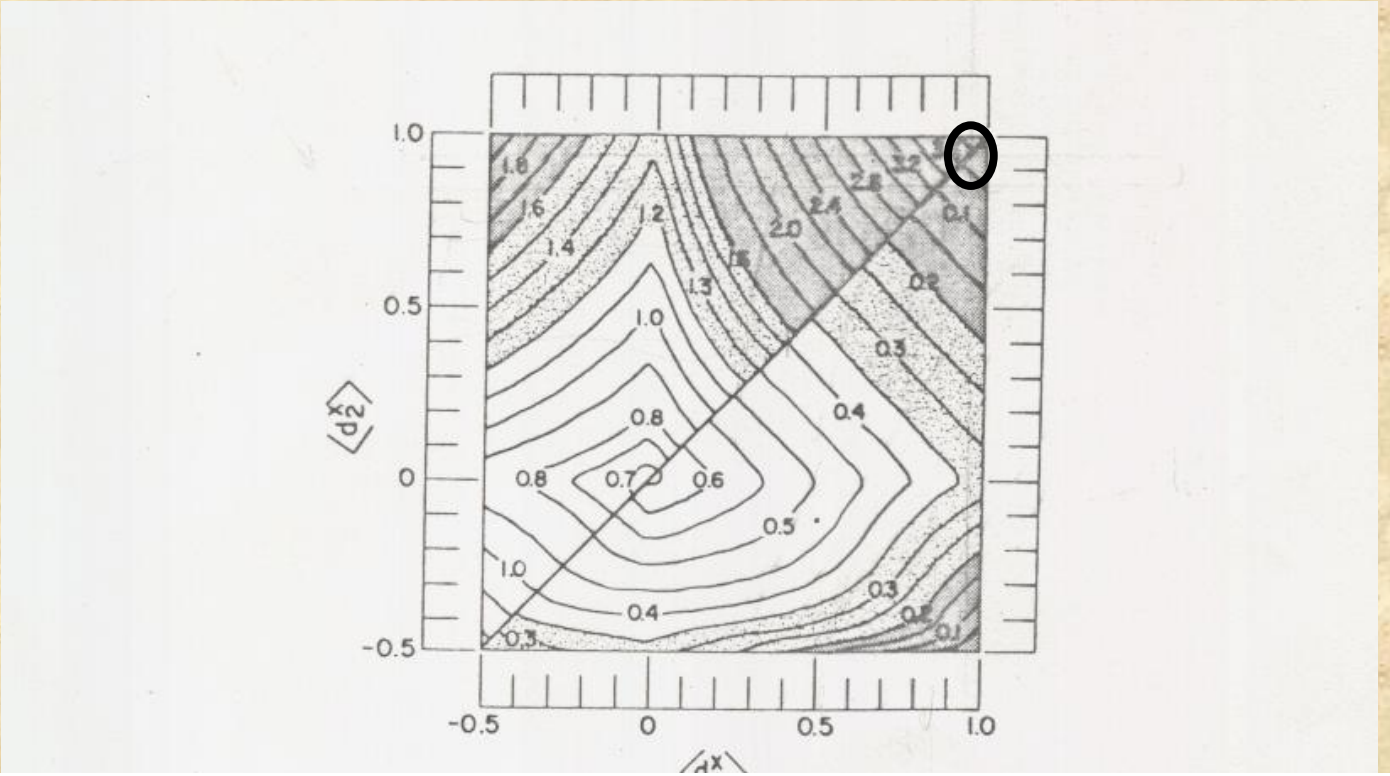

In fact the authors concluded, based on other information, that the distance between DAPI and TNP-GTP bound to tubulin was likely to ~ 30 Angstroms.

BIOPOLYMERS VOL. 13, 1607–1620 (1974)

Energy Transfer in tRNA^{Phe} (Yeast). The Solution Structure of Transfer RNA

W. E. BLUMBERG, R. E. DALE,* J. EISINGER, and
D. M. ZUCKERMAN, *Bell Laboratories, Inc.,*
Murray Hill, New Jersey 07974

TABLE II
Maximum and Minimum Values of the Orientation Factor and Ratio of Derived Separation R to that Obtained Using the Dynamic Random Average (Isotropic) Value $R_{2/3}$

Model[a]		Figure[a]	Y–A	$\langle\kappa^2\rangle$	$R/R_{2/3}$
4(1)	*cc*	10	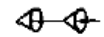	3.13 ± 0.08	1.29 ± 0.01
	cC	11	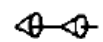	3.13 ± 0.08	1.29 ± 0.01
	Cc	11	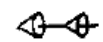	3.13 ± 0.08	1.29 ± 0.01
	CC	12	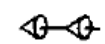	3.13 ± 0.08	1.29 ± 0.01
4(2)	*cc*	13	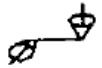	0.115 ± 0.012	0.75 ± 0.01
	cC	14	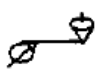	0.115 ± 0.012	0.75 ± 0.01
	Cc	14	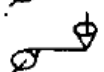	0.115 ± 0.012	0.75 ± 0.01
	CC	15	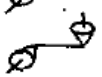	0.115 ± 0.012	0.75 ± 0.01

CCA Terminus—Anticodon Separation

Assuming an average value of 2/3 for κ^2, Beardsley and Cantor[2] estimated the separation between the *Y* base adjacent to the anticodon and acriflavine bound at the CCA terminus of $tRNA^{Phe}$ (yeast) to be about 46 Å. The analysis presented here indicates a possible range of 34–61 Å at the most.

Taking into account the uncertainty in the location of the acriflavine chromophore with respect to the CCA stem (as indicated above it may well be intercalated back into a nearby double-helical region, not necessarily in the CCA limb), the upper limit is reasonably consistent with the 77 Å separation between the extended CCA terminus and the anticodon triplet recently determined by X-ray crystallography.[2]

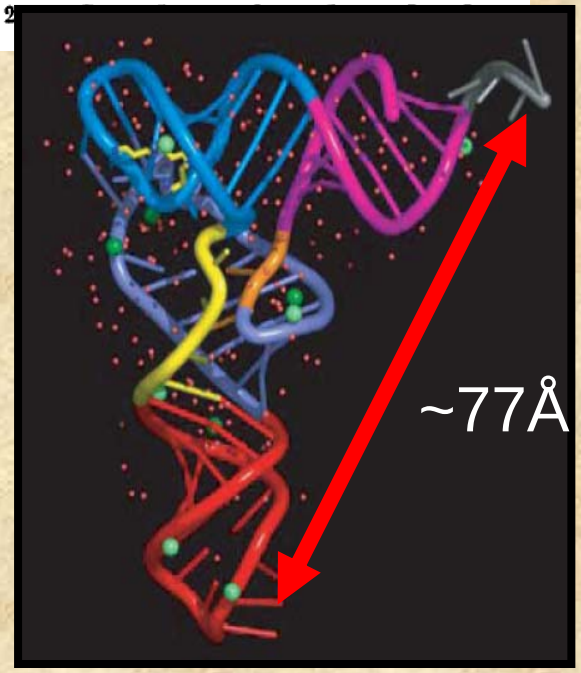

Quantitative distance determinations using FRET – i.e., as a true “spectroscopic ruler” - remain **difficult at best**

But FRET can be very powerful when used to detect changes in a system, such as alterations in distance and or orientation between donor and acceptor attached to biomolecules, i.e., due to ligand binding or protein-protein interactions

The renaissance of fluorescence resonance energy transfer

Paul R. Selvin

Recent advances in fluorescence resonance energy transfer have led to qualitative and quantitative improvements in the technique, including increased spatial resolution, distance range, and sensitivity. These advances, due largely to new fluorescent dyes, but also to new optical methods and instrumentation, have opened up new biological applications.

nature structural biology • volume 7 number 9 • september 2000

The development of Fluorescent Proteins has led to a significant increase in FRET studies

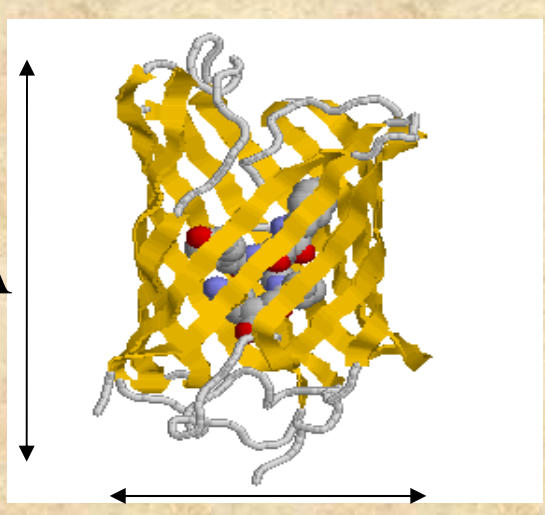

The GFP is fused to the protein of interest and expressed in the organism under study.

Fluorescent proteins with the appropriate absorption and emission properties are chosen as donors and acceptors. Such systems can be used in vitro as well as in vivo

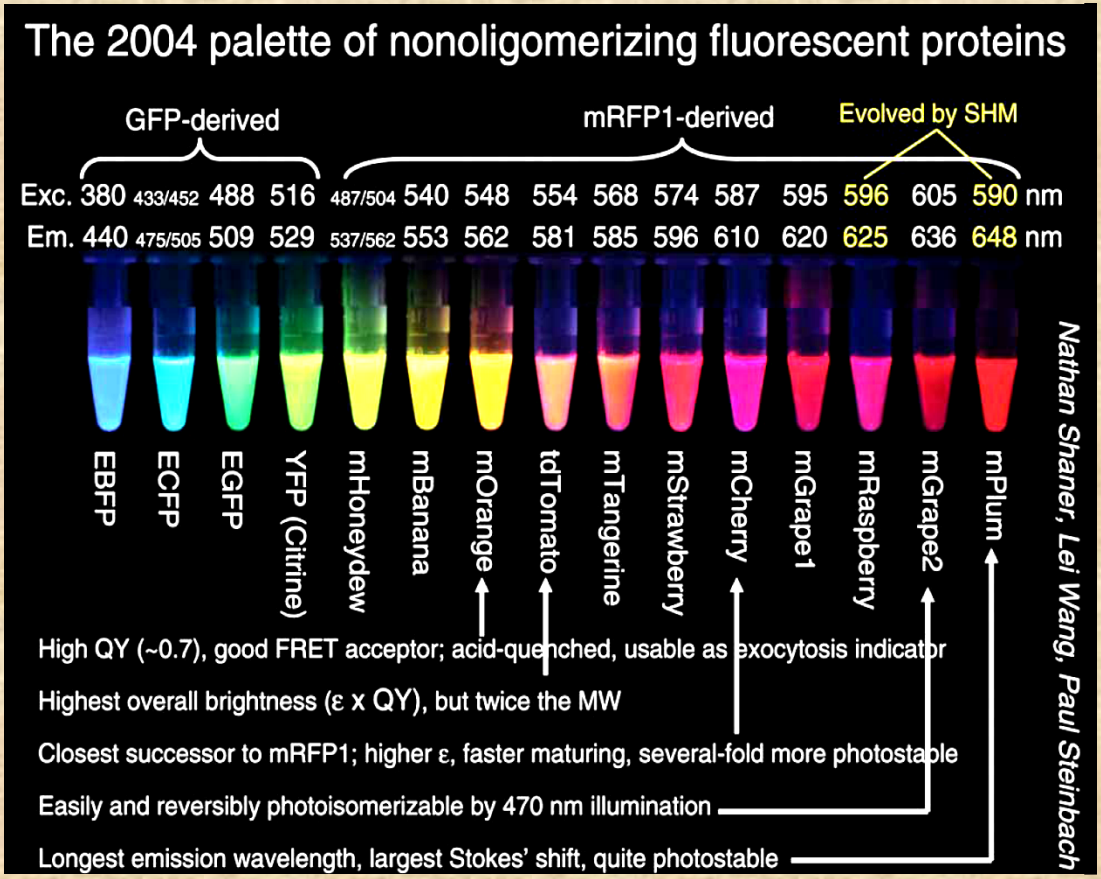

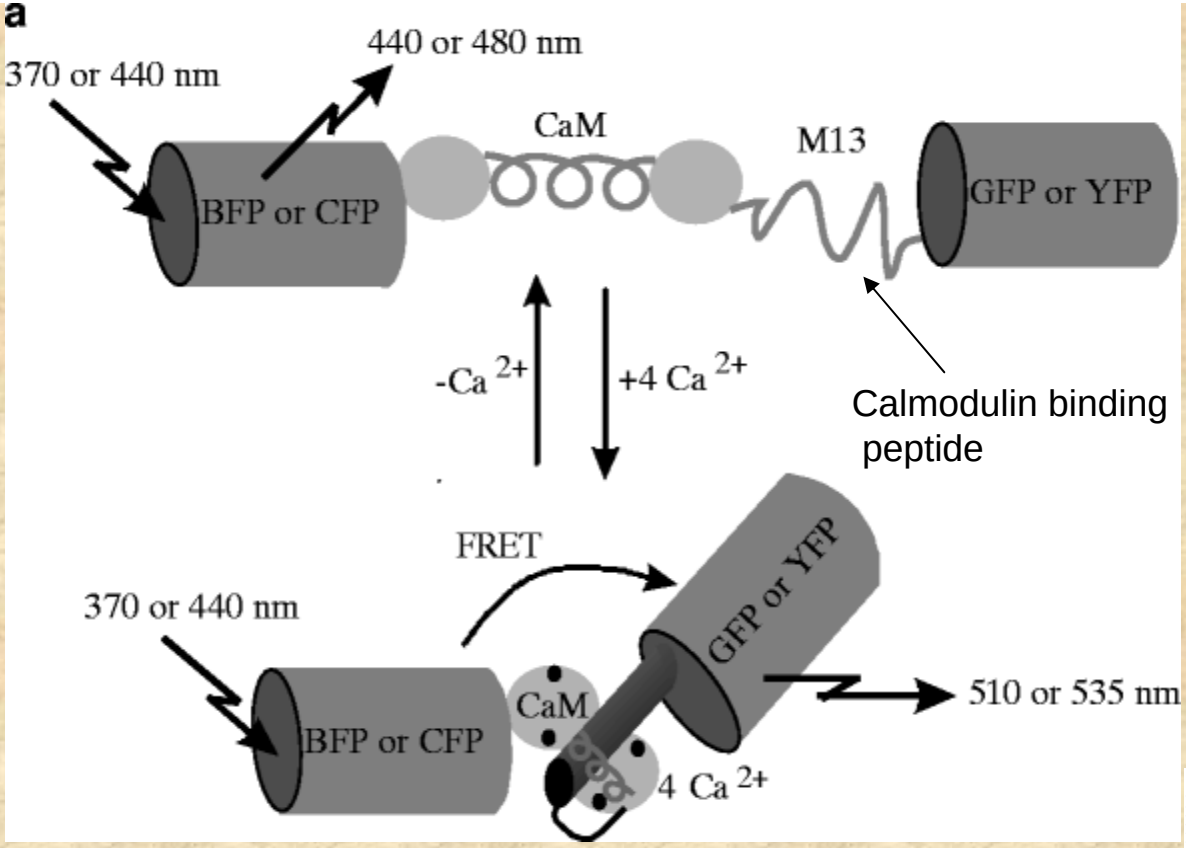

"Cameleon Proteins"

Fluorescent indicators for Ca2+based on green fluorescent proteins and calmodulin:

A. MIYAWAKI, J. LLOPIS, R. HEIM, J. M. MCCAFFERY, J. A. ADAMS, M. IKURA & R. TSIEN: *Nature (1997)* **388**, 882 - 887

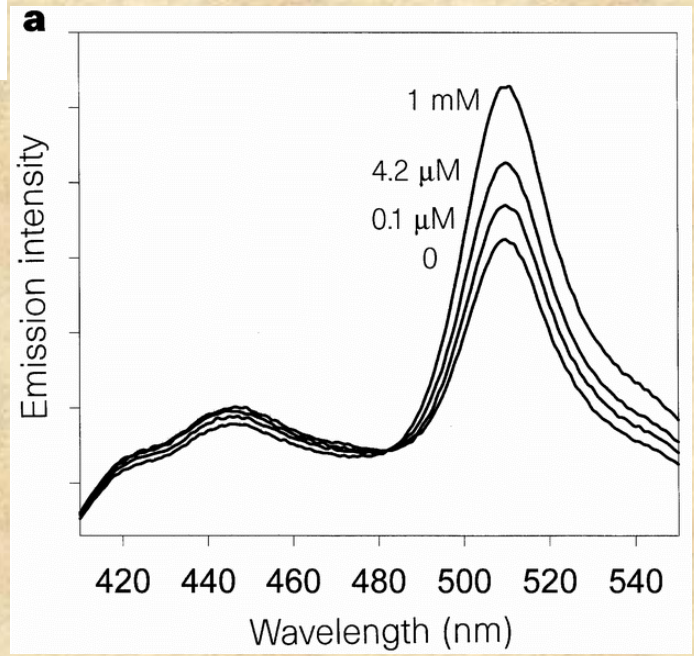

Seeing the Machinery of Live Cells

Roger Y. Tsien and Atsushi Miyawak

Science 19 June 1998:
Vol. 280. no. 5371, pp. 1954 - 1955

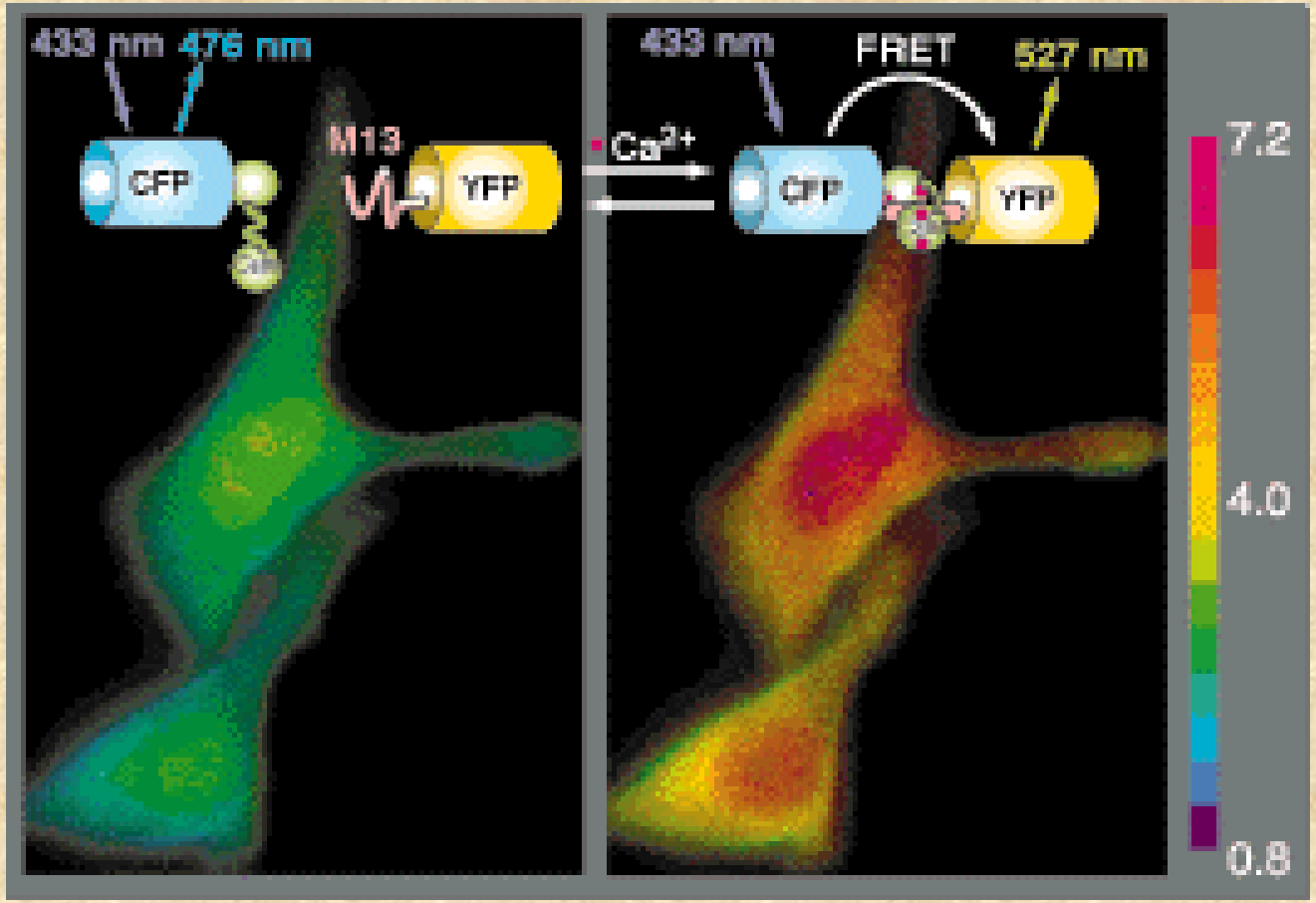

Fig. 1. Imaging by FRET of induced protein-protein interaction in individual live cells. Cyan-GFP-labeled calmodulin (CFP-CaM) and yellow-GFP-labeled calmodulin-binding peptide (M13-YFP) were coexpressed in HeLa cells (14). Pseudocolor hues from blue to magenta indicate increasing ratios of yellow to cyan emissions, resulting either from increased FRET (see overlaid schematic) or excess of YFP over CFP. The left panel shows two cells before stimulation, while the right panel shows the same cells after elevation of cytosolic Ca2+ by 0.1 mM histamine.

FRET in protease assays

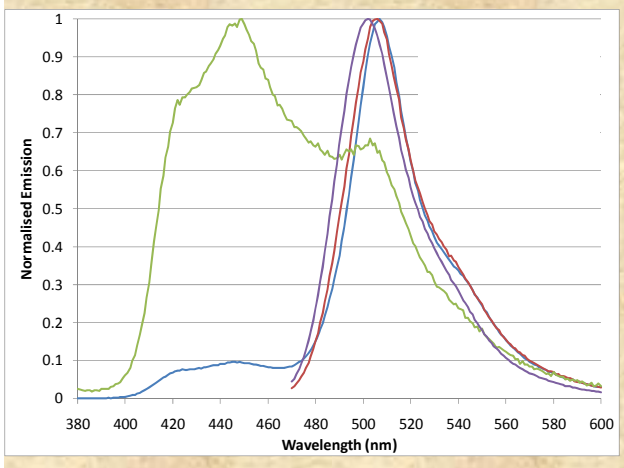

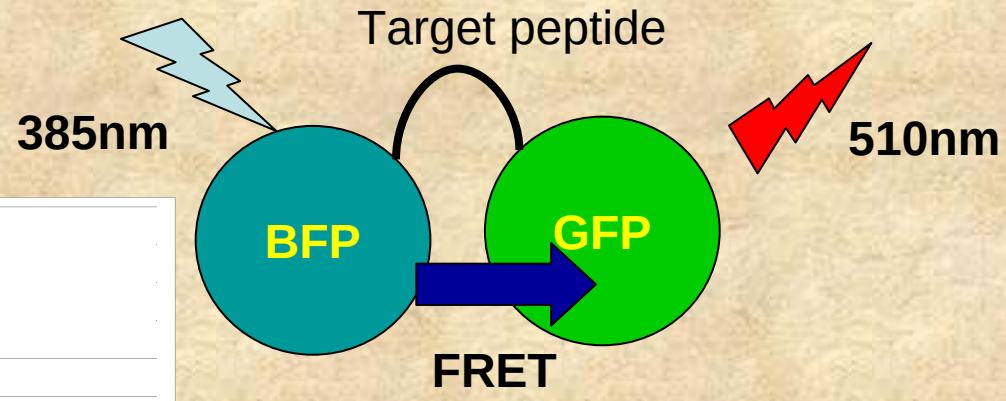

Specific protease

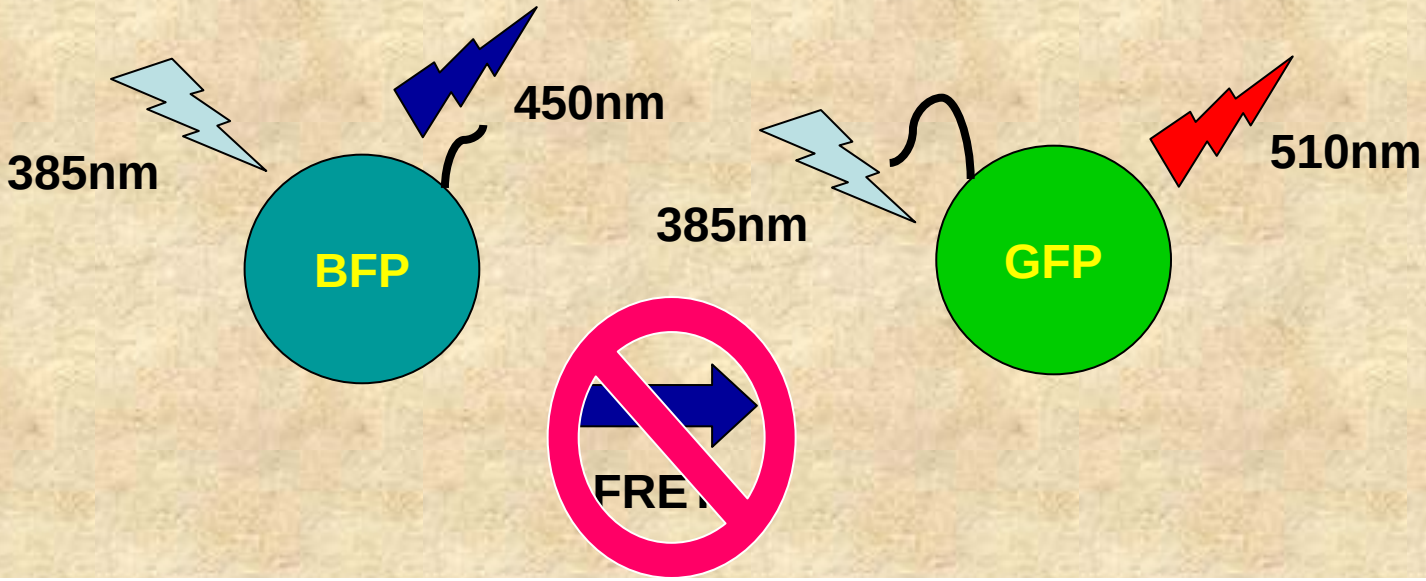

First application of FRET using of Fluorescent Proteins

Gene, 173 (1996) 13–17

GENE 09471

Fluorescence resonance energy transfer between blue-emitting and red-shifted excitation derivatives of the green fluorescent protein *

(FRET; *Aequorea victoria*; fluorescent proteins; factor X_a)

Robi D. Mitra[a], Christopher M. Silva[b] and Douglas C. Youvan[b]

We have constructed a concatemer of two GFP mutants that exhibits FRET. A blue fluorescent protein (BFP5) with an excitation band at 385 nm and an emission band at 450 nm is joined to a red-shifted GFP (RSGFP4) with an excitation band at 488 nm and an emission band at 505 nm. The two mutants are separated by a 20 amino acid flexible peptide linker that contains a Factor X_a protease site. When excited at 385 nm, two emission bands are obtained, one at 450 nm, and another at 505 nm, due to energy transfer from BFP5 to RSGFP4. Upon cleavage of the RSGFP4::BFP5 fusion with Factor X_a, the band at 505 nm disappears, and there is an increase in the fluorescence observed at 450 nm. This is the first demonstration of FRET between two GFP derivatives.

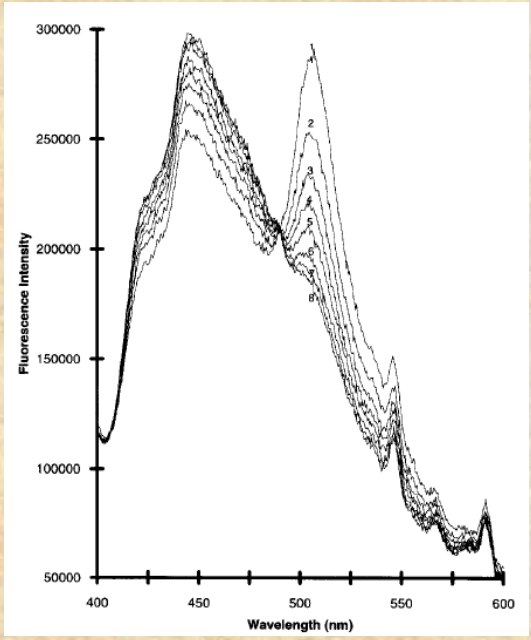

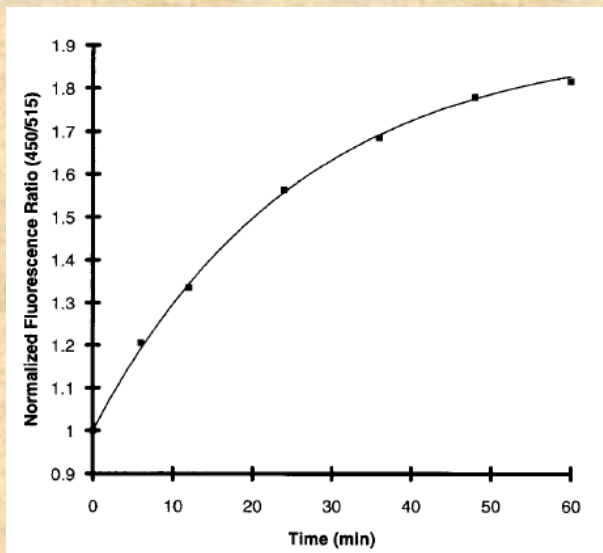

Homo-transfer of electronic excitation energy

So far, we considered the donor and acceptor molecules to be different.However, if the probe excitation spectrum overlaps its emission spectrum, FRET can occur between identical molecules.

« Il suffit qu'un transfert d'activation puisse se produire entre deux molécules voisines d'orientation différentes, c'est a dire portant des oscillateurs non parallèles, pour qu'il en résulte en moyenne une diminution de l'anisotropie de distribution des oscillateurs excites et par suite de la polarisation de la lumière émise. »

(F. Perrin *Ann de Phys.* 1929)

It suffices that a transfer of activation can occur between two neighboring molecules with different orientations, that is with non-parallel oscillators, in order to have, on average, a decrease in the anisotropy of the distribution of excited oscillators, and therefore a decrease of the polarization of the emitted light.

« …L'existence de transferts d'activation est expérimentalement prouvée pour de telles molécules par la décroissance de la polarisation de la lumière de fluorescence quand la concentration croit… »

(F. Perrin *Ann de Phys*. 1932)

…The existence of transfer of activation is proven experimentally for such molecules by the decrease in polarization of the fluorescent light when the concentration is increased…

Electronic energy transfer between identical fluorophores was originally observed by Gaviola and Pringsheim in 1924.

Über den Einfluß der Konzentration auf die Polarisation der Fluoreszenz von Farbstofflösungen.

Von **E. Gaviola** und **Peter Pringsheim** in Berlin.

Mit zwei Abbildungen. (Eingegangen am 24. März 1924.)

Tabelle 2. Uranin in ganz wasserfreiem Glycerin.

C	p	C	p	C	p	C	p
$\frac{1}{4}$	0	$\frac{1}{32}$	6,5	$\frac{1}{256}$	15	$\frac{1}{2048}$	39,2
$\frac{1}{8}$	?	$\frac{1}{64}$	8,1	$\frac{1}{512}$	19,5	$\frac{1}{4100}$	43,5
$\frac{1}{16}$	3,2	$\frac{1}{128}$	11,1	$\frac{1}{1024}$	30,7	etwa $\frac{1}{20000}$	45

(note: uranin is the sodium salt of fluorescein)

Homo-transfer of electronic excitation energy

"…Excitation transfer between alike molecules can occur in repeated steps. So the excitation may *migrate* from the absorbing molecule over a considerable number of other ones before deactivation occurs by fluorescence or other process. Though this kind of transfer cannot be recognized from fluorescence spectra, it may be observed by the decrease of fluorescence polarization…" (Förster, 1959)

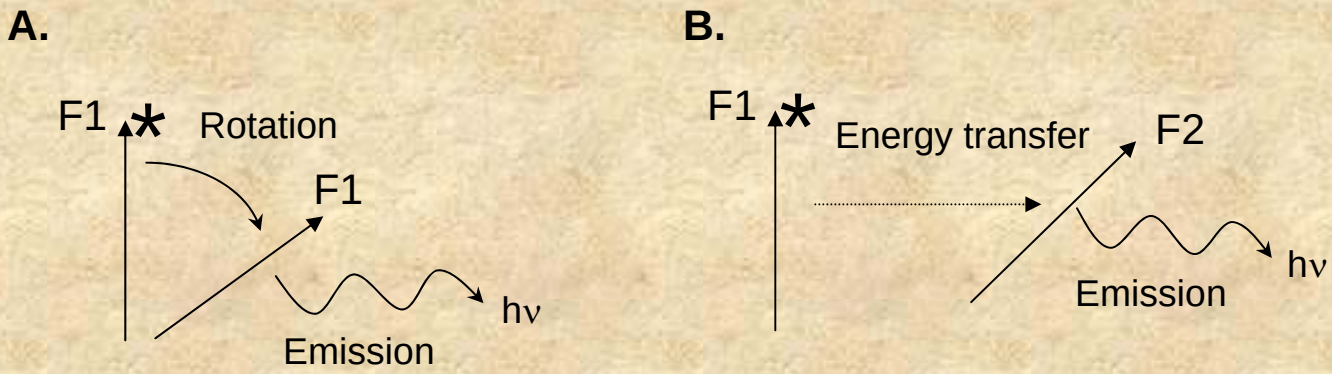

A. Depolarization resulting from rotational diffusion of the fluorophore. The excited fluorophore (F1*) rotates then emits light. **B.** The excited fluorophore (F1*) transfer energy to another fluorophore F2 which in turn emits light.

Weber's Red-Edge Effect

In 1960 Weber was the first to report that homotransfer among indole molecules disappeared upon excitation at the red-edge of the absorption band - this phenomenon is now known as the "Weber red-edge effect".

In 1970 Weber and Shinitzky published a more detailed examination of this phenomenon. They reported that in the many aromatic residues examined, transfer is much decreased or undetectable on excitation at the red edge of the absorption spectrum .

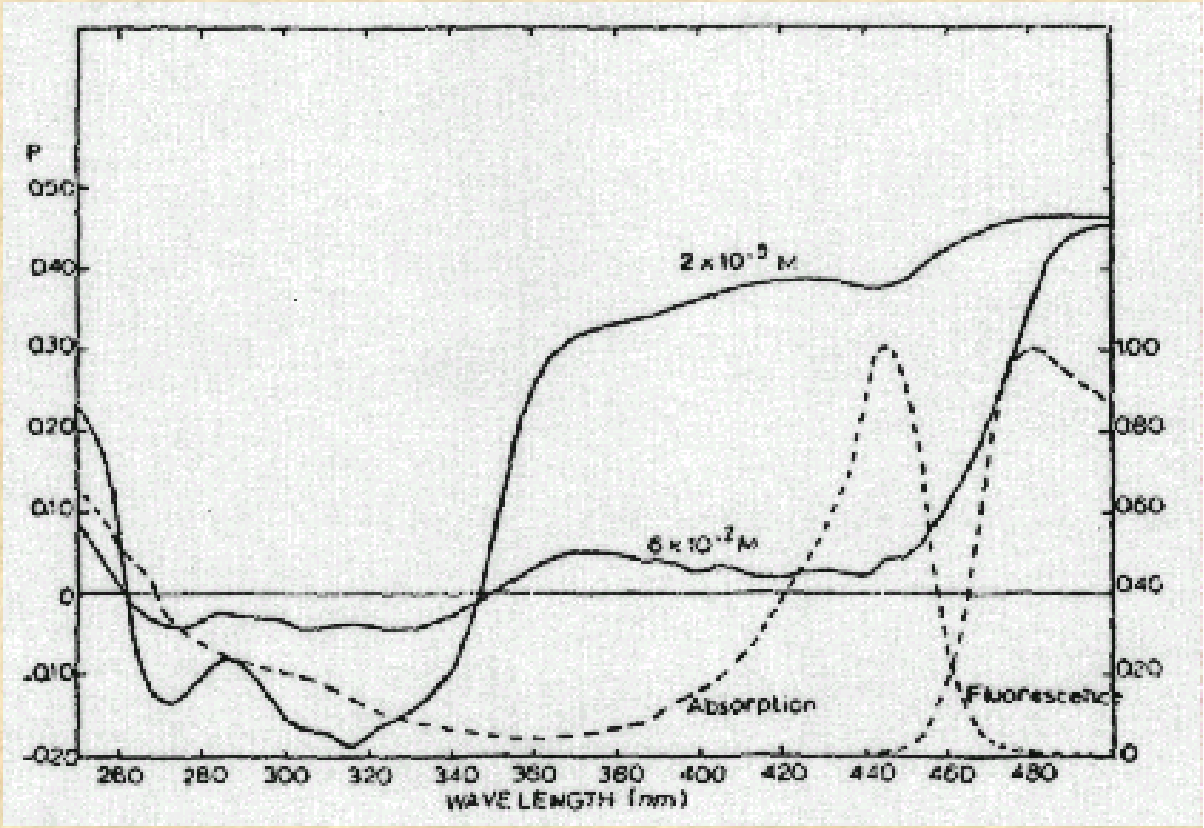

Distance determination using homotransfer

The efficiency of transfer can be calculated from a knowledge of the polarization in the absence and presence of energy transfer.

The steady state expression for the efficiency of energy transfer (*E*) as a function of the anisotropy is given by

$$E = 2(r_d - \langle r \rangle)/(r_d - r_a)$$

Where r_d and r_a are the anisotropy decay of the donor and acceptor only, respectively and $\langle r \rangle$ is the observed anisotropy in presence of both donor and acceptor. If κ^2 =2/3 then r_a = 0 and

$$E = 2(r_d - \langle r \rangle)/r_d$$

An example of homo-FRET used to study protein interactions is the work by Hamman et al (Biochemistry *35*:16680) on a prokaryotic ribosomal protein

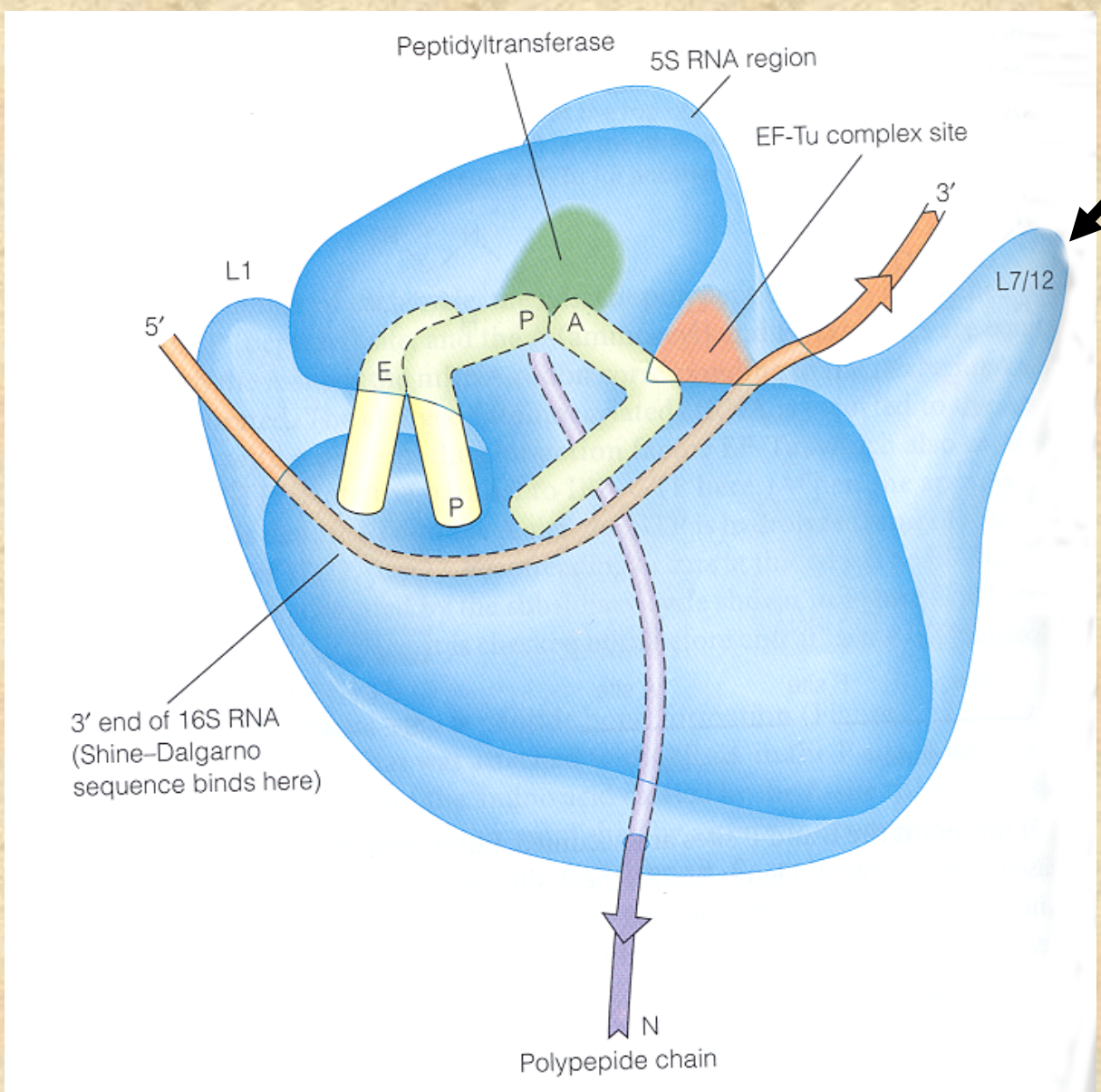

L7/L12 is present as two dimers in the ribosome. An X-ray structure of monomeric C-terminal domains led to the speculation that the C-terminal domains of L7/L12 interacted through hydrophobic surfaces as shown below

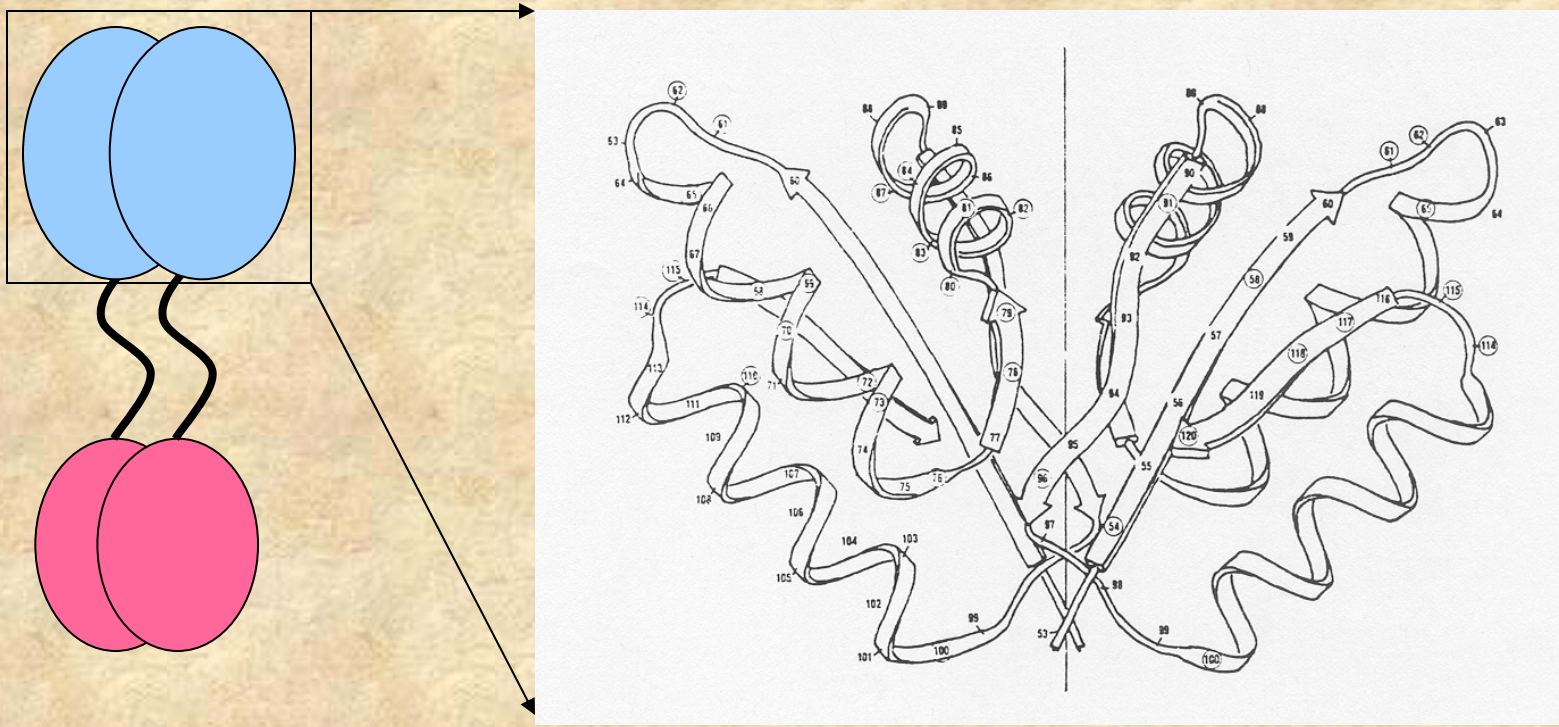

To study this protein fluorescence probes were introduced at specific locations along the L7/L12 peptide backbone.

To introduce these probes at specific locations site-directed mutagenesis was used to place cysteine residues in different locations

Sulfhydryl-reactive fluorescence probes were then covalently attached to these cysteine residues

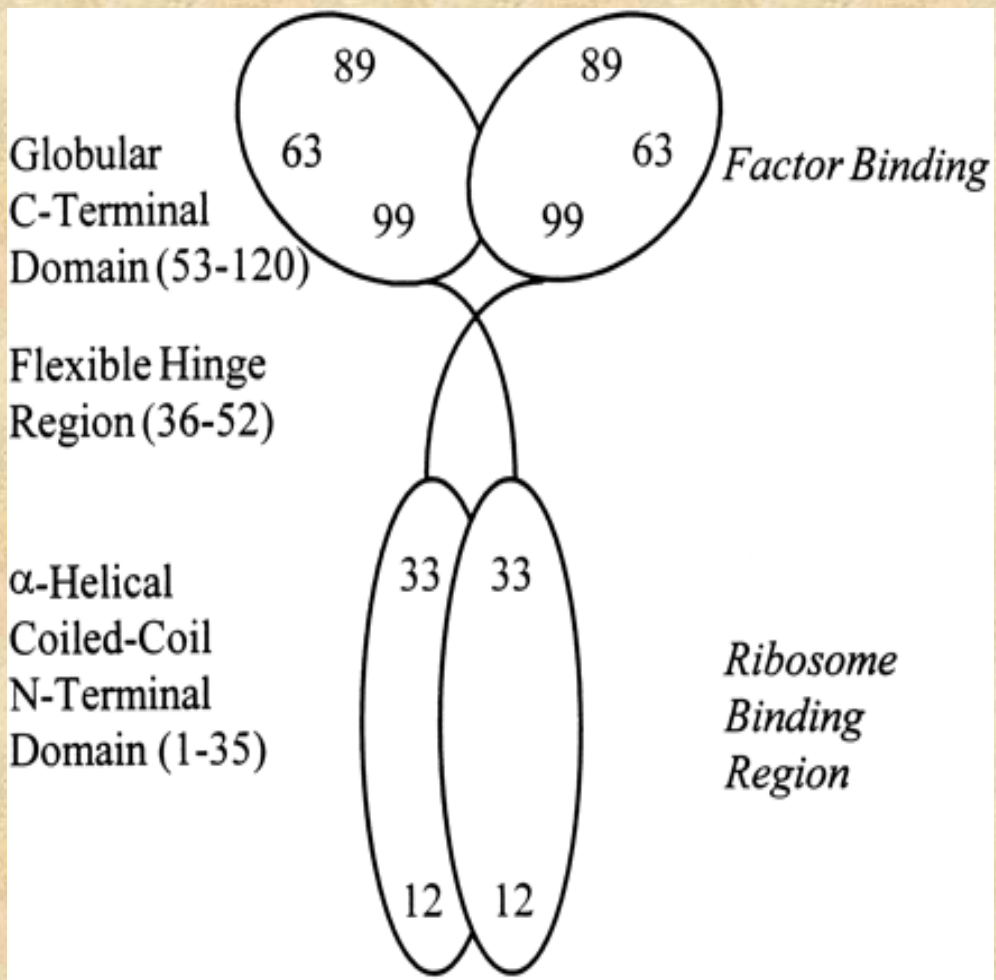

Subunit exchange experiments allowed the preparation of singly labeled dimers

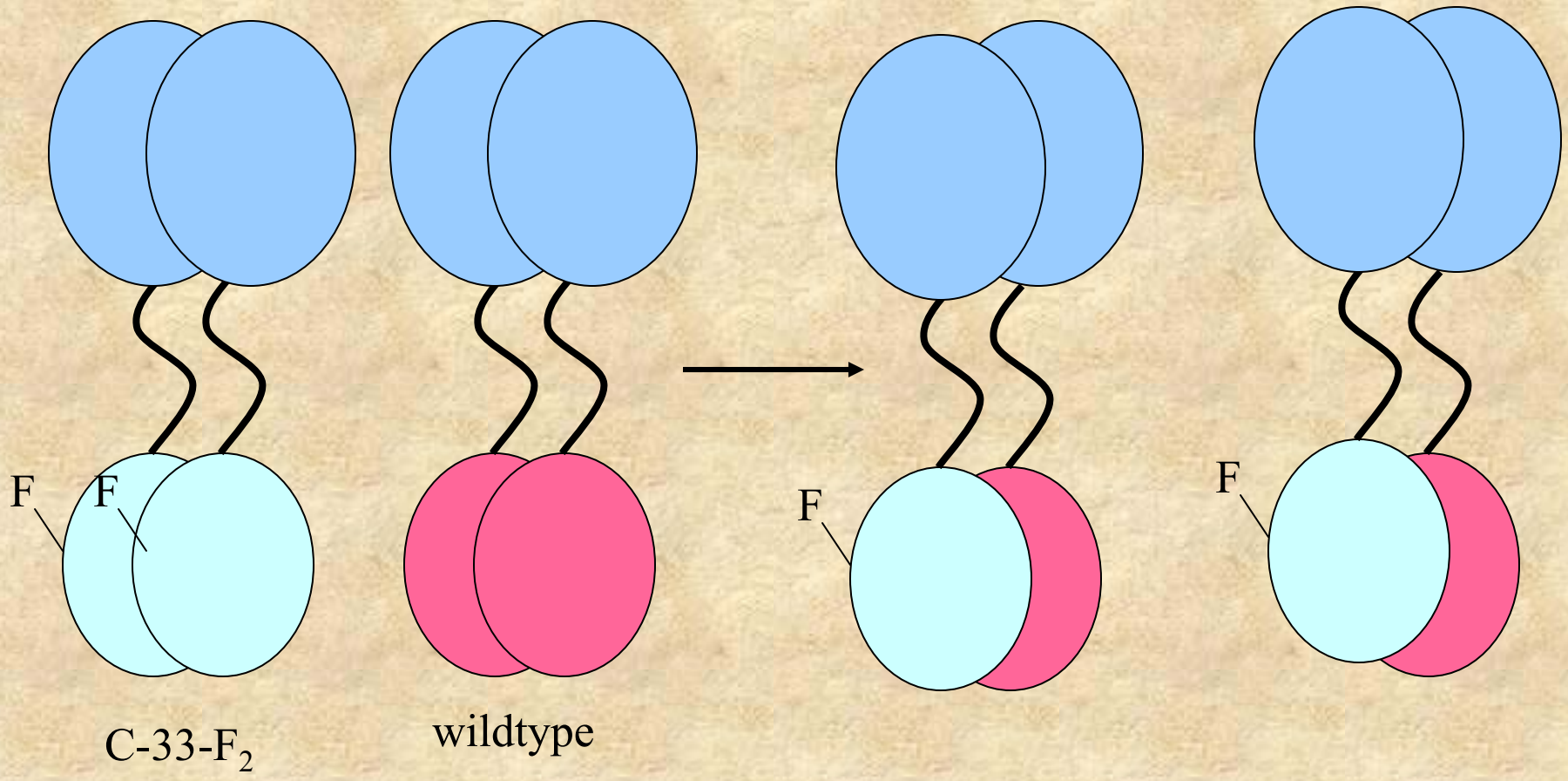

The presence of homoFRET was evident in the excitation polarization spectrum as shown by the Weber Red-Edge Effect.

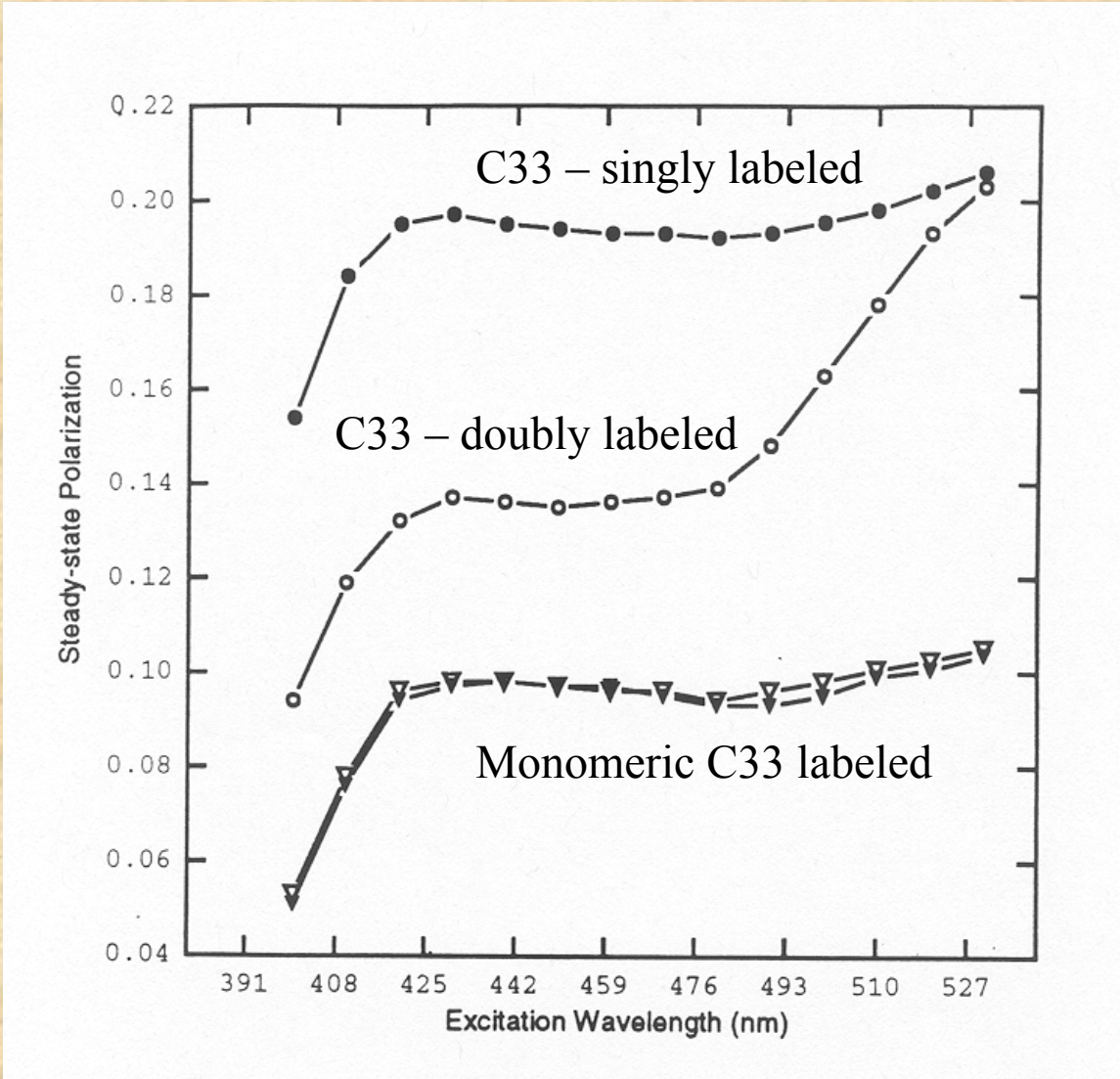

The polarization values, before and after subunit exchange, indicate which residues undergo homoFRET. The polarization data below are for fluorescein labeled constructs before (violet) and after (magenta) subunit exchange

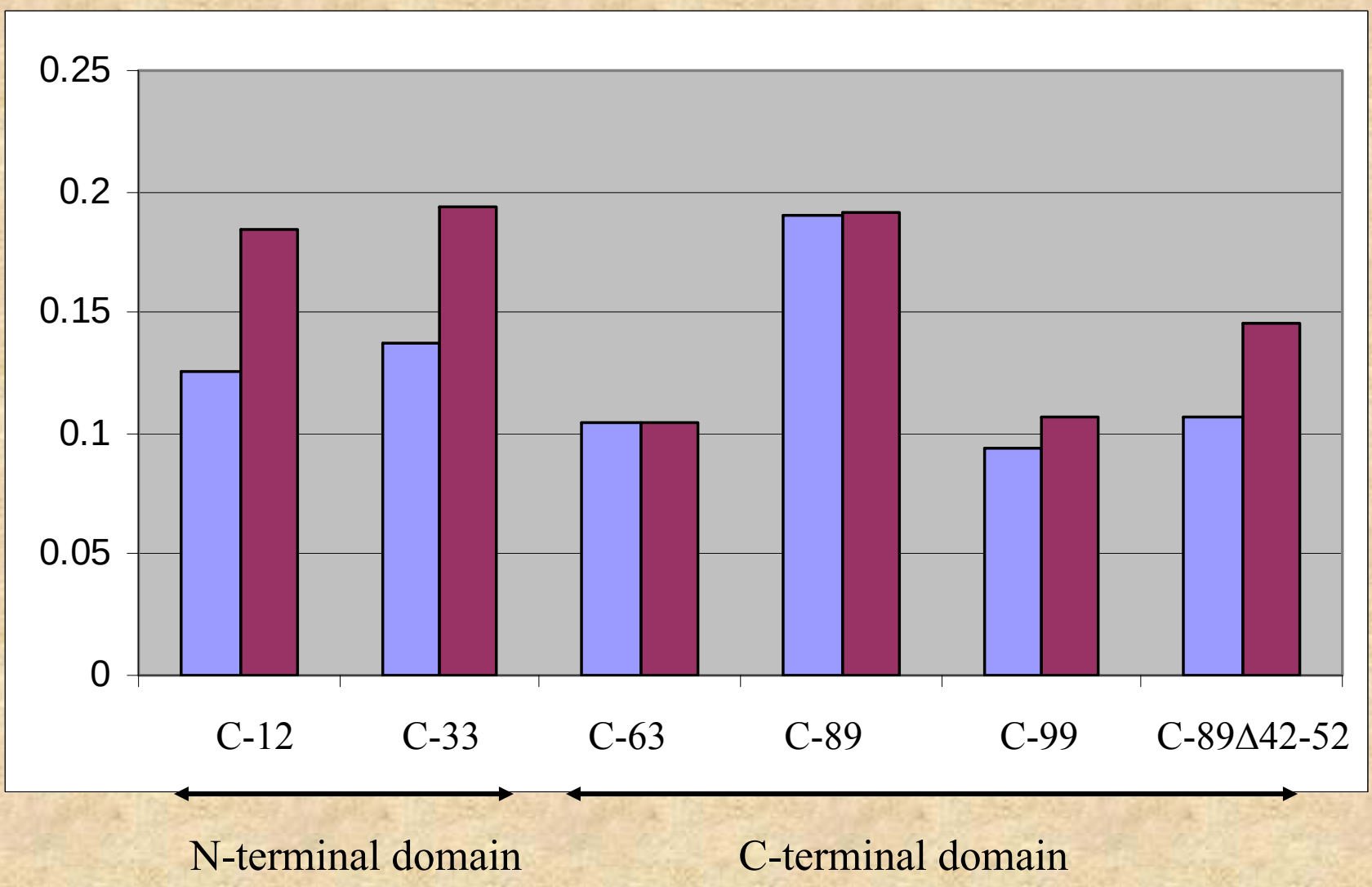

These changes in polarization due to homoFRET allow us to assign maximum proximity values for the C-terminal domains.

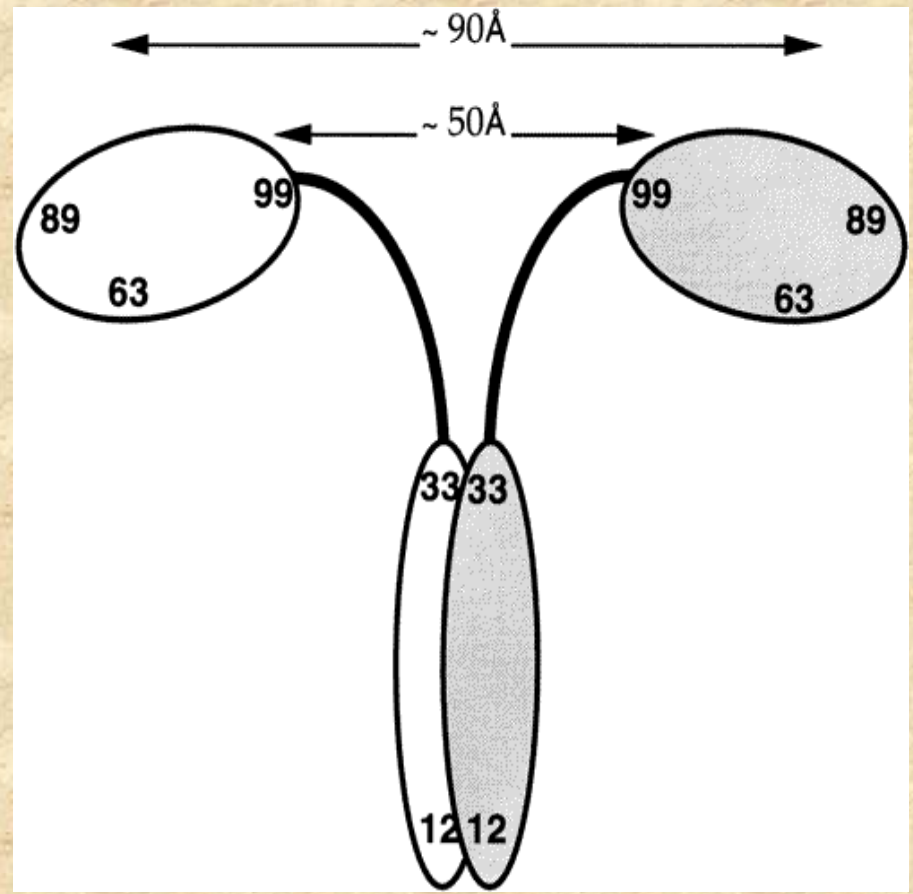

The conclusion is that the C-terminal domains are well-separated – contrary to the original model from the X-ray studies and the usual depictions in the literature

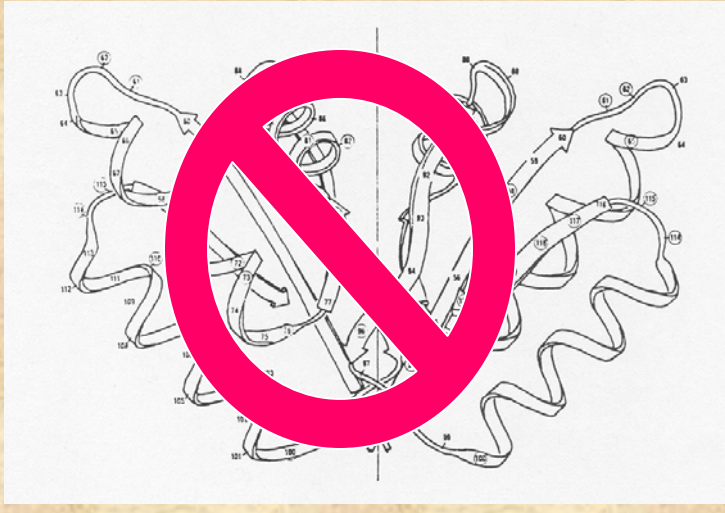

Homo-FRET Microscopy in Living Cells to Measure Monomer-Dimer Transition of GFP-Tagged Proteins

I. Gautier,* M. Tramier,* C. Durieux,* J. Coppey,* R. B. Pansu,† J-C. Nicolas,‡ K. Kemnitz,§ and M. Coppey-Moisan*

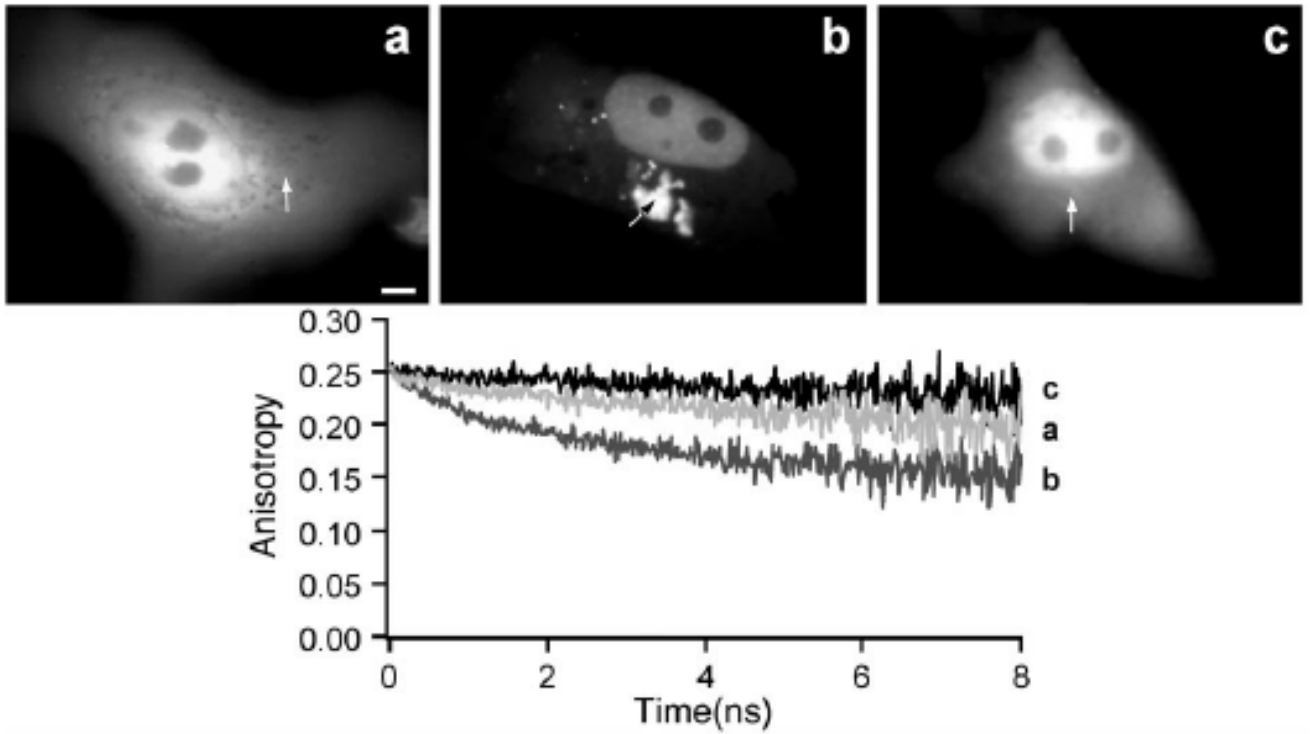

FIGURE 1 Subcellular fluorescence anisotropy decays of $TK_{27}GFP$ and $TK_{366}GFP$ proteins. (*Top*) Steady-state fluorescence images of Vero cells expressing $TK_{27}GFP$ (*a*) and $TK_{366}GFP$ (*b* and *c*). (*a* and *c*) Cells presenting only a diffuse cytoplasmic and nuclear fluorescence pattern; (*b*) Cells containing fluorescent aggregates. (*Bottom*) Time-resolved fluorescence depolarization from a cytoplasmic area of diffuse fluorescence (*a* and *c*) and from an area inside an aggregate (*b*). The subcellular location of the illuminated volume (~1 μm^3) from which the anisotropy decay was performed is indicated by an arrow. For cells containing aggregates, anisotropy decays from nuclear or cytoplasmic area of diffuse fluorescence were similar to that obtained from aggregates (*b*). Bar in *a*, 5 μm.

Biophys J, June 2001, p. 3000-3008, Vol. 80, No. 6

Other examples of homo-FRET *in vivo* can be found in: Tramier et al., 2003 "Homo-FRET versus hetero-FRET to probe homodimers in living cells" Methods Enzymol. 360:580-97.

To summarize this lecture is not intended to prepare you to start FRET measurements immediately but rather to make you aware of the salient principles and pitfalls

Several books on this topic are available as well as MANY articles in the primary literature

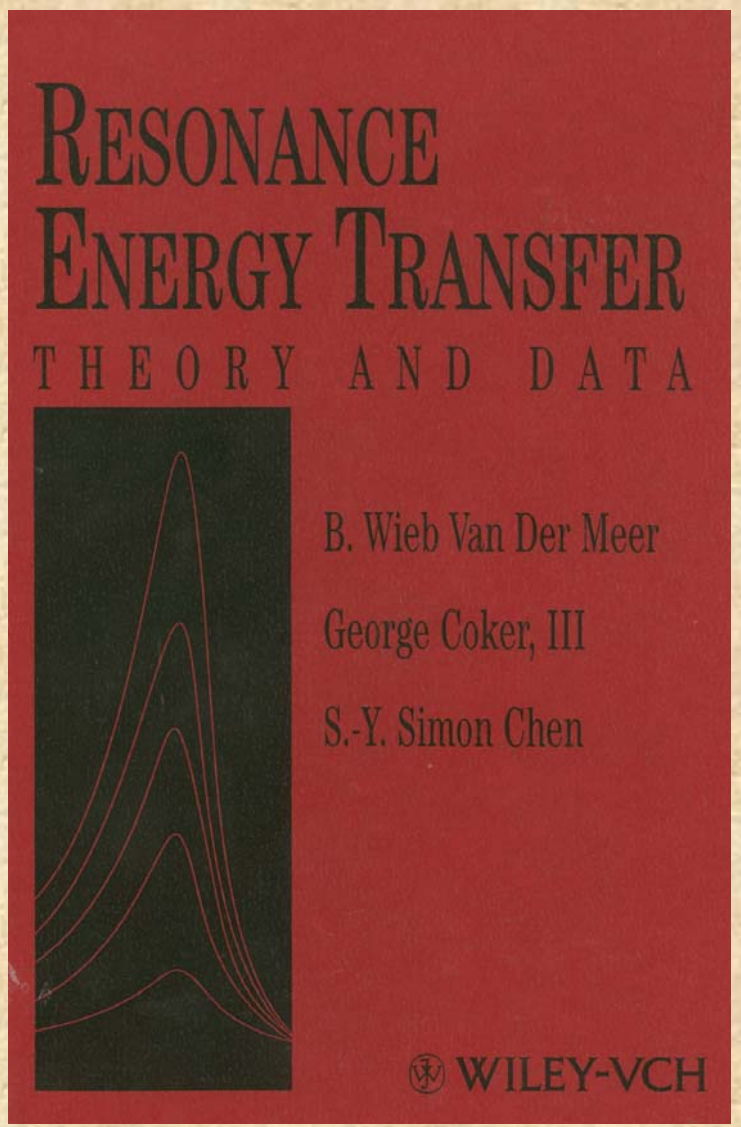

Fluorescence Probes

In vitro *(or In Silico)*

Will be discussed in this course by Ewald Terpetschnig from ISS, Inc.

In vivo (or more accurately in cells)

Will be largely restricted to a brief discussion of Fluorescent Proteins

REVIEW

The Fluorescent Toolbox for Assessing Protein Location and Function

Ben N. G. Giepmans,[1,2] Stephen R. Adams,[2] Mark H. Ellisman,[1] Roger Y. Tsien[2,3]*

SCIENCE VOL 312 14 APRIL 2006

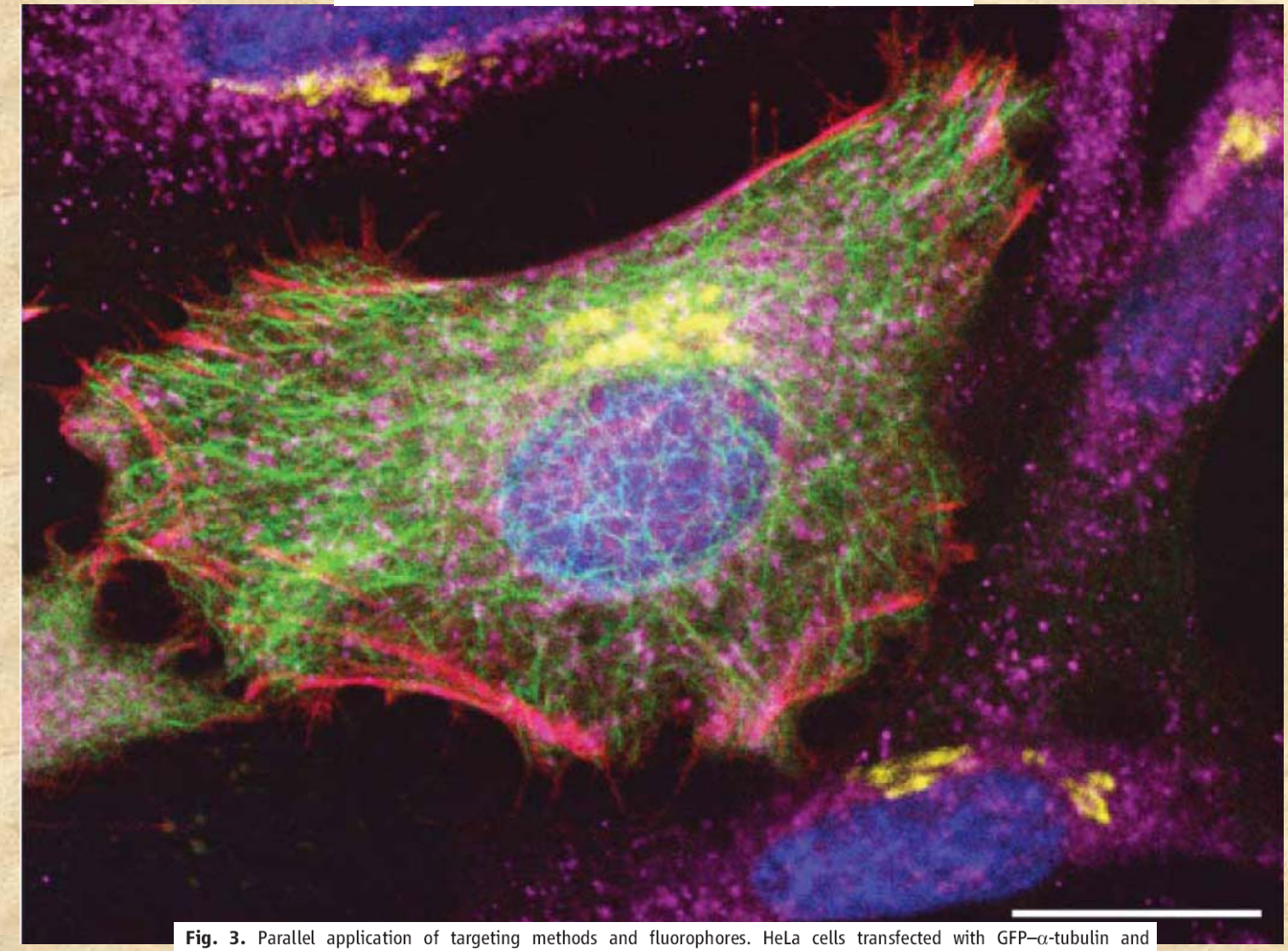

Fig. 3. Parallel application of targeting methods and fluorophores. HeLa cells transfected with GFP–α-tubulin and tetracysteine–β-actin were stained with ReAsH. After fixation, cells were immunolabeled for the Golgi matrix protein giantin with QDs and for the mitochondrial enzyme cytochrome c with Cy5 as indicated. DNA was stained with Hoechst 33342. Images were acquired from Z planes that best represent each structure using excitation and emission wavelengths as indicated. Individual channels are false-colored (middle) and merged (bottom). Scale bars, 20 μm.

Green Fluorescent Protein

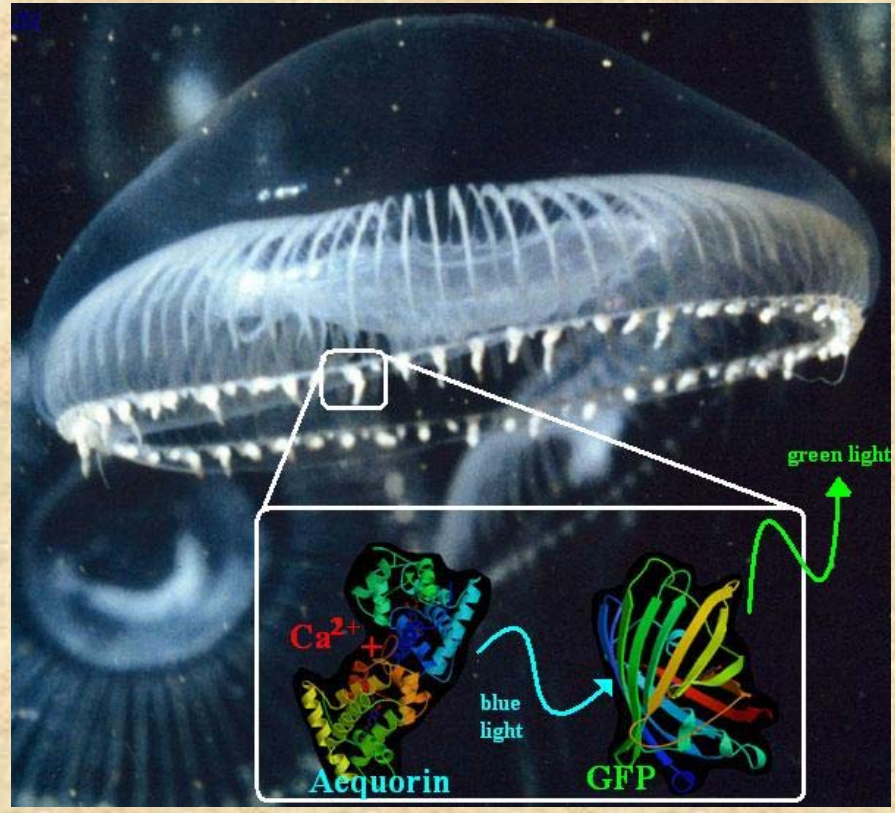

Aequorea victoria jellyfish

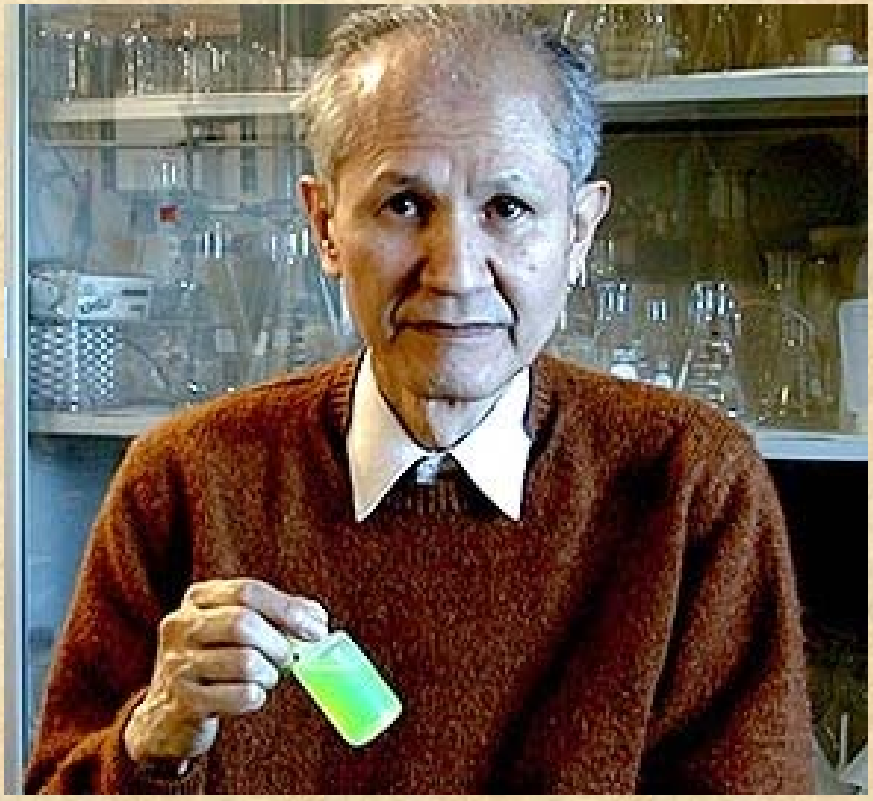

Osamu Shimomura

Shimomura O, Johnson F, Saiga Y (1962). "Extraction, purification and properties of aequorin, a bioluminescent protein from the luminous hydromedusan, Aequorea". *J Cell Comp Physiol* **59**: 223-39.

“The jellyfish *Aequorea* and its light-emitting organs”

O. SHIMOMURA:*Journal of Microscopy, Vol. 217, Pt 1 January 2005, pp. 3–15*

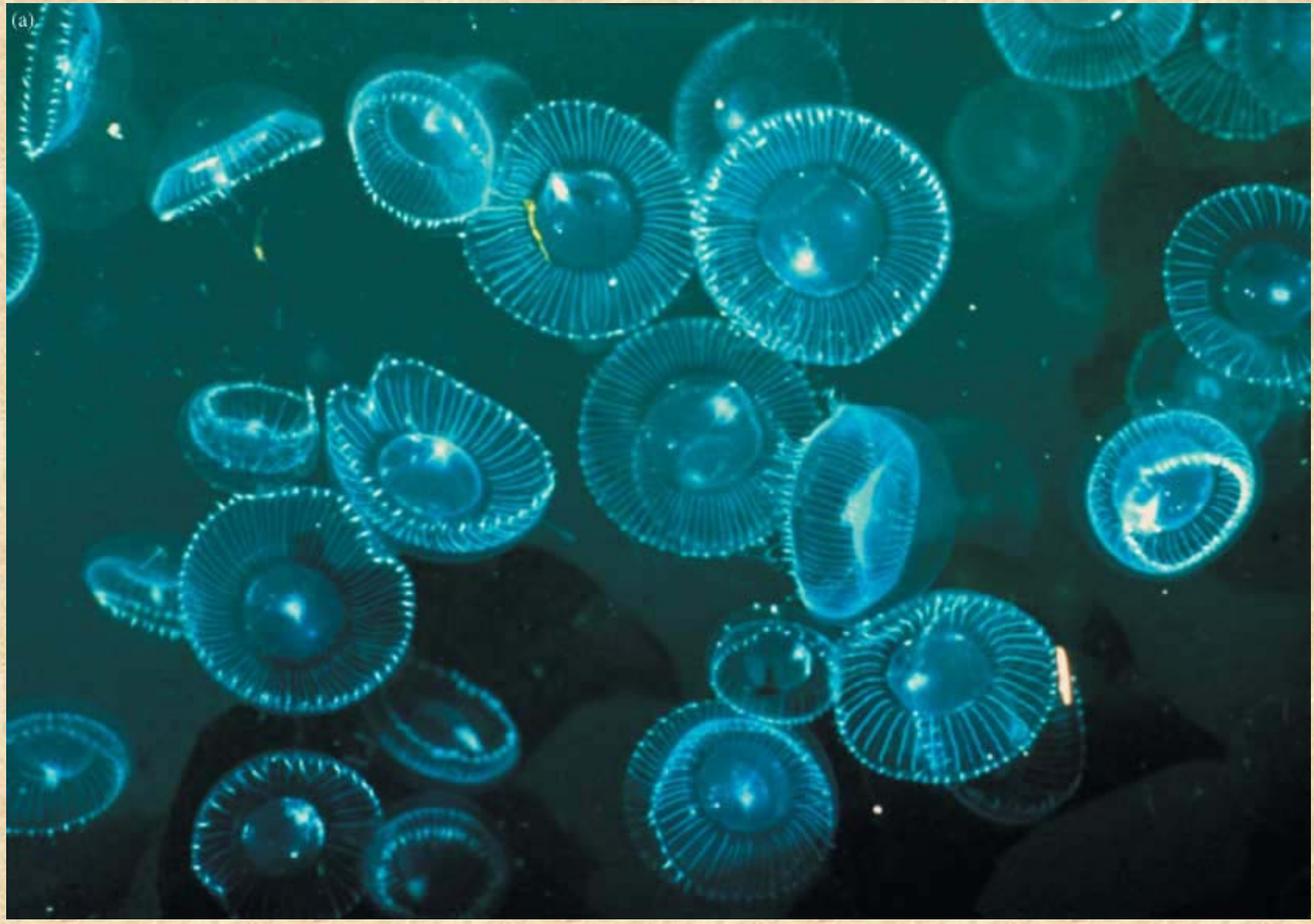

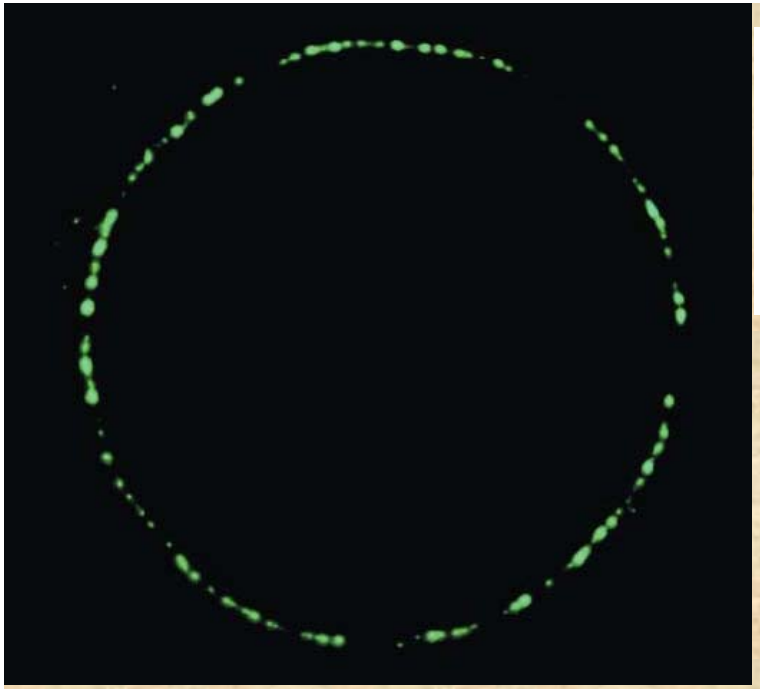

Intermolecular Energy Transfer in the Bioluminescent System of *Aequorea*†

Hiroshi Morise, Osamu Shimomura, Frank H. Johnson,* and John Winant

2656 BIOCHEMISTRY, VOL. 13, NO. 12, 1974

Materials and Methods

Aequorin. The material used in this study was extracted and purified from some 30,000 specimens of *Aequorea*

70 mgs of purified GFP were obtained.
The 30,000 jellyfish weighed about 1.5 tons

The outer ring of the jellyfish had to be isolated. Intially scissors were used but then a "ring-cutting" machine was built

Aequorea cutting machine by Johnson

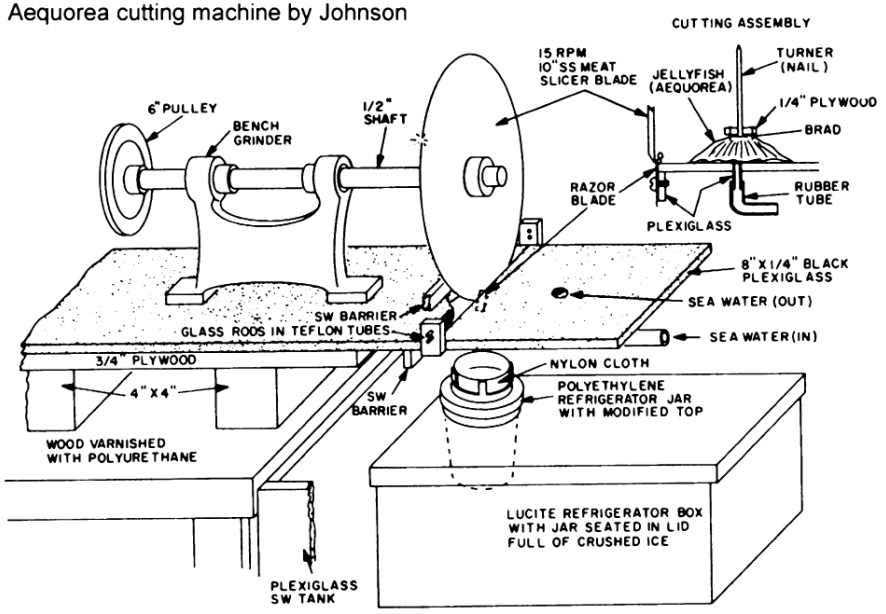

Crystallized GFP

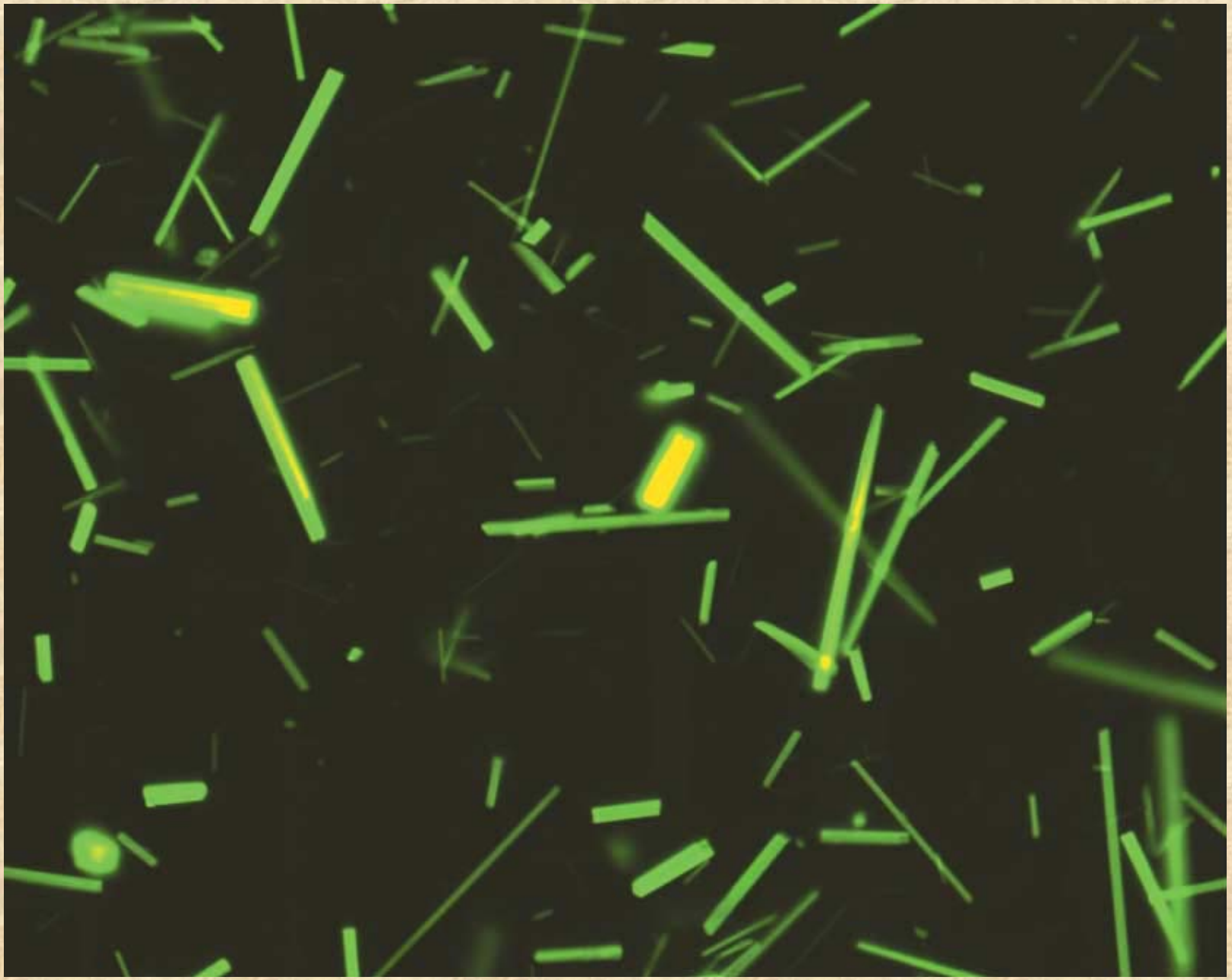

RESEARCH ARTICLE

The molecular structure of green fluorescent protein

Fan Yang, Larry G. Moss[1], and George N. Phillips, Jr.*

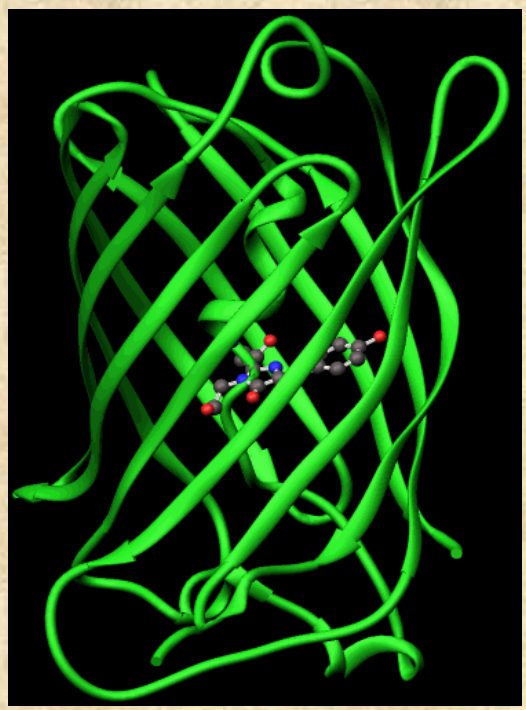

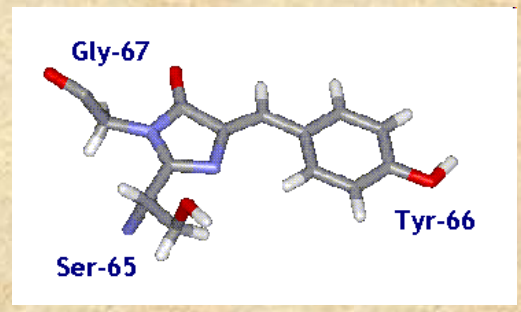

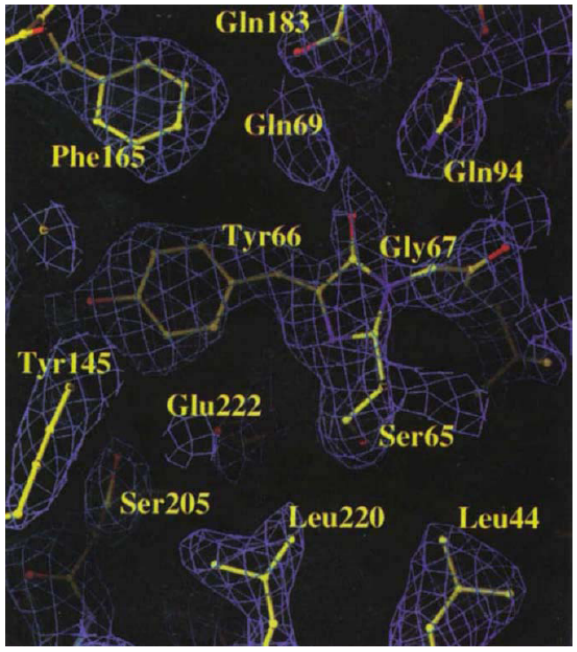

The GFP chromophore is formed via a posttranslational cyclization reaction involving the three amino acids serine 65, tyrosine 66 and glycine 67

This scenario was proposed in the paper that first presented the primary seqeunce of GFP

Gene, 111 (1992) 229–233
 0378-1119/92/$05.00

22

GENE 06296

Primary structure of the *Aequorea victoria* green-fluorescent protein

(Bioluminescence; Cnidaria; aequorin; energy transfer; chromophore; cloning)

Douglas C. Prasher[a], Virginia K. Eckenrode[b], William W. Ward[c], Frank G. Prendergast[d] and Milton J. Cormier[b]

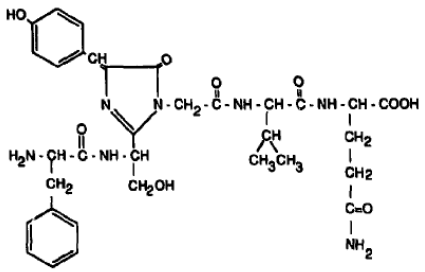

Fig. 1. The chemical structure of the chromophore in *Aequorea* GFP (W.W.W., unpublished). The cyclized chromophore is formed from the trimer Ser-dehydroTyr-Gly within the polypeptide by an unknown mechanism.

THE GREEN FLUORESCENT PROTEIN

Roger Y. Tsien
Howard Hughes Medical Institute; University of California, San Diego; La Jolla, CA 92093-0647

Annu. Rev. Biochem. 1998. 67:509–44

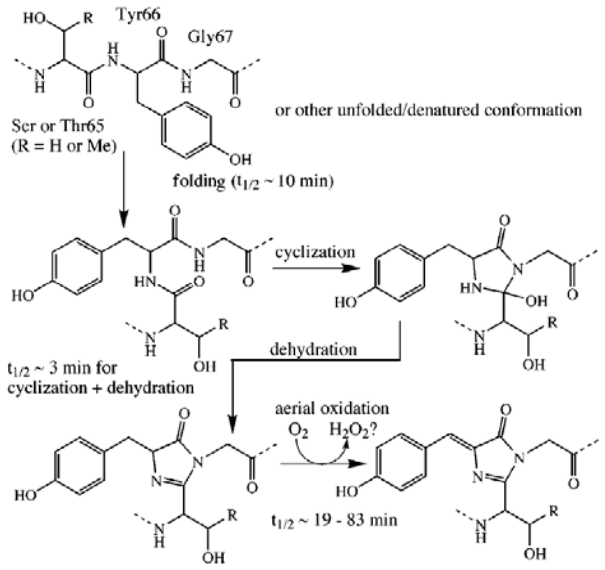

Figure 2 Mechanism proposed by Cubitt et al (22) for the intramolecular biosynthesis of the GFP chromophore, with rate constants estimated for the Ser65 → Thr mutant by Reid & Flynn (23) and Heim et al (25).

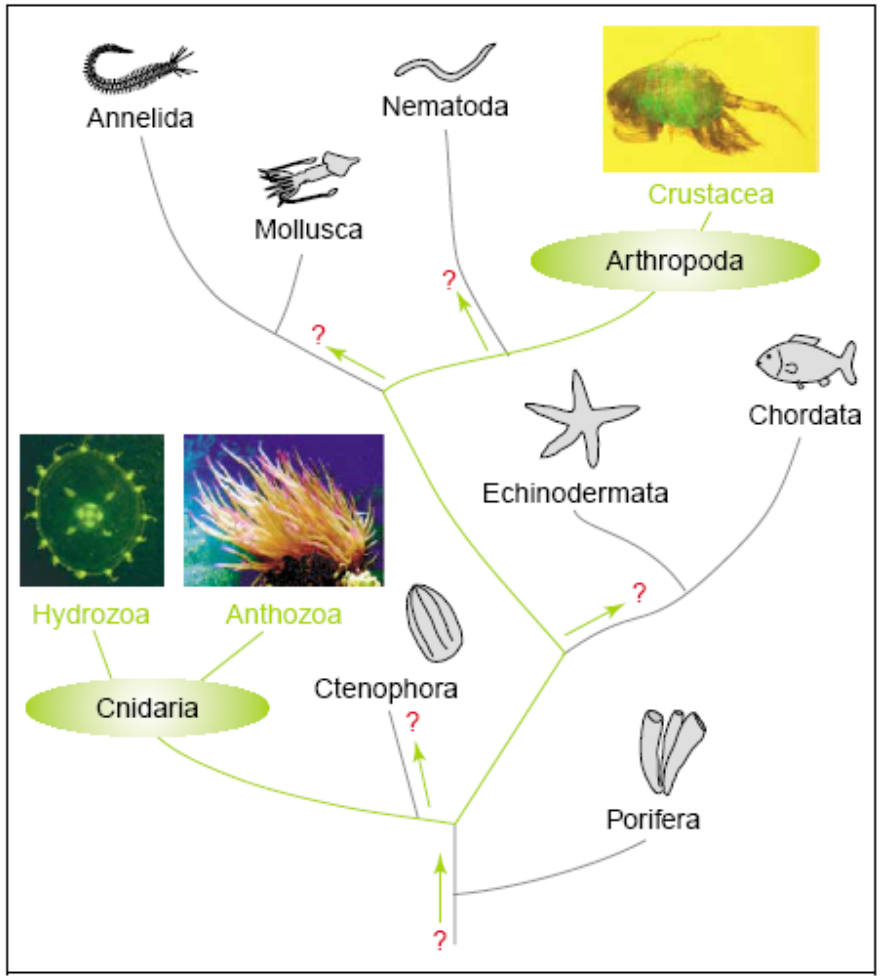

Figure 1. Positional relationship of the fluorescent protein-producing organisms on the phylogenetic tree. The phyla Cnidaria and Arthropoda (where GFP genes were found) and the branches connecting these phyla are highlighted in green. Photos show organisms representative of each phylum expressing GFP-like proteins: jellyfish *Phialidium* showing yellow fluorescence; sea anemone *Anemonia sulcata* with purple tentacle tips; and a copepod displaying green fluorescence. Question marks indicate possible, but unexplored, pathways of the evolution of FPs.

Review TRENDS in Biotechnology Vol.23 No.12 December 2005

Fluorescent proteins as a toolkit for *in vivo* imaging

Dmitriy M. Chudakov, Sergey Lukyanov and Konstantin A. Lukyanov

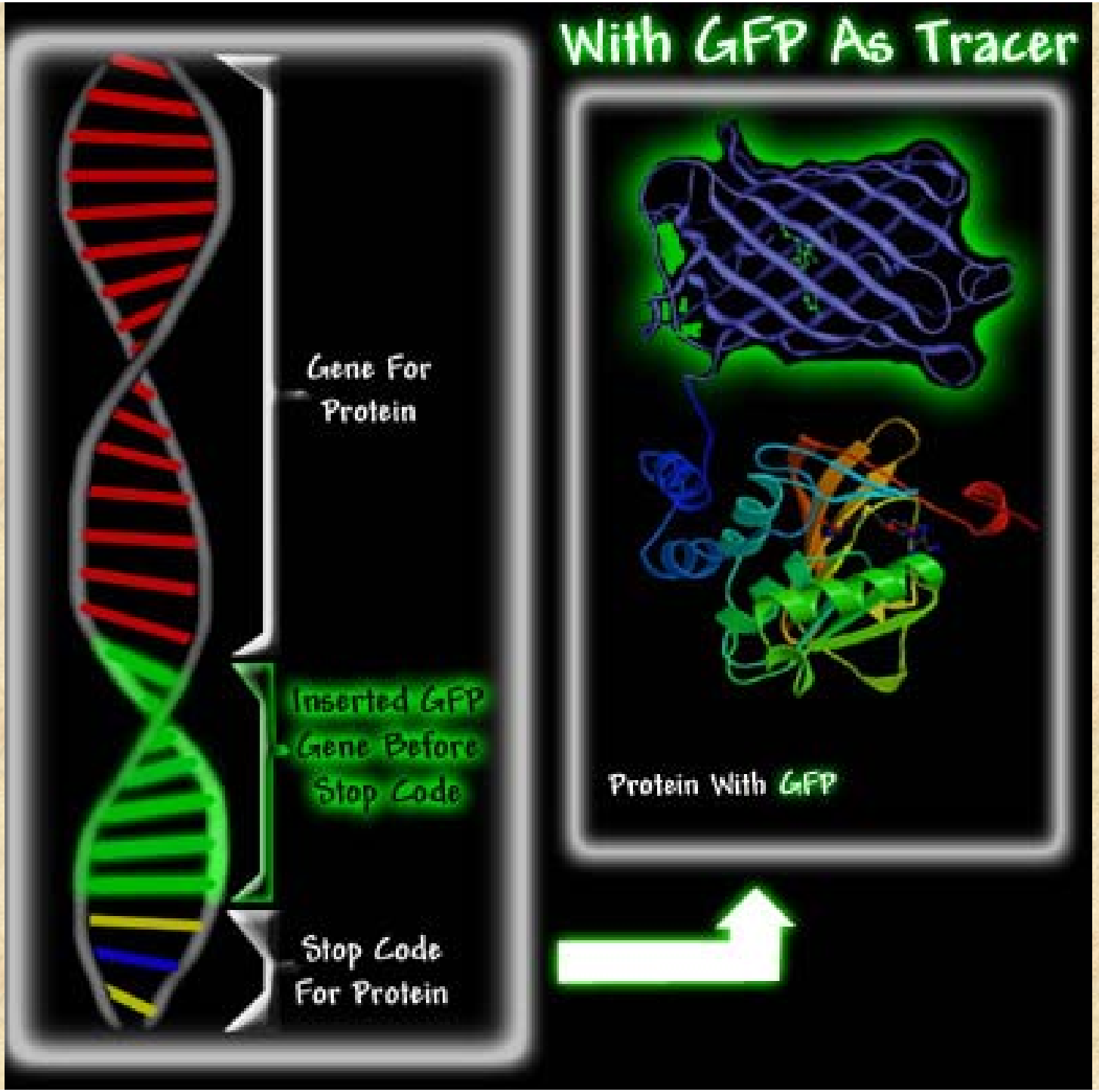
With GFP As Tracer
Gene For Protein
Inserted GFP Gene Before Stop Code
Stop Code For Protein
Protein With GFP

Ryuzo Yanagimachi

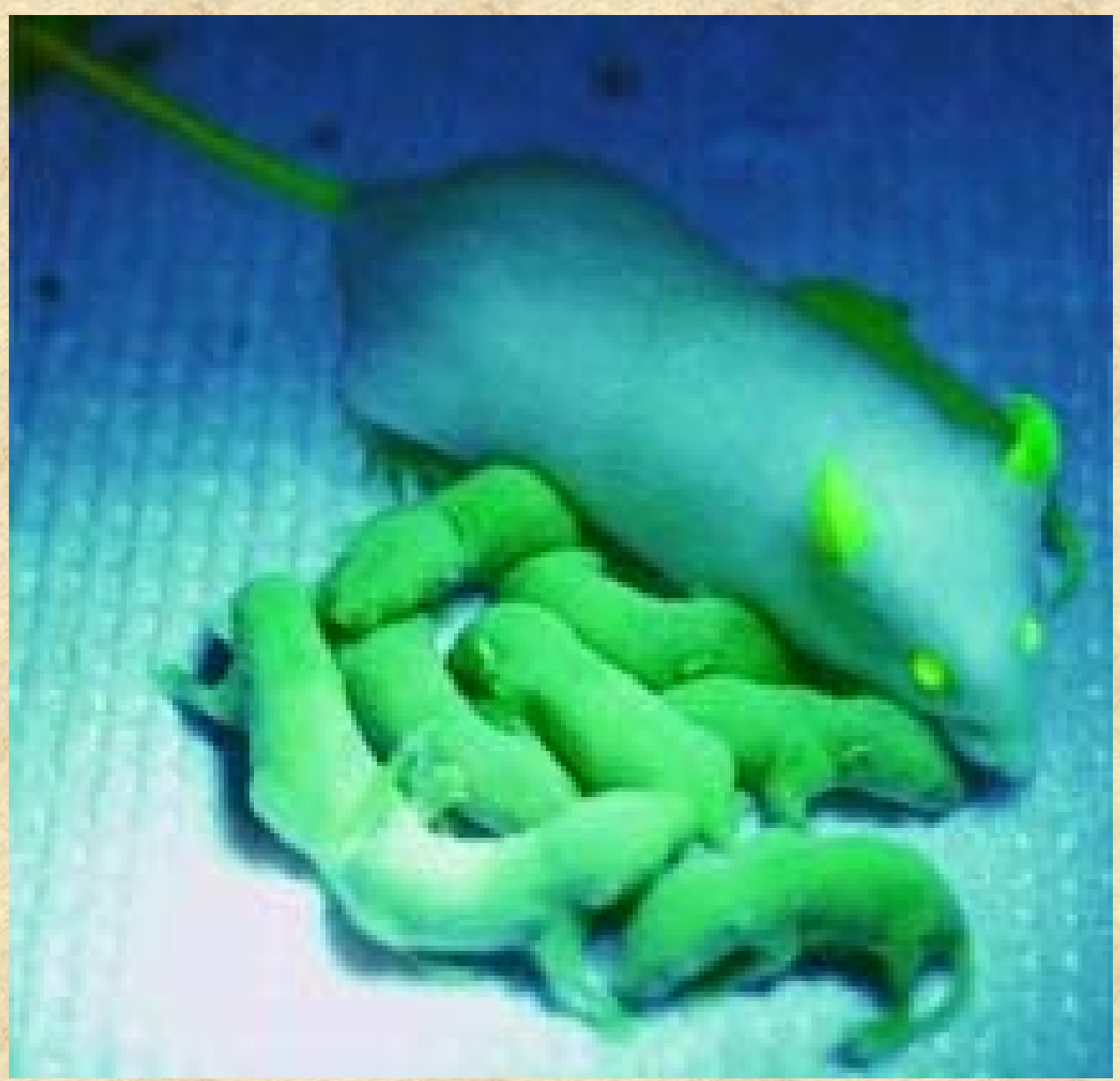

A number of new GFP proteins have been made using site directed mutagenesis to alter the amino acids near the chromophore and thus alter the absorption and fluorescence properties.

Proc. Natl. Acad. Sci. USA
Vol. 91, pp. 12501–12504, December 1994
Biochemistry

Wavelength mutations and posttranslational autoxidation of green fluorescent protein

(*Aequorea victoria*/blue fluorescent protein/*Escherichia coli*/imidazolidinone)

ROGER HEIM*, DOUGLAS C. PRASHER†, AND ROGER Y. TSIEN*‡

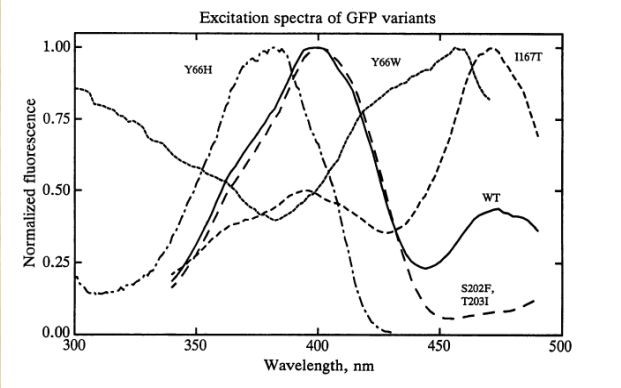

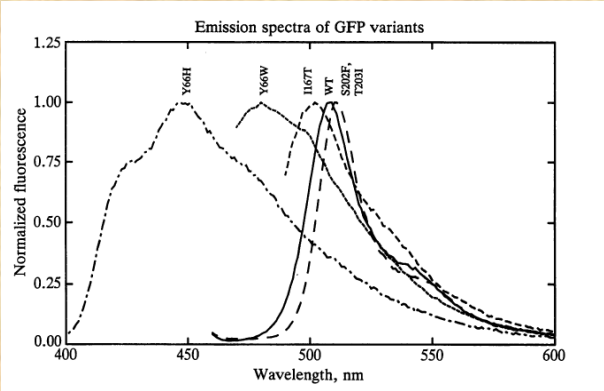

For all these reasons, it would be interesting to convert the *Aequorea* GFP excitation spectrum to a single peak, preferably at longer wavelengths. The cDNA was therefore subjected to random mutagenesis by hydroxylamine treatment or PCR. Approximately six thousand bacterial colonies on agar plates were illuminated with alternating 395- and 475-nm excitation and visually screened for altered excitation properties or emission colors. Although this number of colonies falls far short of saturating the possible mutations of a protein of 238 residues, interesting variants have already appeared.

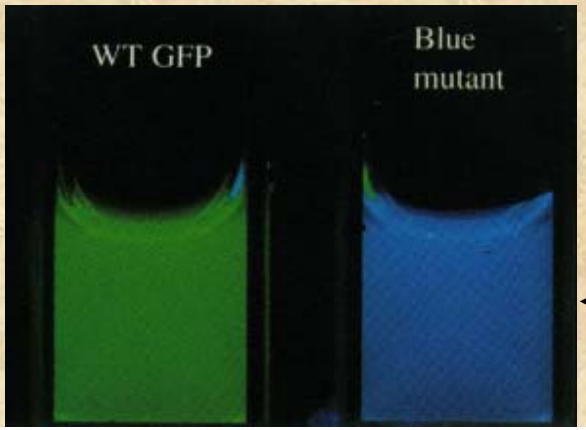

Tyr-66 replaced by His

Journal of Cell Science 120, 4247-4260

Advances in fluorescent protein technology

Nathan C. Shaner[1], George H. Patterson[2] and Michael W. Davidson[3]

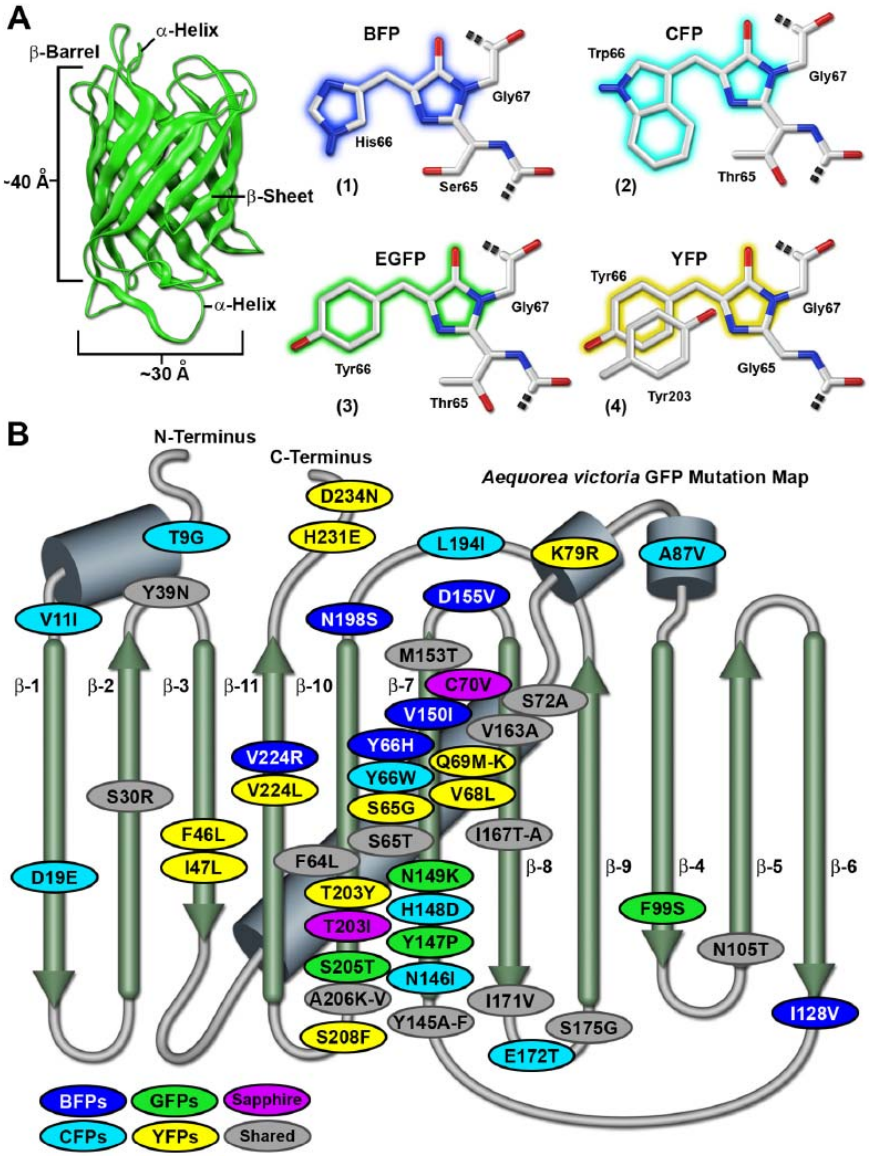

Fig. 1. (A) FP β-barrel architecture and approximate dimensions, and chromophore structures of common *Aequorea* FP derivatives. (1) BFP, (2) CFP, (3) EGFP, (4) YFP. The tryptophan residue (Trp66) in (2) is illustrated in the cis conformation as occurs for Cerulean derivatives (Malo et al., 2007) rather than the trans isomer that is common to CFP and related variants. Portions of the chromophores that are conjugated and give rise to fluorescence are shaded with colors corresponding to the emission spectral profile. (B) *Aequorea* GFP mutation map showing common mutations superimposed on a topological layout of the peptide structure. β-sheets are numbered and depicted as thin, green cylinders with an arrow pointing towards the C-terminus, whereas α-helices are depicted as gray cylinders. Mutations are color-coded to represent the variants to which they apply: BFPs (blue), CFPs (cyan), GFPs (green), YFPs (yellow), Sapphire (violet), folding, shared and monomerizing (gray). Note that almost 75% of the mutations are located in the central helix and in β-sheet strands 7, 8 and 10. In general, wavelength-specific mutations occur near the central helix containing the chromophore, whereas folding mutations occur throughout the sequence. Many of the cyan and yellow FP mutations introduced near the termini of the proteins resulted during the CyPet and YPet mutagenesis efforts (Nguyen and Daugherty, 2005). Several of the sfGFP folding mutations (S30R, Y39N, F99S and N105T) also occur away from the chromophore. The monomerizing mutation A206K is useful for all known GFP derivatives, but is replaced by A206V in sfGFP and EBFP2.

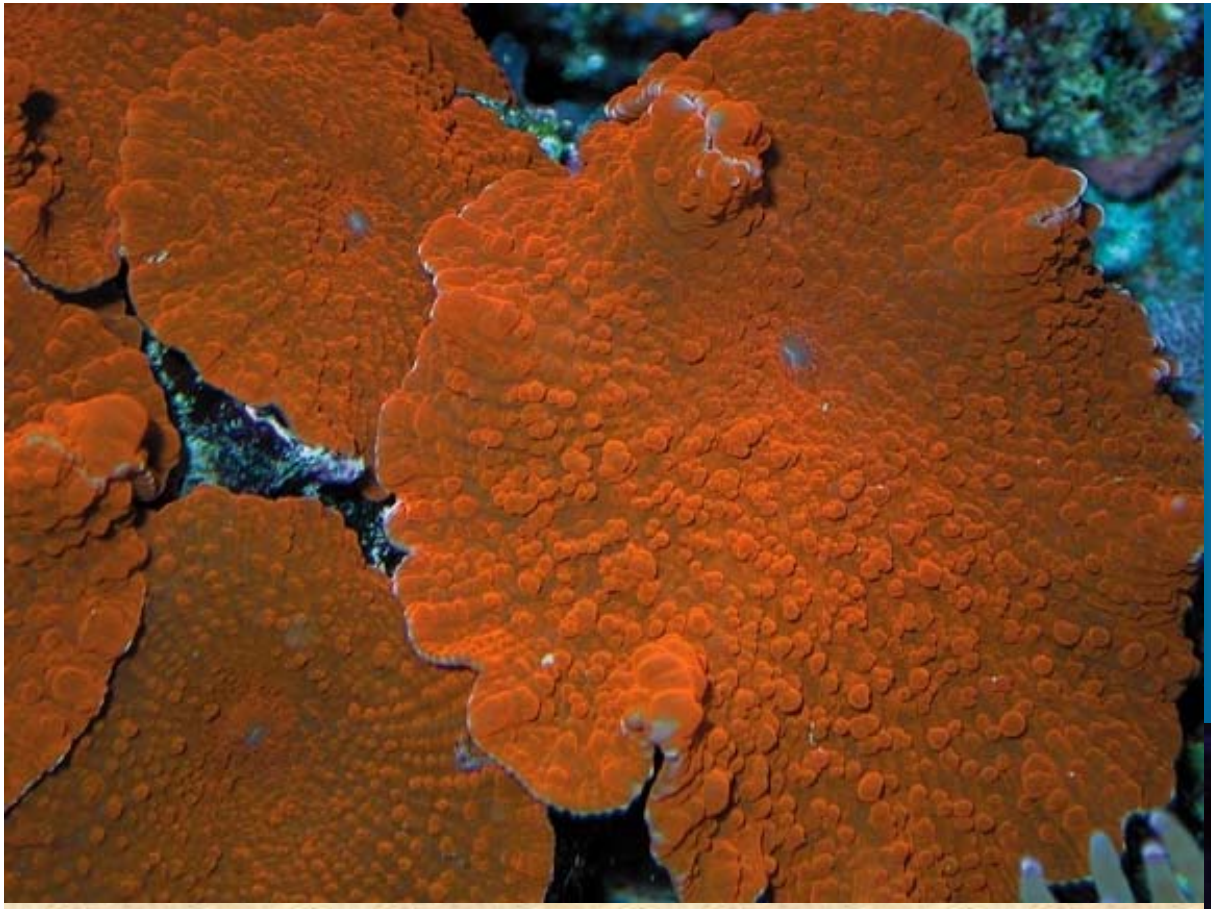

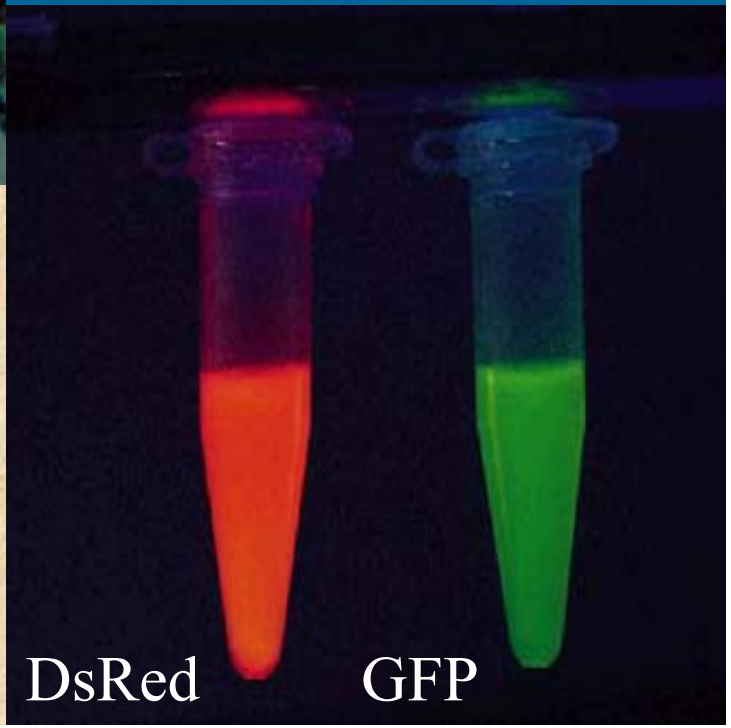

Another increasingly popular fluorescent protein is DsRed - originally isolated from the IndoPacific sea anemone relative *Discosoma* species

Journal of Cell Science 120, 4247-4260

Advances in fluorescent protein technology

Nathan C. Shaner[1], George H. Patterson[2] and Michael W. Davidson[3]

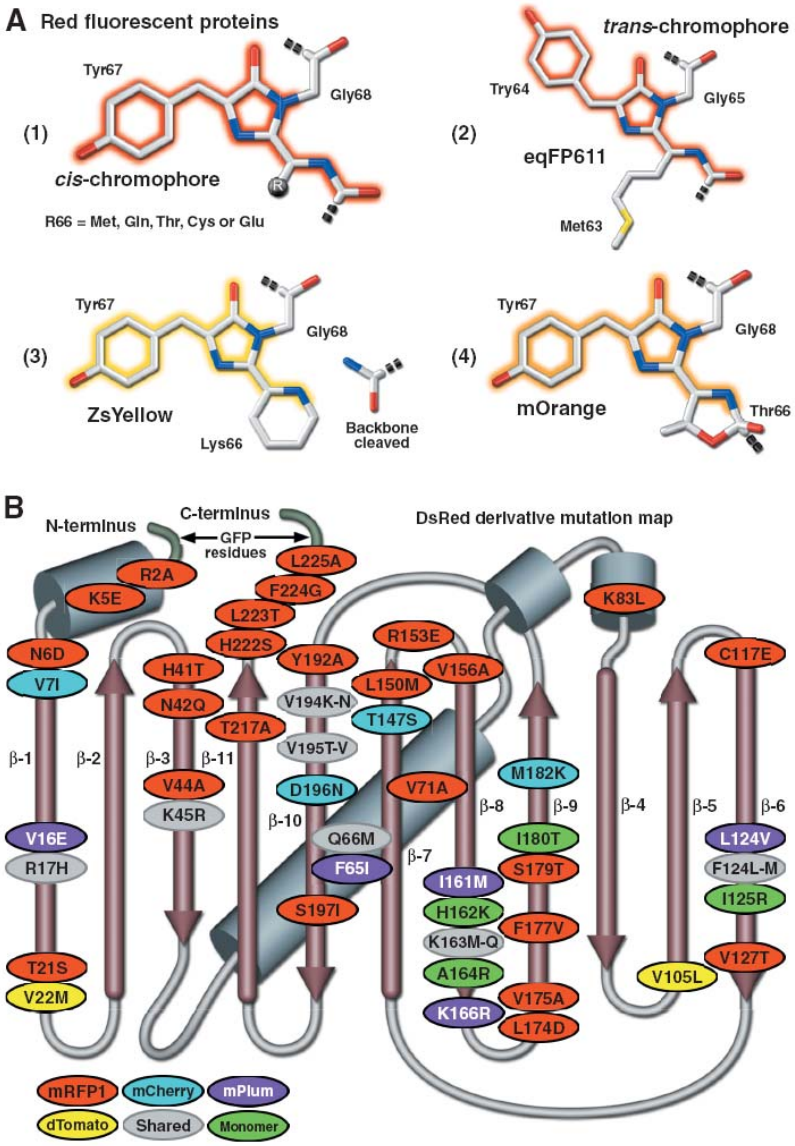

Fig. 2. (A) Chromophore structural variation in yellow, orange, and red FPs. (1) FPs derived from DsRed and other reef coral organisms thought to have a cis-chromophore. The residue at position 66 can be Met, Gln, Thr, Cys or Glu. (2) eqFP611, a red variant derived from *Entacmaea quadricolor*, is the only known FP featuring a trans-chromophore (Petersen et al., 2003). (3) ZsYellow (also zFP538), derived from the button polyp *Zoanthus*, features a novel three-ring chromophore that is created when the lysine residue at position 66 cyclizes with its own α-carbon to form a tetrahydropyridine ring conjugated to the chromophore (Remington et al., 2005). (4) mOrange, one of the mFruit proteins (Shaner et al., 2004), also features a three-ring chromophore where Thr66 cyclizes with the preceding carbonyl carbon to yield a partially conjugated oxazole ring (Shu et al., 2006). (B) DsRed mutation map showing mutations of useful variants superimposed on a topological layout of the peptide structure. β-sheets are numbered and depicted as thin, red cylinders with an arrow pointing towards the C-terminus, whereas α-helices are depicted by gray cylinders. Extensions of the N- and C-termini due to the addition of amino acids derived from GFP to improve fusion performance are shaded in light green. Mutations are color-coded to represent the variants to which they apply: mRFP1 (red), mCherry (cyan), mPlum (violet), dTomato (yellow), monomerizing mutations (green) and shared mutations (gray). Note that unlike the cluster of mutations surrounding the chromophore for *Aequorea* GFP variants (Fig. 1), red FP mutations are distributed throughout the sequence.

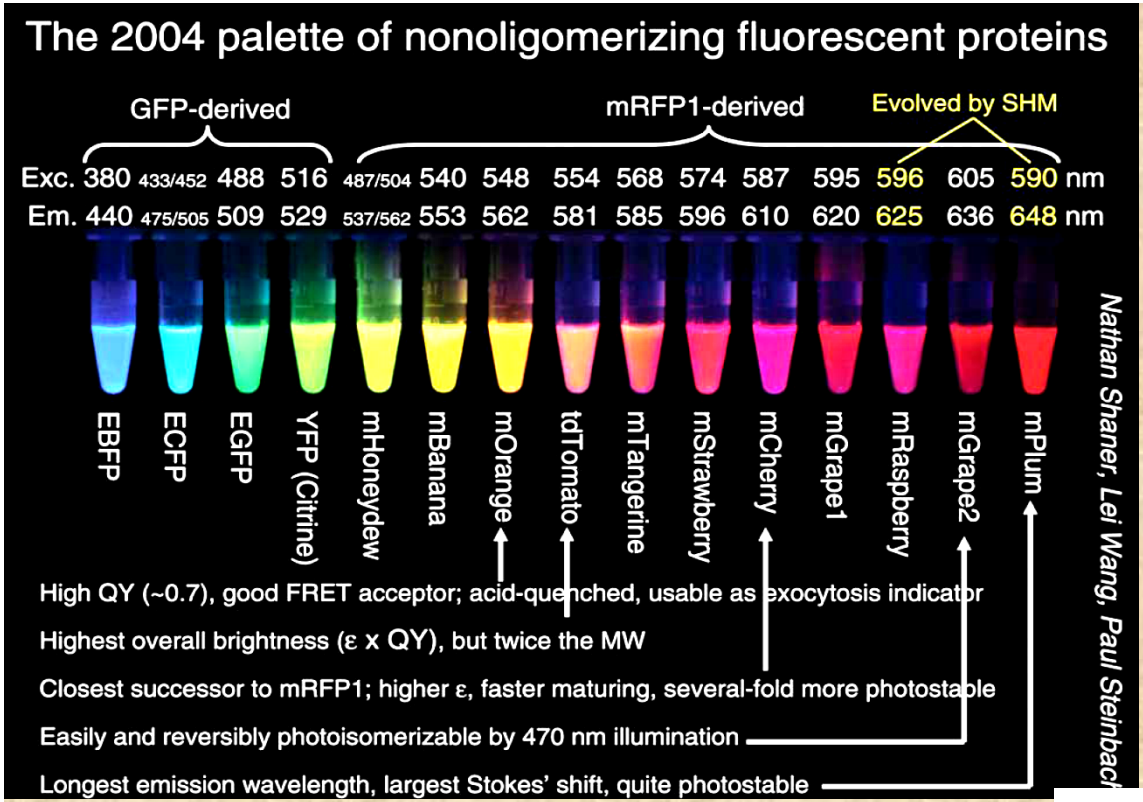
The 2004 palette of nonoligomerizing fluorescent proteins
GFP-derived
mRFP1-derived
Evolved by SHM
Exc. 380 433/452 488 516 487/504 540 548 554 568 574 587 595 596 605 590 nm
Em. 440 475/505 509 529 537/562 553 562 581 585 596 610 620 625 636 648 nm
EBFP
ECFP
EGFP
YFP (Citrine)
mHoneydew
mBanana
mOrange
tdTomato
mTangerine
mStrawberry
mCherry
mGrape1
mRaspberry
mGrape2
mPlum
High QY (~0.7), good FRET acceptor; acid-quenched, usable as exocytosis indicator
Highest overall brightness (ε x QY), but twice the MW
Closest successor to mRFP1; higher ε, faster maturing, several-fold more photostable
Easily and reversibly photoisomerizable by 470 nm illumination
Longest emission wavelength, largest Stokes' shift, quite photostable
Nathan Shaner, Lei Wang, Paul Steinbach

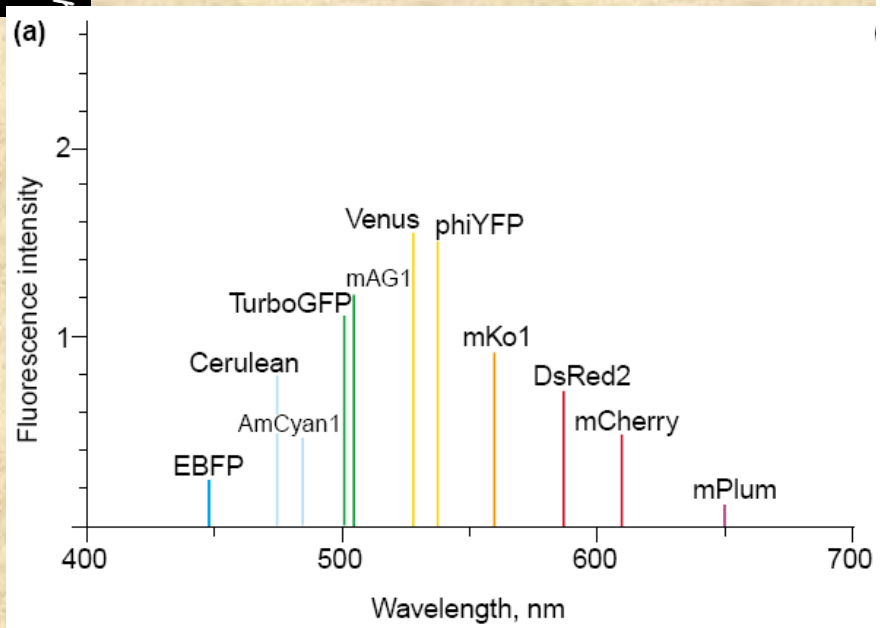
(a)
Fluorescence intensity
2
1
Venus
phiYFP
mAG1
TurboGFP
mKo1
Cerulean
DsRed2
AmCyan1
mCherry
EBFP
mPlum
400
500
600
700
Wavelength, nm

But of course Nature has already experimented with color detection and site-directed mutagenesis

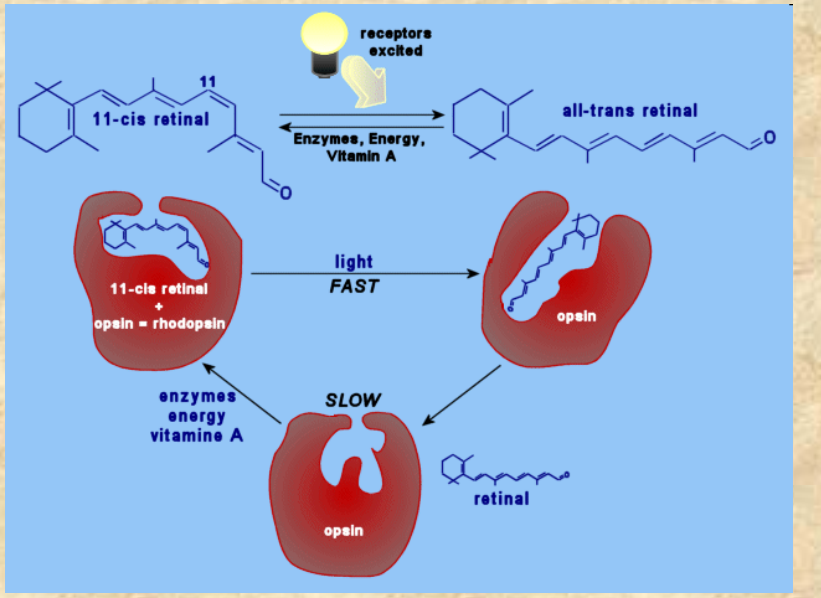

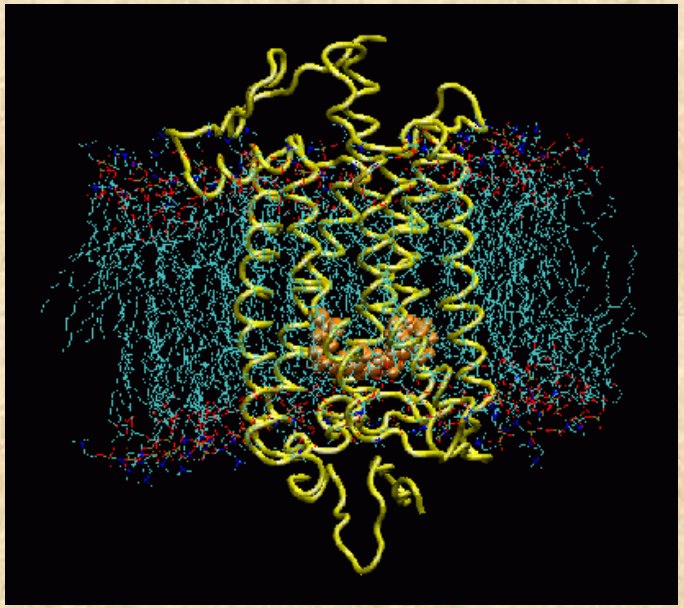

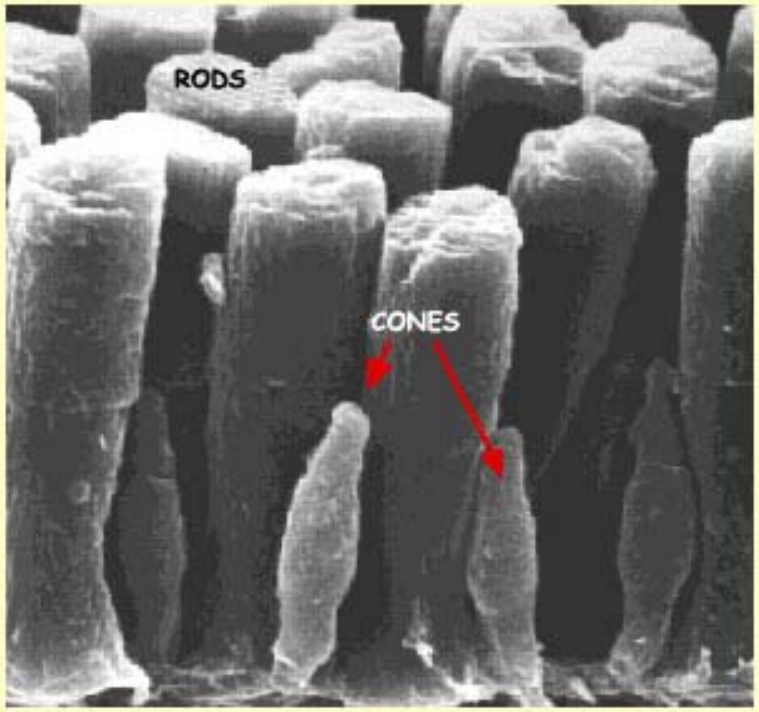

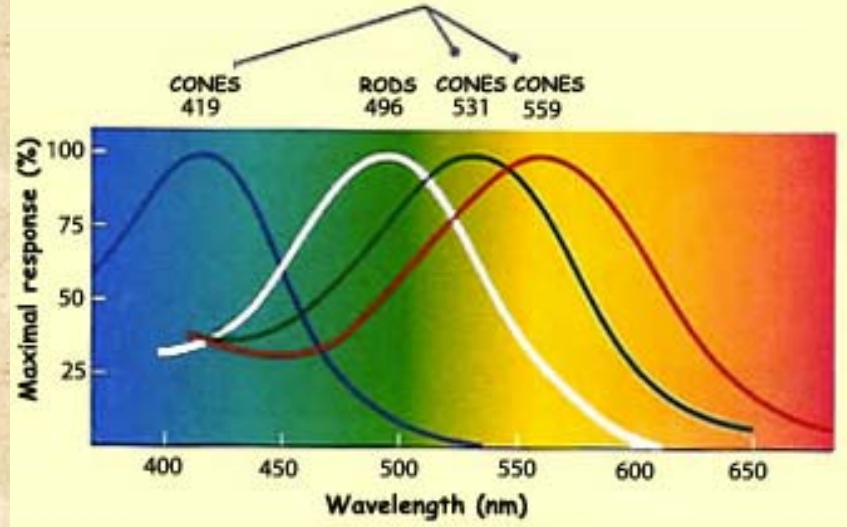

Sharpe et al. • Human Red, Green, and Red-Green Hybrid Cone Pigments

J. Neurosci., December 1, 1998, *18*(23):10053–10069

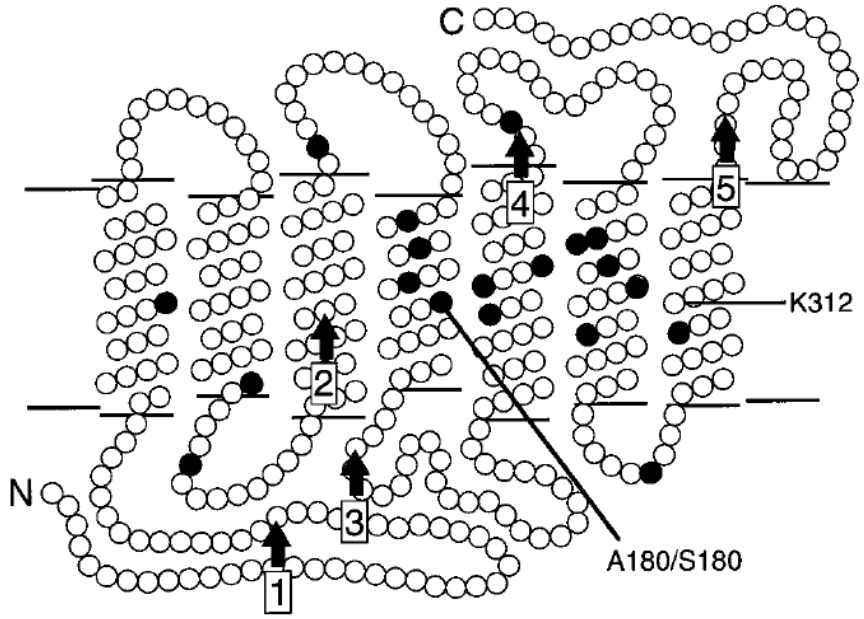

Figure 3. Schematic diagram of the human red and green pigments in the membrane. The N terminus (*N*) faces the extracellular space, and the C terminus (*C*) faces the cytosol. Each *filled circle* represents a position that differs between red and green pigments in the set of sequences studied here; these are positions 65, 111, 116, 153, 171, 174, 178, 180, 230, 233, 236, 249, 274, 275, 277, 279, 285, 298, and 309. The locations of lysine[312] (*K312*), the site of covalent attachment of 11-*cis* retinal, and the polymorphic serine/alanine at position 180 (*A180*/*S180*) are indicated. The five intron positions are indicated by *vertical arrows*.

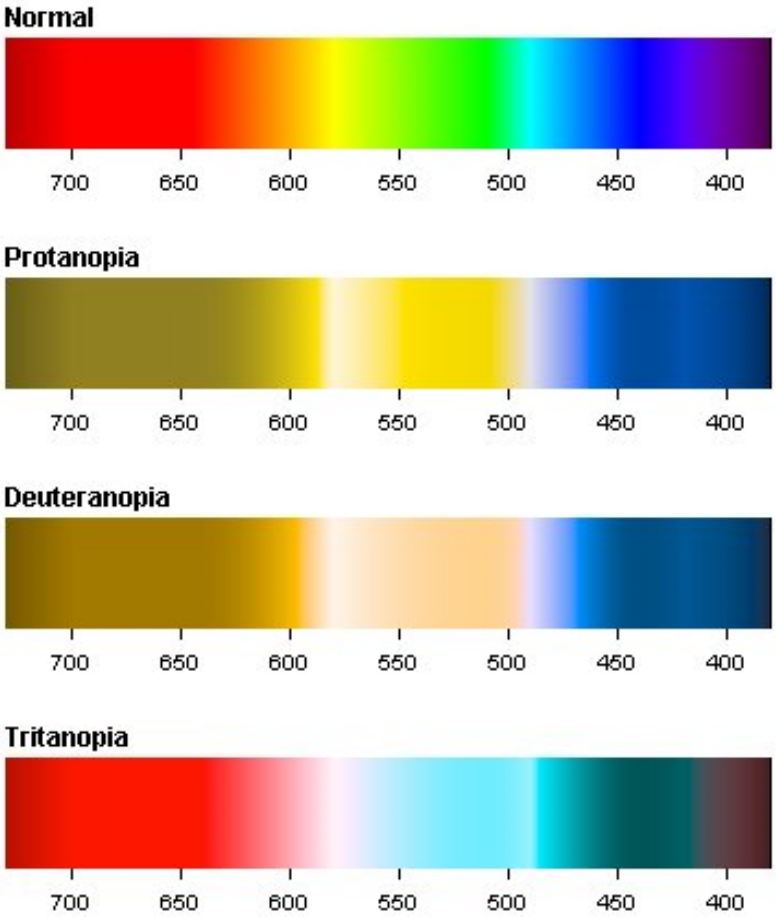

http://www.internettg.org/newsletter/mar99/spectrum.jpg

FlAsH-EDT2 labeling (FlAsH tag)

Specific Covalent Labeling of Recombinant Protein Molecules Inside Live Cells

B. Albert Griffin,* Stephen R. Adams, Roger Y. Tsien†

SCIENCE VOL 281 10 JULY 1998

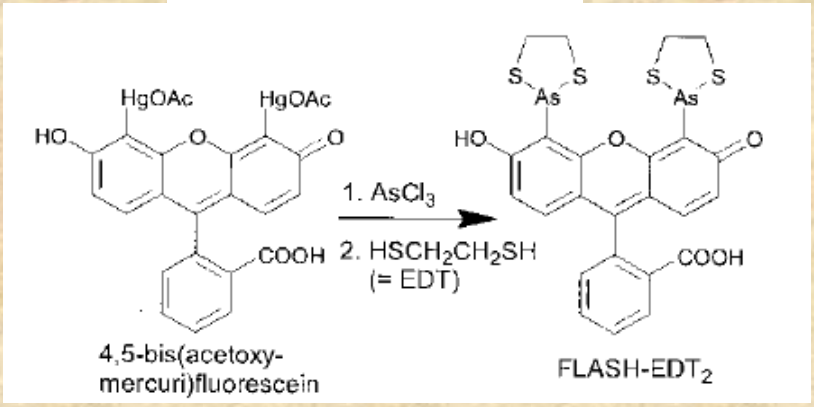

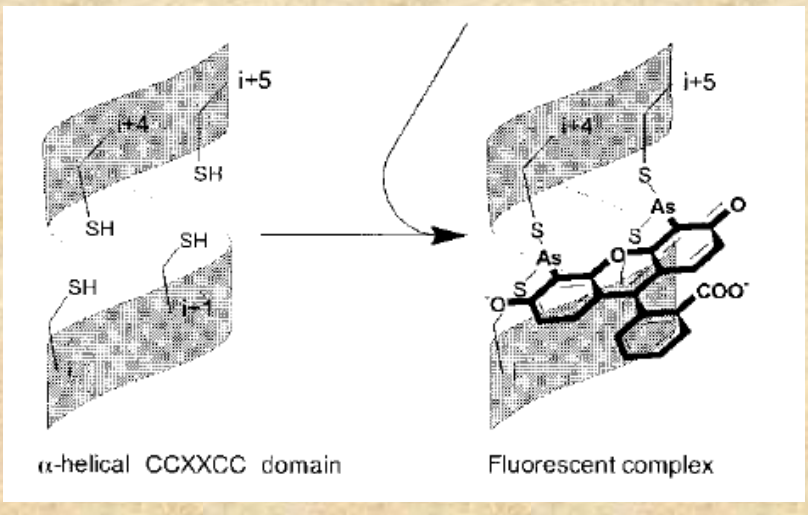

The original motif "CCXXCC" often gave rise to significant nonspecific background.

The use of the "CCPGCC" motif led to reduced background

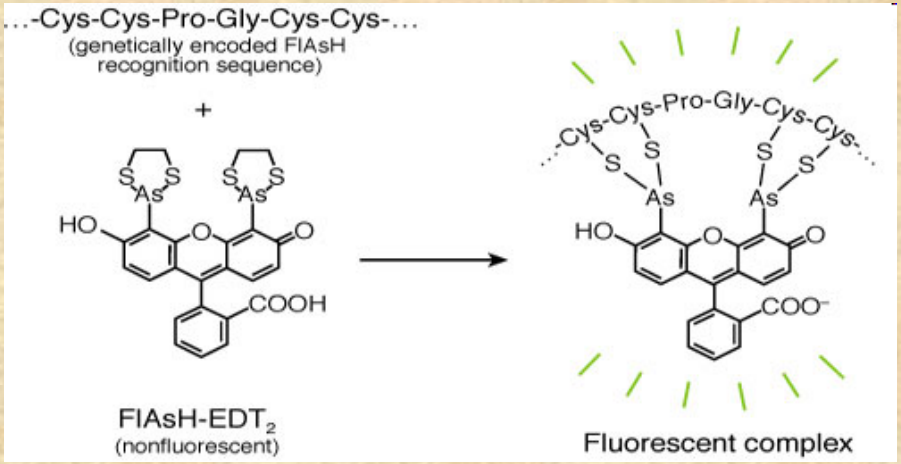

New motifs include "HRWCCPGCCKTF" and "FLNCCPGCCMEP"

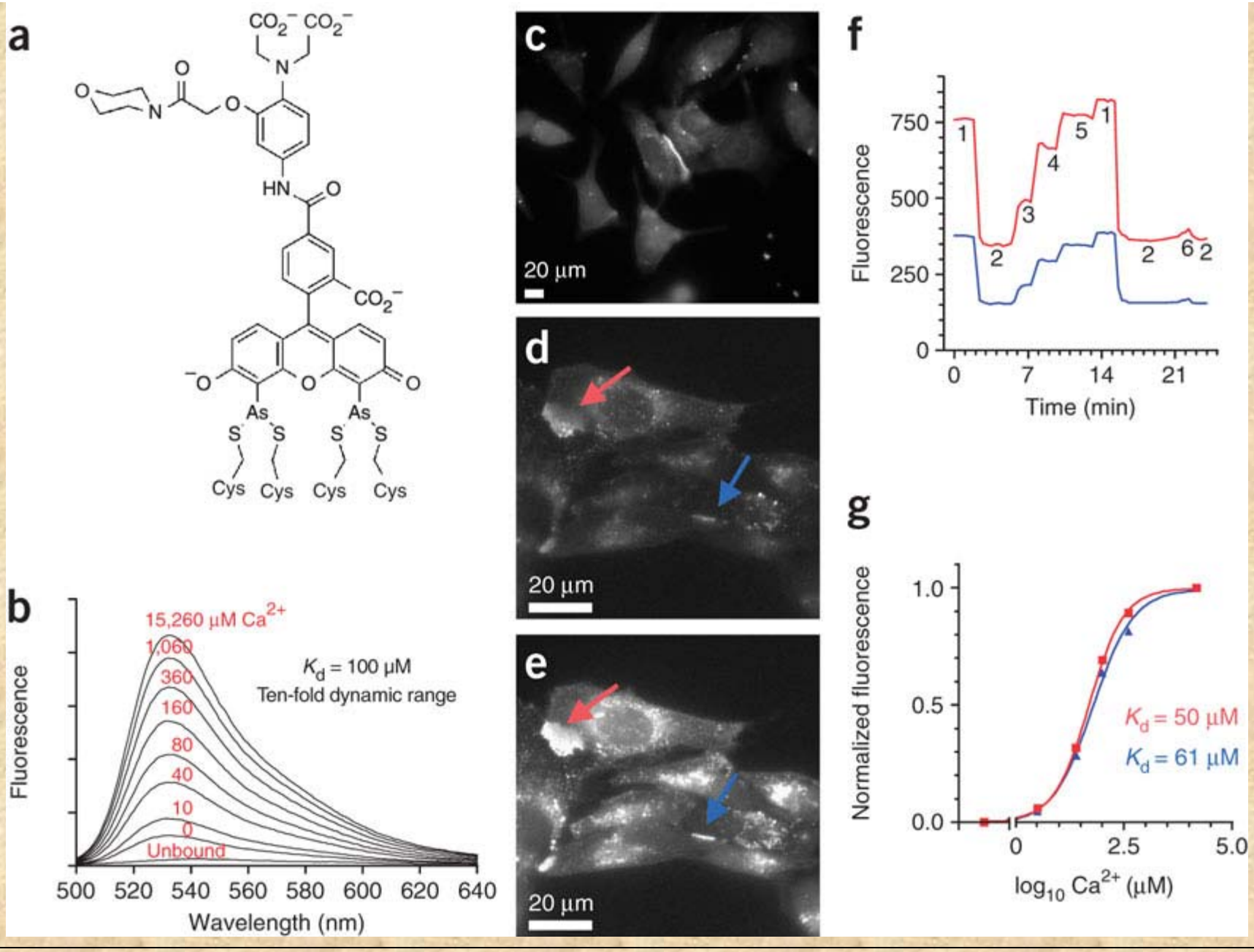

Calcium Green FlAsH as a genetically targeted small-molecule calcium indicator

Oded Tour, Stephen R Adams, Rex A Kerr, Rene M Meijer, Terrence J Sejnowski, Richard W Tsien & Roger Y Tsien

Nature Chemical Biology 3, 423-431 (2007)

ReAsh

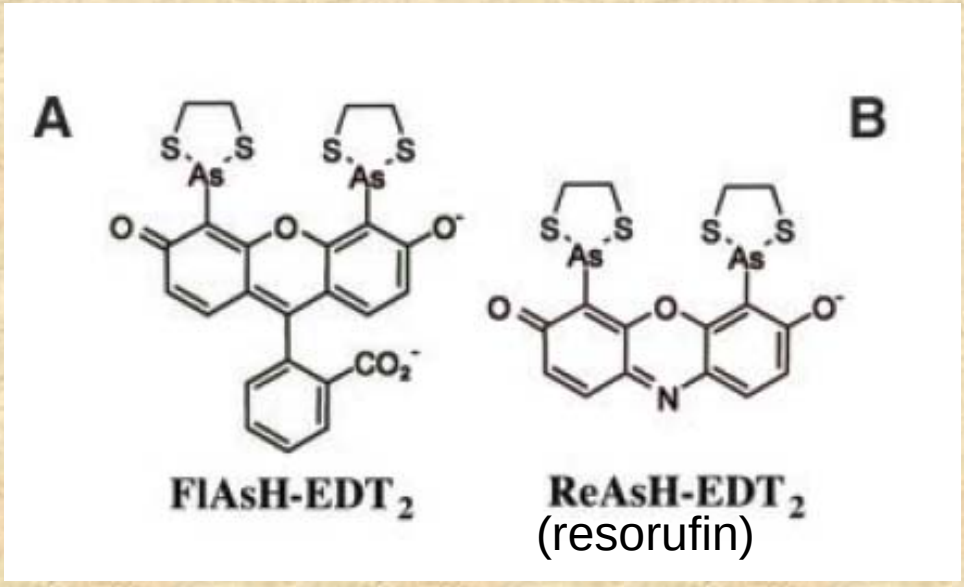

Multicolor and Electron Microscopic Imaging of Connexin Trafficking

Guido Gaietta,[1] Thomas J. Deerinck,[1] Stephen R. Adams,[2] James Bouwer,[1] Oded Tour,[2]* Dale W. Laird,[3] Gina E. Sosinsky,[1] Roger Y. Tsien,[2]* Mark H. Ellisman[1]†

SCIENCE VOL 296 19 APRIL 2002

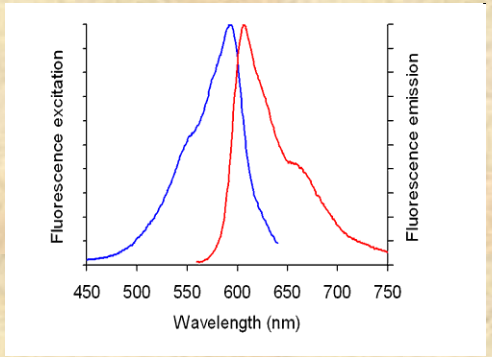

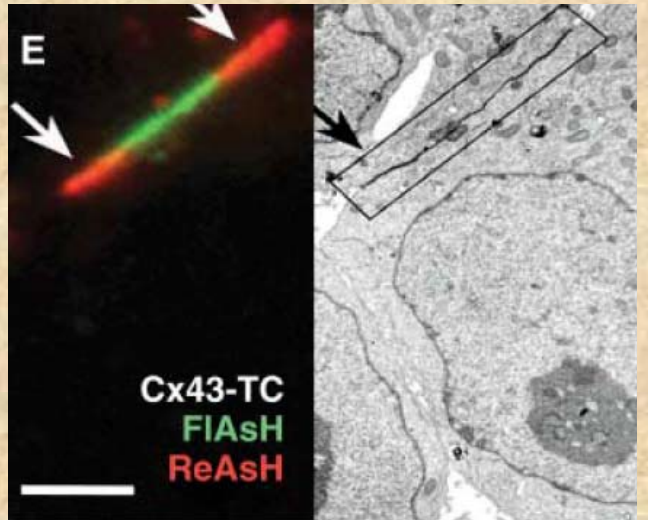

Tetracysteines on connexin43 were pulse-labeled with FlAsH (green) and subsequently ReAsH (red), thus distinguishing old from new connexins, respectively. ReAsH is also visualized in EM using photooxidation (E) (right).

Bimolecular Fluorescence Complementation (BiFC)

Nat Biotechnol. 2003 May ; 21(5): 539–545.

Simultaneous visualization of multiple protein interactions in living cells using multicolor fluorescence complementation analysis

Chang-Deng Hu and **Tom K. Kerppola***

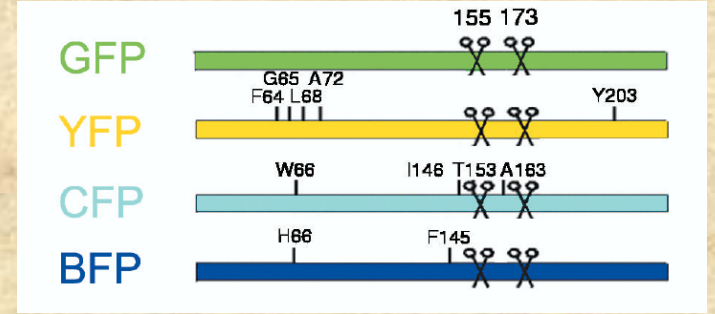

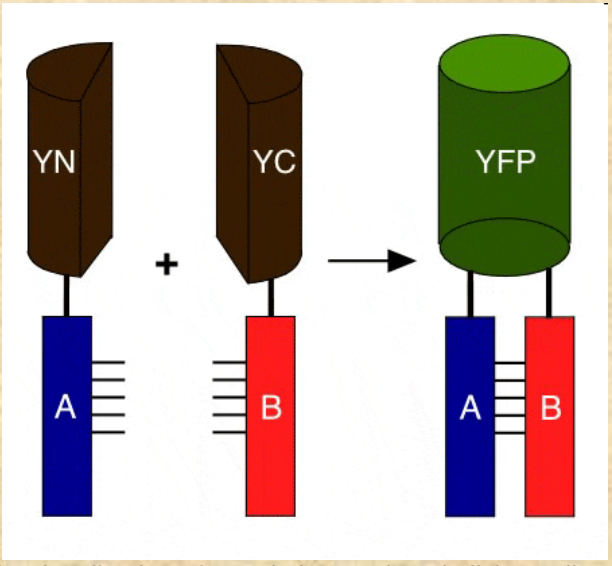

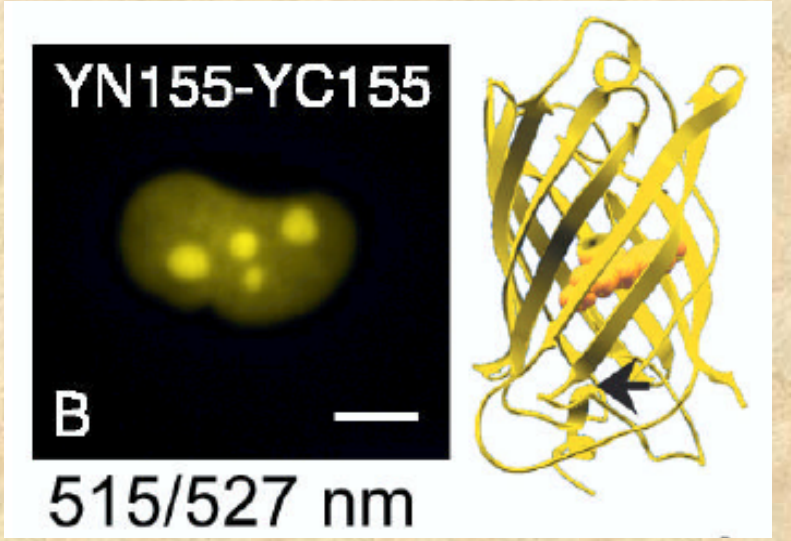

Hu et al., Visualization of protein interactions in living cells using bimolecular fluorescence complementation (BiFC) analysis. Curr Protoc Protein Sci. 2005 Sep;Chapter 19:Unit 19.10.

Other Approaches

J|A|C|S COMMUNICATIONS

Published on Web 08/24/2009

Genetic Incorporation of a Small, Environmentally Sensitive, Fluorescent Probe into Proteins in *Saccharomyces cerevisiae*

Hyun Soo Lee, Jiantao Guo, Edward A. Lemke, Romerson D. Dimla, and Peter G. Schultz*

Department of Chemistry and the Skaggs Institute for Chemical Biology, The Scripps Research Institute, 10550 North Torrey Pines Road, La Jolla, California 92037

J. AM. CHEM. SOC. 2009, *131*, 12921–12923

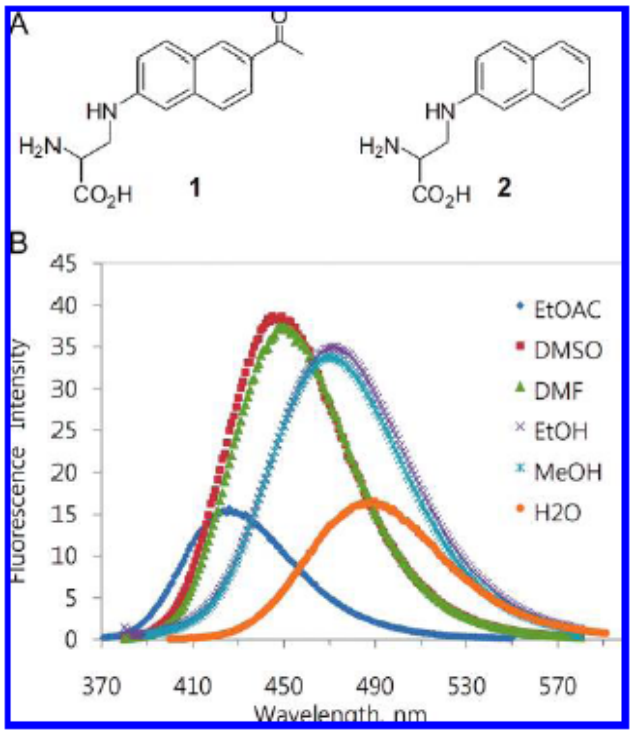

Figure 1. (a) Chemical structures of Anap (**1**) and Nap (**2**). (b) Fluorescence spectra of **1** in various solvents; samples were excited at 350 nm.

To genetically encode this amino acid in *Saccharomyces cerevisiae*, an orthogonal *Escherichia coli* amber suppressor tRNA/leucyl-tRNA synthetase ($tRNA^{Leu}_{CUA}$/LeuRS) pair[12] was used on the basis of previous experiments[7a,13] which showed that LeuRS mutants can accommodate unnatural amino acids with large hydrophobic side chains. To alter the specificity of LeuRS so that it aminoacylates $tRNA^{Leu}_{CUA}$ with Anap and no endogenous amino acids, a LeuRS library was constructed by randomizing five residues

That’s all!!!